The Fluorescent Tube-Lamp Integrating Chamber

By

C.R.Durrheim

Submitted in partial fulfilment of the
requirements for the degree of
Master of Science
in the
School of Physics
University of KwaZulu-Natal
2008

Durban
2008

Supervisor

Preface

The work carried out in this dissertation was performed at the University of Natal, Durban from March 2003 to September 2005 under the supervision of Dr. M. J. Alport and Prof. T. B. Doyle.

These studies represent the original work and have not been submitted in any form to another university. The work presented is that of the author's. Mathematical techniques are not original but the applications to the problems in this dissertation are unique. No study has been previously documented with regard to the cylindrical chamber. The author is not aware that the fluorescent tube-lamp has been previously analyzed using the techniques in this study. All equation deductions and analysis is original, as are the physical deductions and approximations leading up to the chamber measurement equation.

Author's signature: _____

Acknowledgements

Abstract

The objective of this project is to design a facility that will characterize the electrical and optical properties of both tubular and the more recent compact fluorescent tubes. The first stage of this project, which is the subject of this dissertation, was to design, build, test, and model a cylindrical light integrating chamber.

An integrating chamber capable of measuring 2-metre long fluorescent tubes was built at the University of KwaZulu-Natal, South Africa. To approximate an infinitely long tube, precisely mounted planar mirrors were placed at opposite ends of the cylinder. The reflectance of diffusive reflective paint and mirrors enter into calculations and were investigated experimentally using a Jarrel-Ash optical spectrometer.

The light flux was finally measured for various chamber lengths and compared with a mathematical model. Total light power output from the lamp was calculated and compared with the electrical power input, and the lamp efficiency deduced.

Accurate calculations required that the light field surrounding a cylindrical diffuse source be modeled mathematically. The reflection coefficients of the mirrors were not unity and the equations had to be modified to include this effect.

The mathematical model was solved using a combination of analytical and numerical techniques.

The model results were compared with measurements. The final result includes a mathematical description of the integrating chamber, and a flux-density plot of the space surrounding the fluorescent tube.

The Fluorescent Tube-Lamp Integrating Chamber

List of Contents

Table of Figures

Page

Table of Tables

1. Introduction

The distribution of light intensity and the efficiency of light sources are of prime economical importance in the lighting industry. Most industrial activity takes place inside buildings, and adequate lighting is essential for productivity and the comfort of workers. Aspects such as glare and contrast can significantly affect the performance and cost-effectiveness of lighting installations. It is therefore highly desirable that the distribution of light from one of the most common sources, namely the cylindrical fluorescent lamp, be well understood and quantified.

Knowledge of the radiation pattern around a lamp enables engineers to design luminaires that efficiently distribute light, and allow for the reasonable determination of light levels in the working environment prior to installation. Combined with such calculations, the experimental measurement of the flux density at various points in space with the aid of an appropriate lux-meter also allows for an estimation of lamp power output and hence also for a determination of the deterioration of the lamp with time.

The integrating chamber allows for an accurate measurement of the total light power output of an individual lamp. Spherical chambers are virtually exclusively used throughout the scientific and engineering community, due to ease of theoretical results. Such a chamber is, however, not practical from long lamps, such as the cylindrical fluorescent lamp. The cylindrical chamber described in this dissertation, presents a compact, affordable solution for cylindrical fluorescent lamps, in that the physics of light reflection within such a chamber, is fully described.

The cylindrical chamber hosts a cylinder coated on the inside with a diffuse highly reflective white paint. The end-walls are presented with mirrors, which emulate the conditions of an infinitely long chamber and lamp, thereby improving light integration and simplifying calculations. One of the mirrors is movable to accommodate a variety of lamp-lengths. A light-meter sensor is positioned midway between the mirrors. The

reading translates into a measure of the total light power output of the lamp. See Figure 4-2 in Section 4.2.2 where the apparatus is discussed in detail.

It is a requirement in the lighting industry for small sections of the lamp to be measured individually. Holes are therefore cut into the centres of the mirrors to accommodate the translation of a fluorescent tube through the reduced chamber.

The approach to analyzing the cylindrical chamber is similar to that commonly used for the spherical chamber .i.e. multiple reflections from the source are integrated over the surface of the chamber. However the method here is simplified by noting that the total absorbed light power is exactly the light power of the lamp. On the other hand, the analysis is complicated by the mirrors possessing a reflectance f_m < 1. Statistical ratios were incorporated to account for the adjustable distance between the mirrors. Finally it was noticed that light incident on a diffuse surface had to be treated uniquely. The incident ray cannot be regarded as comprising orthogonal components as in the case of specular reflection. A statistical weighting was introduced to rectify the final measurement equation.

Light levels within the chamber were measured for sectional lengths of the same lamp. Hence a profile of light intensity versus chamber length was obtained. The primary aim of this dissertation is to obtain a theoretical formulation of the measured profile. To this end, it was necessary to measure the reflectance of the mirrors accurately, and to determine the diffusivity of the paint. In order to facilitate calculations with a pseudo-infinitely long chamber (due to mirrors), the light intensity surrounding a diffusive emitting cylinder (a fluorescent tube in this case) was calculated using boundary projection onto a unit sphere. This method of integrating over a sphere, greatly simplifies calculation, and is based on the diffusive nature of the lamp, as well as uniformity of intensity over its surface. An experiment was performed to confirm the results, but is not described in detail in this dissertation, as it is regarded as detracting from focus on the chamber. Briefly, a lamp was suspended about two meters above the floor (on the roof of a building), that was covered by a non-reflective black sheet. The experiment was

performed at night; hence there were no reflective or emissive surfaces in the vicinity. The light intensity was measured at several positions in space surrounding the lamp, and experimental results compared favorably.

This dissertation begins with a literature survey, presenting other commonly used chambers and an instance of the modeling of a cylindrical chamber for measuring laser scattering. Chapter 3 introduces the basic concepts of the physics of a fluorescent lamp, as well as some of the terminology used in subsequent chapters. Chapter 4 attempts to familiarize the reader with the practicalities of using an integrating chamber, including the basis for constructing the cylindrical chamber with diffusive paint, end-mirrors etc. Chapter 5 details the analysis of light surrounding a cylindrical fluorescent lamp, finally presenting the graphical result, but more importantly, the formula which is used in Chapter 6. Chapter 6 forms the core of the dissertation. The cylindrical chamber is analyzed in detail, and a mathematical model is developed. The final result is a measurement equation describing the dependence of calculated light power on chamber length. Finally, conclusions and suggestions are discussed in Chapter 7. The subsequent appendices present details of experiments performed, as well as mathematical derivations that are lengthy and would otherwise distract the reader from the core of the topic in discussion.

The author is unaware of any research having been performed on such cylindrical, as opposed to the spherical integrating chambers. The mathematical derivations for the cylindrical chamber, presented herein are, therefore, original to the present author.

2. Literature Survey

An extensive literature search has not revealed any research having been done on a cylindrical integrating chamber using mirrors. A cylindrical shape with end-cones has been used by Simpson *et al* [1] to integrate light from a laser-scattering target. In this experiment, scattering from the target is non-uniform, hence the choice of a cylinder rather than a sphere. The cones are required to compliment the geometry of the external lens system, and due to their nature of directed scattering, the chamber is not applicable to the fluorescent tube. The experimental setup is reproduced in Figure 2-1 below.
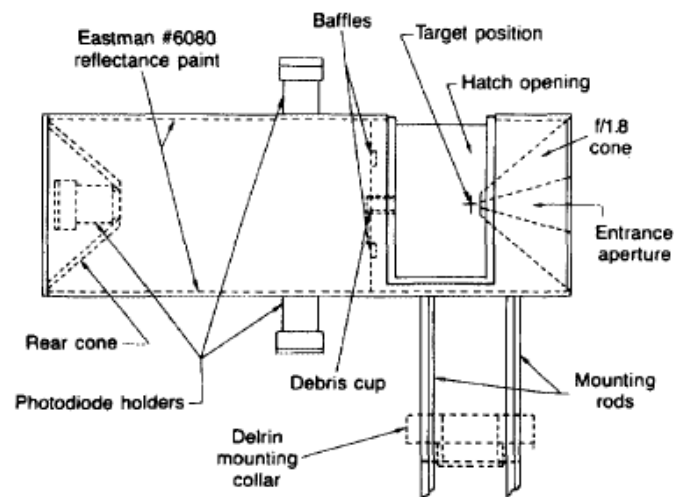
Figure 2-1

A cylindrical chamber used for integrating light from a laser-scattering target.
Note the use of diffusive end-cones [1].

On the other hand, a spherical integrating chamber is utilized extensively in both industry and research, and for various applications. A typical sphere is shown below in Figure 2-2.

The large port in the foreground usually performs the function of a uniform diffuse light source [2].

The basic principle of operation of an integrating chamber is that there is multiple scattering of light from a light source placed within the chamber to the extent that the reflecting surface exhibits a perfectly uniform radiance (due to spatial light integration) that is accurately measurable.

Figure 2-2

A photograph of a typical integrating sphere. The port in the foreground
serves as a uniform light source [2].

The objective of measuring the luminance of a source is achieved by placing a sensor at a small port in the chamber wall. Alternatively, a larger port can be used as a source of precisely known uniform intensity as required, for example, in the field of spectroscopy [3].

A high degree of reflectance of the inner surface, combined with high diffusivity, ensures a high degree of scattering, which in turn ensures a high degree of uniformity of radiance from the sphere inner surface, as well as an enhanced radiance level.

The simplest theoretical model of an integrating sphere assumes a highly reflective surface of uniform reflectance and uniform smoothness. Since the function of the chamber relies on multiple reflections, the result becomes highly sensitive to the surface reflectance. Uniform reflectance implies a reflectance that is constant over the visual spectrum, *and* does not vary from place to place along the chamber surface. Any deviation from uniform spectral reflectance is amplified by the nature of multiple reflections. It is vital therefore that the surface material exhibits a uniform flat spectral response so that all spectral components are equally represented for measurement.

Paint, which is commonly used as the reflecting/diffusing material, is difficult to apply in a manner that results in a smooth surface. For example, the stroke of a brush may lead to elongated depressions in the painted surface. Furthermore, reflectance will have some dependence on the thickness of the paint since some degree of light penetration occurs in all paints.

The type of paint used should therefore also have a consistency such that all samples possess identical properties. Barium Sulphate is a common component of such highly reflective/diffusive paints. House-paint usually contains titanium-oxide, which is slightly absorbent in the blue end of the visible spectrum [4].

The spectral selectivity of reflective paint, in the visible region, has been investigated by Walsh and Barnett [5]. They have demonstrated the effect of selectivity and have presented some solutions. One choice is to ascribe a colour temperature to the lamp, and to calculate a correction factor using laws of Black-body radiation, in particular, Wien's Law.

Paint stability with respect to time, temperature and humidity, and paint washability are also important considerations.

Another widely used material is Spectralon, a thermoplastic PTFE based resin developed by Labsphere [4]. Use has been made of Spectralon's compressibility to minimize gaps between the components of a geodesic chamber frame, by Shitomi *et al* [6].

The company, Labsphere, based at 231 Shaker st., North Sutton, New Hampshire, U.S.A.; (website: **www.labsphere.com**), produces a range of coatings including Duraflect, Infragold and Spectraflect

Aside from the surface, other important factors include the surface area of constructions within the chamber such as lamp supports and direct-beam baffles, and the size of the port in relation to the chamber.

The ideal integrating sphere equation for the intensity *I* at the surface is given by

$$I = \frac{\Phi_s}{4\pi r^2} \frac{f}{1-f} \quad W.m^{-2}$$

where Φ_s is the total flux from the source and *f* is the surface reflectance. The equation for the sphere is quite uncomplicated and simple to prove, as shown in Appendix G, and the sphere is therefore a favorable choice of shape for the integrating chamber in general.

While the particular purpose of the *cylindrical* chamber is to measure intensities of elongated (i.e. high aspect ratio) lamps, the integrating *sphere* is suited to a wider range of applications. Some common uses are listed below:

- Light collection from internal or external source (lamp measurement photometry)

- Laser power measurements [7]

- LED spectral and SPD measurements

- Reflectance of either specular or scattering samples

- Total or diffuse only transmittance measurements

- Cosine receptors

- Uniform light sources

The principle of the integrating sphere has also been applied in the investigation of absorption measurement, by Lerebourg *et al* [8]. In this experiment the chamber was filled with the liquid sample to be investigated. When light is transmitted through a medium, some light is absorbed, while the remainder is scattered. The integrating sphere can collect and measure all light except the absorbed light, and in this way the absorbed light energy can be deduced. Bastin *et al* [9] have investigated solid samples.

The Monte Carlo method has been applied by Hanssen and Prokhorov [10], to the integrating sphere in the radiation source arrangement, in order to obtain the radiance at the sphere surface, and the external irradiance due to a port. The radiance from the port, which can then be known accurately, is highly uniform over the port surface, to the extent that the sphere can be used as a calibration source. Details have been documented by Brown and Johnson [11].

Other uses for the integrating sphere include the measurement of emissivity, as described by Saunders *et al* [12], and in the field of microscopy where the sample is placed within a sphere to remove contrasts in the sample, as described by Kiguchi and Kato [13].

3. Basic Concepts

3.1 Introduction

The total light output of a lamp can be measured by means of a 4π integrating chamber; i.e. one which reflects light from all directions back into the chamber. The light intensity at the surface is measured, in order to deduce the total light output power. Such a chamber is ideally suited for sources with small dimensions, e.g. incandescent globes. The total light output of a small lamp is ordinarily measured using a spherical integrating chamber.

Conventional 2-meter long cylindrical fluorescent lamps suggest the use of a cylindrical integrating chamber, rather than a spherical chamber, which would need to be at least 5 meters in diameter in order to obtain the desired light integration. Such a cumbersome chamber would favour permanent installation, since it is too large to be easily transported. Furthermore, such a chamber would be costly to produce.

This dissertation shows that the total light output of a long cylindrical lamp can be accurately measured using a portable cylindrical light-integrating chamber, of length no longer than the lamp. The end result relies on a knowledge of the radiation pattern for a cylindrical diffuse transmissive surface. The light intensity surrounding a cylindrical lamp will, therefore, be analyzed as a prelude to finding the measurement-equation for the chamber.

Note that the integrating cylinder designed for this investigation had the facility to allow for the measurement of power output of a short lamp section, as a function of distance along the length of lamp. This is an important consideration for lamp designers and end-users.

3.2 Terminology

For the purpose of the present analysis, the long axis of the lamp was assumed as aligned along the *z*-axis in the Cartesian system as shown in Figure 3-1. A list of term definitions is given in Appendix E.
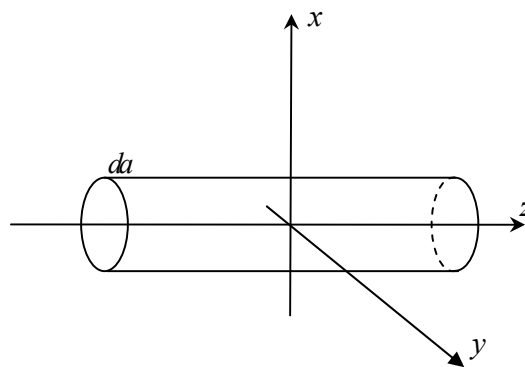
Figure 3-1

The orientation of the fluorescent tube and chamber with respect to Cartesian axes.

3.3 The Fluorescent Tube Lamp

The light from a fluorescent tube is generally emitted from a fluorescent powdered layer, coating the inside surface of a sealed glass tube. See Figure 3-2 below. The layer is significantly diffusive such that the emission closely approximates Lambertian character.

Fluorescence results from the irradiation of the fluorescent layer by photons emitted from the plasma encapsulated in the sealed tube. The plasma is generated by an electrical discharge through a suitable gas along the length of the tube.

Electrodes at the ends of the tube take the form of filaments, which can be heated by a current to enable spontaneous liberation of electrons into the gas.

Boundary layer behavior in the plasma in the vicinity of the filaments gives rise to a reduction in light output from the regions immediately surrounding the electrodes. This phenomenon is commonly known as 'cathode fall'. The end result is a loss of overall efficiency of the lamp, and a tube therefore does not have an entirely uniform light intensity over the outer surface.

The performance of the lamp is, furthermore, somewhat dependent on the physical state of the filaments. The high operating temperature of the filament contributes substantially to the deterioration of emissivity over the operational lifetime. The lifetime of the lamp is, in fact, mainly determined by the condition of the filaments.

It has been established that several measurable parameters of the operating lamp provide a reasonable indication of the remaining lifetime of the cathodes. One of those parameters is the emission profile along the length of the lamp. It is of interest to a lamp designer, therefore, to be able to measure the light output from the lamp as function of position along its length.
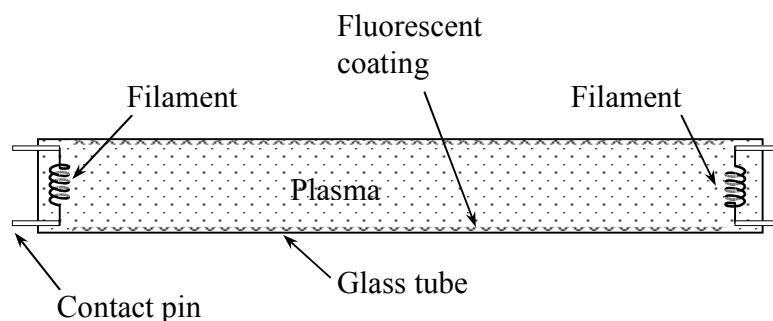
Figure 3-2

The basic construction of a fluorescent tube lamp.

4. Design criteria for the Integrating Chamber

The integrating chamber should obviously be designed to ensure that the optical radiation in the chamber, which impinges on a detector (thereby providing a measurable signal), has a quantifiable dependence on total lumen output of a lamp (or a local segment of it), which, ideally, can be obtained with a relatively straightforward analytical or numerical algorithm in terms of the lamp and chamber parameters.

The total lumen output of a lamp, as well as the light intensity distribution along its length (in the case of a cylindrical lamp), is useful in the manufacturing and consumer industries. Knowledge of the total lumen output enhances quality control of the manufacture process and provides a criterion for comparison between products. The intensity profile along the length of commercial tubes provides, *inter alia*, information on the quality and remaining lifetime of the lamp filaments, which are obviously important considerations.

The spherical integrating chamber will first be discussed as an introduction to the use of integrating chambers in general.

4.1 The Spherical Integrating Chamber

The spherical integrating photometer comprises a sphere coated on the inside surface with a highly reflective diffusive material. The source is placed at the centre, behind a baffle, that blocks light traveling directly from the lamp toward the sensor. The baffle is an essential requirement if the transmitting surface, e.g. lamp filament, is small.
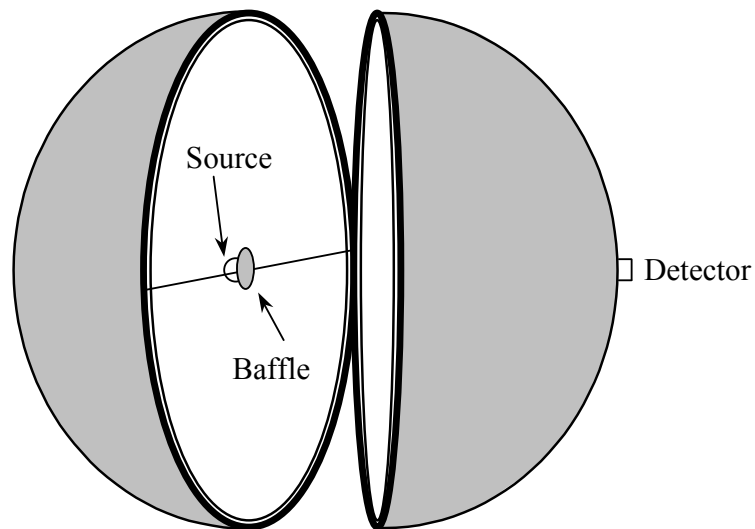
Figure 4-1

An exploded illustration of a spherical Integrating chamber.

The effects of source anisotropy are largely reduced by the use of a highly reflective/ diffusive surface (reflectance $f = 0.97$ for the paint used in this model). Multiple reflections of light in the chamber enhance the integrating functionality of the sphere, which is directly related to the average number of reflections a photon undergoes before absorption. Excellent integration has the effect of causing the light intensity to be approximately constant everywhere on the inside surface. Thus, at any arbitrarily chosen position on the surface, a small area can be used to obtain a measure of the total lumen output from the lamp.

A gain factor G, more commonly known as the *sphere multiplier*, can be ascribed to the chamber (see Labsphere [3], p5). G is the ratio of measured light intensity at a point on the chamber inner surface directly due to the lamp, to that with the chamber reflective surface included. Note that $G \geq 1$, with $G = 1$ by definition, for a non-reflective wall. The gain factor is easily measured by placing a calibrated source at the centre of the chamber,

and recording the light intensity at the chamber surface, by means of a suitable light-sensor and light-meter.

Effective light integration will necessitate the use of a chamber of more than 5 meters in diameter for a typical fluorescent lamp tube of 2 meters in length, as has been stated. The reason is as follows. Due to the cylindrical shape of the emitting surface of the lamp, the emissive characteristics in the vicinity of the lamp are far removed from that of a point source. Hence the chamber surface is required to be far away enough that the cylindrical lamp approximates a point source. The gain factor for such a large chamber will be quite low, due to the large area of the reflective surface in relation to the source intensity, with a corresponding reduction in integration efficiency.

4.2 The Cylindrical Integrating Chamber

Effective light integration necessitates the requirement that the cylindrical chamber diameter be sufficiently large in comparison with the lamp diameter, so that local bright zones on the lamp do not affect measured values.

The compact design of a cylindrical chamber makes it an attractive alternative to the spherical model, for cylindrical fluorescent lamps. Further discussion will therefore concentrate on the cylindrical chamber only.

4.2.1 Main Objectives

The main objective of this project was to obtain a mathematical model for the cylindrical integrating chamber with end-mirrors (see Figure 4-2 below), i.e. a relationship is required between measured incident light intensity and total emitted light power. The mathematical model is complicated by the imperfect reflectance of the end-mirrors.

A secondary objective is to characterize the radiation field around a cylindrical fluorescent lamp. The ideal result would be an equation describing the constant-intensity trajectories (isolines) as a family of curves.

The chamber equation should enable, indirectly, the measurement of total light output of a lamp, as well as the light output of a longitudinal section of the lamp. The chamber system should not be sensitive to small variations in length or position of the lamp, or light-sensor location.

4.2.2 *The Apparatus*

The chamber cylinder consists of a hollow cylindrical tube, in which the lamp is inserted axially. Perfectly reflective planar mirrors, supporting the lamp inside its ends, would effectively enable the lamp to possess the optical properties of an infinitely long tube (see Figure 4-2 below).

The chamber cylinder radius is larger than that of the lamp by a factor of approximately 20. This proportion was chosen as a compromise between the gain factor G of the chamber and the degree of integration of light within the chamber. Such a chamber would effectively have no ends or edges (where two surfaces meet at differing orientations), and would approximate to the ideal situation of an infinitely long cylinder. Analysis would then be simplified since the flux in the chamber would be uniform.

However, as will be discussed later, practical mirrors have a reflectance $f < 1$. Consequently there must be some non-uniformity of the flux, but certain assumptions will be made to simplify the calculations.
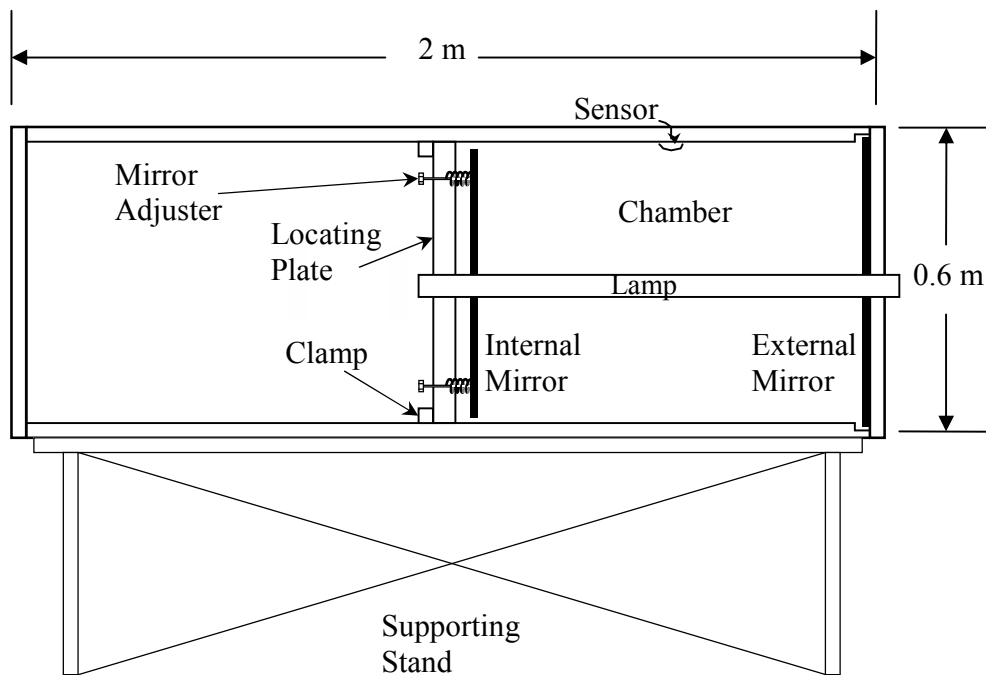
Figure 4-2

A diagrammatical view of the chamber used in this project. Note that the chamber is designed for tubes of various lengths. Mirrors are ideally surface coated.

Light intensity over a small area at a point P, on the chamber surface, was measured by means of a light-sensor, which consists of a diffuse transmissive dome, surrounding a photodiode. This is a so-called "cosine-corrected" device. The dome produces a response at the photodiode, such that the photodiode current is proportional to the cosine of a ray arriving on the dome, with respect to the photodiode surface norm.

The associated light meter was capable of measuring up to 200,000 lux, with a resolution of $\pm$ 20 lux and an accuracy of 1%. The light sensor was placed on the chamber wall, halfway along the chamber, to ensure symmetry. This symmetry results in simplified calculations.

It may be a requirement in industry, for a measurement to be made at a specified section along the lamp. The method may be used to construct an intensity profile along the length of the lamp. The profile can yield information about the condition of the lamp electrodes.

Power radiated from a small section along the lamp surface can be measured by placing the mirrors as close to one another as necessary. The lamp is then translated through holes in the mirror centers to obtain an overall intensity profile.

The internal mirror, which is located to select the chamber length, is required to be circular in order to fit into the cylindrical chamber, and is therefore made of Perspex, which is less costly to machine. The external mirror was made of 4 mm thick glass, for the sake of rigidity, and a square cut sufficed, since it was mounted on the door. See Figure 4-3 below.
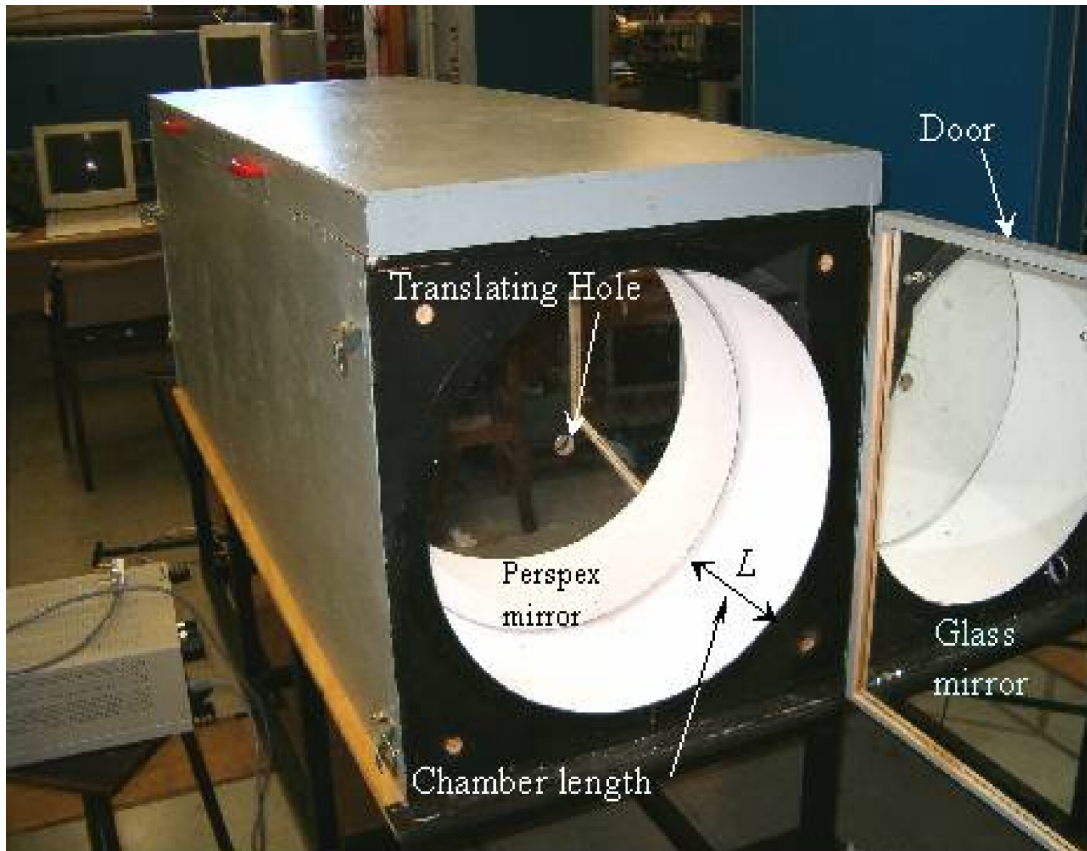
Figure 4-3

A photograph of the side view of the chamber. Here the chamber is set up with an interval $L = 20$ cm by moving the internal Perspex mirror along the axis of the chamber

The Perspex mirror was mounted onto a plywood backing to impose rigidity, and then onto a plywood base with adjustable sprung supports for fine adjustment of mirror orientation.

In order to fix the internal mirror at some point in the chamber cylinder, rubber-buffered clamps were installed onto the base so that it could be secured into position by exerting a force on the chamber wall. The force was applied via clamps, by means of cams, as shown in Figure 4-4.
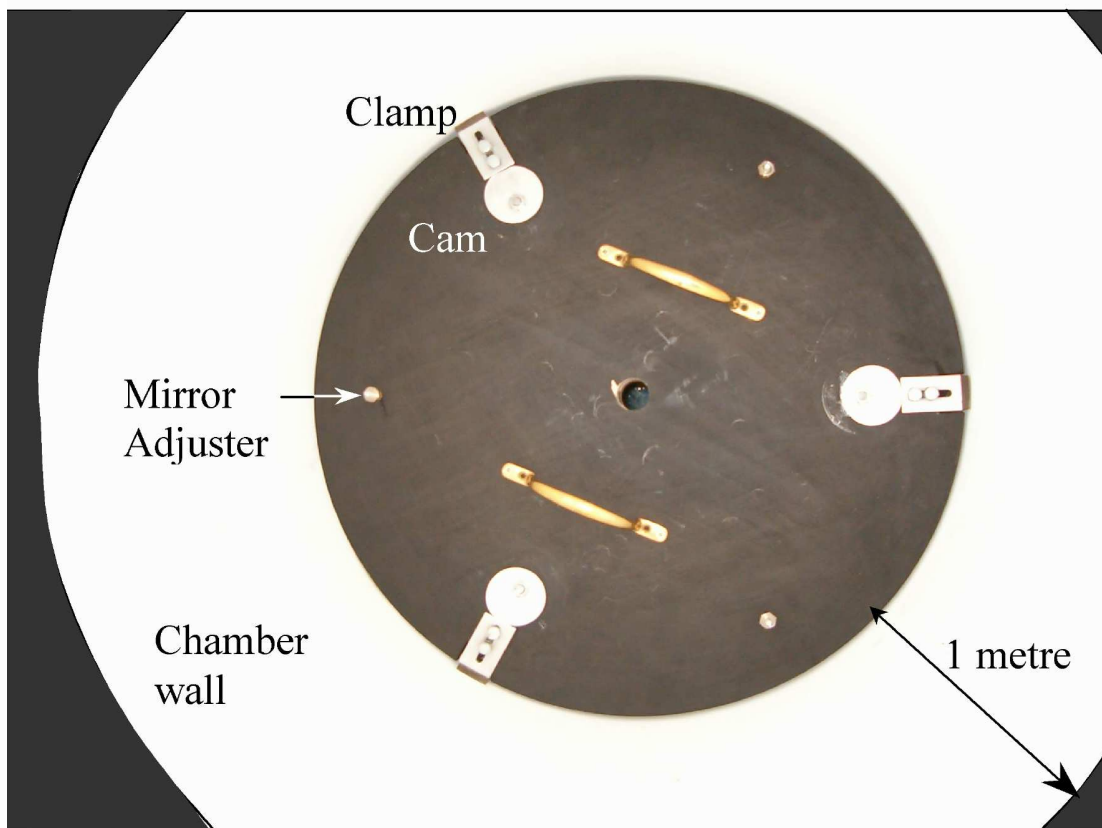
Figure 4-4

A rear view of the internal mirror mount, which was located inside the chamber. The mount was positioned a distance of 1 metre from the near end. Note how uniform the surrounding chamber brightness appears to the camera regardless of distance.

The chamber was constructed according to the following specifications:

Chamber Specifications

Chamber length:	$L = 2.0$ m	
Chamber diameter:	$2R = 0.57$ m	
Mirror reflectance, glass:	$f_{mg} = 0.86$ (see Appendix A)	
Mirror reflectance, Perspex:	$f_{mP} = 0.83$ (see Appendix A)	
Paint reflectance:	$f_p = 0.97$ (as specified by Plascon)	

Tolerances

Lamp centralization: ±1 mm

Mirror azimuth: negligible

Mirror position: ±2 mm

The mirror reflectance was determined empirically, as described in Appendix A. The value of paint reflectance that was used, is the value quoted by Plascon, the supplier of the paint.

Note that mirror azimuthal error could be eliminated by observing the curvature of the infinitely long virtual chamber through a peep-hole in the end mirror. The peep-hole edge results in multiple concentric circles presented at the centre of the remote mirror. If the mirrors are not orthogonal to the cylinder axis, the circles will be progressively offset from the centre, with increasing reflection order.

4.2.3 A First Discussion

If the light intensity due to an isolated lamp is measured at some arbitrary point in space, an indication of the lamp intensity may be obtained. Nothing, however, can be inferred about the total flux output from the lamp. Nor can the intensity at a point on the surface of the lamp be quantified.

Placing the lamp into a 4π reflective chamber enables the integration of light rays, and a measurement that includes contributions from all points on the lamp. For this purpose, a highly reflective and diffusive white surface (usually paint) must be applied to the inner surface of the chamber. The chamber forms a closed system, and if it can be characterized, it will produce information on the total light flux generated by the lamp.

To first order, the mathematical approach to model the cylindrical chamber, is to consider an infinitely long lamp with uniform surface intensity, located axially in an infinitely long chamber. In this case the light intensity at the chamber wall is easily calculated.

To approximate this situation for a realistic lamp of finite length, in a chamber of finite length, it is necessary to provide suitable surfaces at the ends of the chamber cylinder. For this purpose, in an initial trial setup, the chamber was provided with end walls that were coated with the same diffusive paint that was used for the cylinder walls.

Measurements on this system revealed that there were regions of extreme intensity near the edges of the cylinder. This complicates the analysis considerably, especially if the chamber end-walls are quite close together, as is the case when measuring lamp intensity profiles.

The system was therefore modified by replacement of the painted end-walls with specular mirrors, which has the following advantages:

1) With perfectly reflective mirrors placed at each end of the lamp, the chamber and lamp may be regarded as being made up of a real section of one lamp length, and two virtual sections of infinite length. The virtual lengthening of the system enhances the degree of integration of light, in the sense that any variation in intensity near the end of the real chamber, will be "smoothed out" by the neighboring virtual lamp and chamber, reflected by the mirror.

2) Mirrors are not diffusive, and the extremities will not form intense local zones.

3) Certain approximations may be applied with regard to the pseudo-infinite nature of the virtual zone of the chamber.

The use of mirrors resolved some problems, but introduced a new one: namely, the chamber was required to be exactly as long as the lamp, as otherwise the virtual lamp

would include undesirable repetitive gaps. In order to accommodate the various lamp-lengths available on the market, the chamber was constructed with a movable internal mirror, to facilitate adjustment of its length.

A real fluorescent lamp may not radiate perfectly uniformly along its entire length. The end-effect, due to proximity with the electrode (the so-called cathode fall), results in reduced intensity near the ends of the lamp. Variations in the thickness of the fluorescing medium throughout the lamp, result in corresponding variations in light output. However, the strong integrating potential of the chamber is expected to minimize the significance of these variations.

The fluorescent tube-lamp surface is engineered to be Lambertian to a large degree. In this model, the lamp fluorescent material has been assumed to exhibit a perfectly Lambertian surface, i.e. one that does not digress from cosine behavior, as the observation angle varies from $-\pi/2$ to $\pi/2$ radians, with respect to the surface norm.

However, a transmissive medium such as the fluorescent powder coating/ tube glass combination cannot be both transmissive and perfectly Lambertian, due to lamp internal reflection at large angles of ray incidence on the tube glass.

Furthermore, since the fluorescent powder coating is quite thin, photons passing through it are scattered less as the angle with the lamp surface norm decreases. The nett result is that the emission profile may lie intermediately between a Lambertian ($\cos\theta$) and a square cosine ($\cos^2\theta$) behavior. Deviation from Lambertian behavior will be more significant for larger angles of incidence, where $\cos^2\theta$ is maximally different from $\cos\theta$. At large angles, however, the proportion of flux contributed relative to the total flux, is small. Thus the deviation will be assumed as negligible.

An infinitely long *virtual* lamp will decrease in 'surface' intensity, with axial distance from its mid-point, since the reflectance of a mirror is always less than unity. The intensity within the chamber is therefore dependent on the length of the real lamp, and

hence also on the real chamber length. When the mirrors are very close together, a larger set of intervals must be summed to produce a meaningful result, so that the imperfect mirror reflectance becomes a more significant factor, and will therefore be included in calculations.

By comparison with an incandescent lamp, the emitting surface of a fluorescent tube is quite uniform, and the surface area is known. If there is a local bright spot, it is not expected to be very much brighter than the neighboring surface emission, due to the large tube surface area and general continuity of the fluorescing medium. Therefore a baffle was not required in the chamber.

The light arriving at a point on the chamber wall comes from the lamp, from the painted chamber wall, and end-mirrors. Due to multiple reflections, the calculation might be expected to involve a differential equation. However, the solution turns out to be a geometric series if it is assumed that the intensity does not vary along the real chamber wall. In reality, the mirrors cause a small monotonic variation in wall intensity from the centre to the end of the real chamber. A more detailed discussion will be given later.

For large angles of incidence, rear-coated mirrors reflect some light off the glass front surface, thereby slightly decreasing the effective distance between mirrors. Multiple reflections also occur between the opposite surfaces of a rear-coated glass or Perspex mirror, resulting in further absorption and scattering. This effect may need to be included in the solution when the mirrors are close together. Front-coated mirrors are ideal, but increased cost is a consideration.

The option of using non-reflecting surfaces for end-walls was considered for comparison with the situation involving mirrors. However, in this case, a large unknown proportion of light flux would be absorbed by the end-walls, and the degree of scattering would be greatly reduced, so that a measuring device will not produce an accurate indication of total flux.

5. Analysis of the Fluorescent Tube-lamp

5.1 Introduction

Various approaches to finding the light intensity around a tube-lamp were considered.
The lamp shape, being cylindrical, suggests the use of cylindrical coordinates in the
Cartesian system. However, the diffusivity and uniformity of the lamp surface suggest the
use of spherical coordinates, as will be shown. Some methodologies will now be
discussed.

5.2 Methodology

It might be supposed that the simplest approach to analyzing the light intensity around the
tubular lamp is to integrate the radiance over the surface of the lamp. The resulting
integral is, however, complicated by the angular dependence of the integrand. The
angular limits of the integral vary with the distance from the lamp, and the integral results
in compound fractions (an attempt to separate the integrand into partial fractions results
in separate integration terms which tend toward infinity as the distance from the point of
observation to the lamp is increased).

An alternative scheme is to represent the compound fractions as a series, but then
manipulation becomes extremely cumbersome.

A far easier method, reliant on the Lambertian nature of the lamp surface, was utilized. It
must first be observed that the flux from any elemental area on the lamp, projected into a
given solid angle subtended at a point P, is a constant (for a given local intensity of the
lamp). This applies irrespective of the shape of the emissive area, and is a direct
consequence of the Laplacian $\nabla^2 \Phi = 0$, which applies only to the radial component, since
the situation for the radial component emulates that of a conservative vector field, in the

Lambertian case; i.e. the flux density varies as cos θ, as for a vector field [14]. Figure 5-1 below shows the projection of the lamp onto a sphere surface.
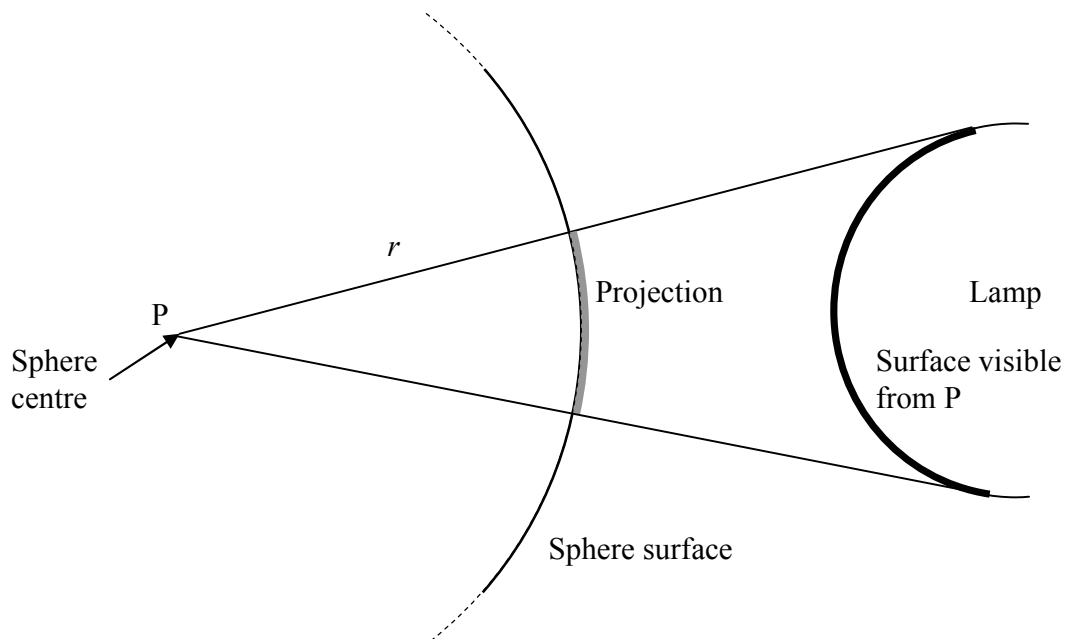
<u>Figure 5-1</u>

The projection of an area on a cylindrical lamp onto a sphere of radius r. The sphere is centered at an observation point P.

It will now be shown, using simple geometry, that the Lambertian surface intensity does indeed appear uniform to an observer at P, irrespective of the surface shape or its distance.

Point source rays

Increasing
point source
density
$\Phi \propto 1/\cos\theta$

Lamp surface

Decreasing
point source
intensity
$\Phi \propto \cos\theta$

θ
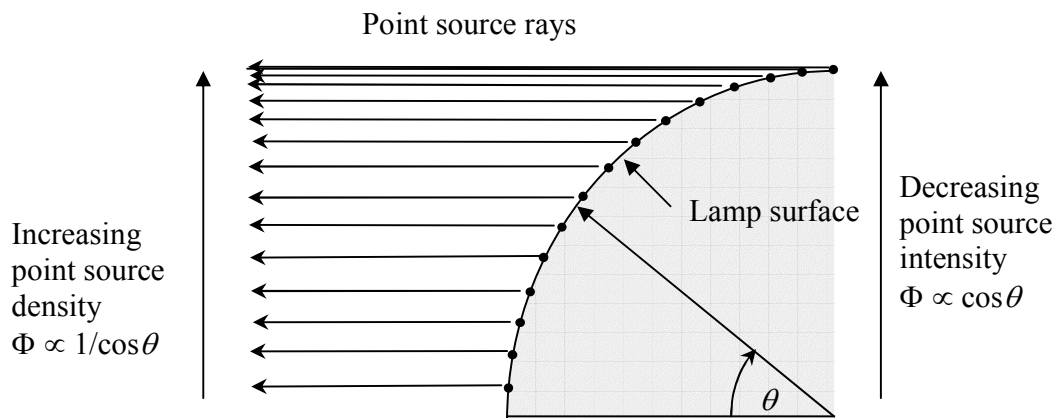
<u>Figure 5-2</u>

Light intensity as a function of position on the lamp surface, as observed from the direction
of a point P in space.

Referring to Figure 5-2 above, several point sources are displayed at even intervals along
a quadrant of the surface of the lamp. From the direction of observation, it can be seen
that the point source density increases with lateral distance from the lamp axis, i.e. with
increasing θ. In Figure 5-3, it can be seen that the lateral distance between two
consecutive point sources, as observed from the direction of a point P in space, is
proportional to $\cos\theta$. Now, the point source density is inversely proportional to the
distance separating them, i.e. $I \propto 1/\cos\theta$.
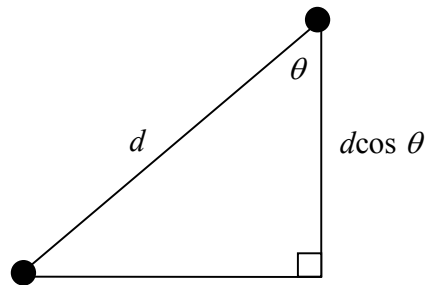
Figure 5-3

The lateral distance between two neighboring point sources. The distance d

is the separation between point sources. The lateral distance is affected by θ,

the angle between the surface norm and the direction of observation.

Now since the intensity of the point sources decreases as $\cos\theta$, and the density of the point sources increases as $1/\cos\theta$, with increasing θ, the proportionalities cancel each other out exactly, so that the light intensity does not vary with the shape of the lamp surface.

It must be stipulated here that any variation in the distance from point P to each respective point source has not yet been considered. However, as a consequence of the Laplacian again, the distance does not affect the calculations. For, consider an elemental area δa on the surface of two spheres of differing radii R and r respectively. Since the elemental areas are defined to be identical in size, we have $\phi_1 R^2 = \phi_2 r^2$ where ϕ_1 and ϕ_2 are the solid angles subtended at point P by the respective areas. Then $\phi_2 = \phi_1 R^2/r^2$, i.e. the solid angle is inversely proportional to the square of the distance of P from the source. Refer to Figure 5-4 below. The projected area becomes $\phi_2 R^2 = \phi_1 R^4/r^2 = \delta a\, R^2/r^2$ (by substitution). Thus it is shown that the area is proportional to $1/r^2$. The variation in elemental area therefore emulates the $1/r^2$ behavior of light intensity with distance r from the source.
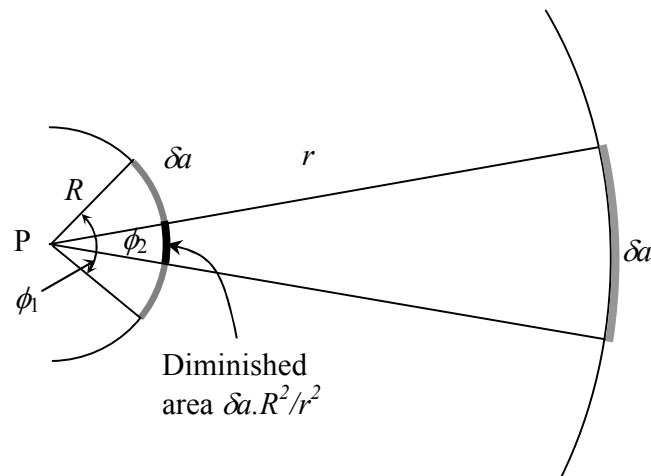
Figure 5-4

The variation of the size of the projection of an elemental area *da*

onto a solid sphere of radius *R*, with changing distance *r* of the source.

The easiest approach, therefore, is to integrate, using a fixed elemental solid angle, over the projection area of the lamp onto a spherical surface with centre focal point P, which will then yield the total flux from the lamp at P. Figure 5-5 below gives an indication of the shape of the projection to be expected from a cylindrical lamp.

Since the lamp surface is regarded as uniform, it is sufficient to project only the boundaries of the source onto the sphere, and then to calculate the area (on the sphere) inside these boundaries, using integral calculus. In the case of a cylindrical tube, the boundary turns out to be fairly simple, as shown in Section 5.2.2.

Although the lamp is cylindrical, it has been shown that the calculations are greatly simplified using projection onto a sphere. Therefore, considering that the boundary of the integral lies on a sphere, the calculations will use spherical coordinates, rather than cylindrical coordinates.
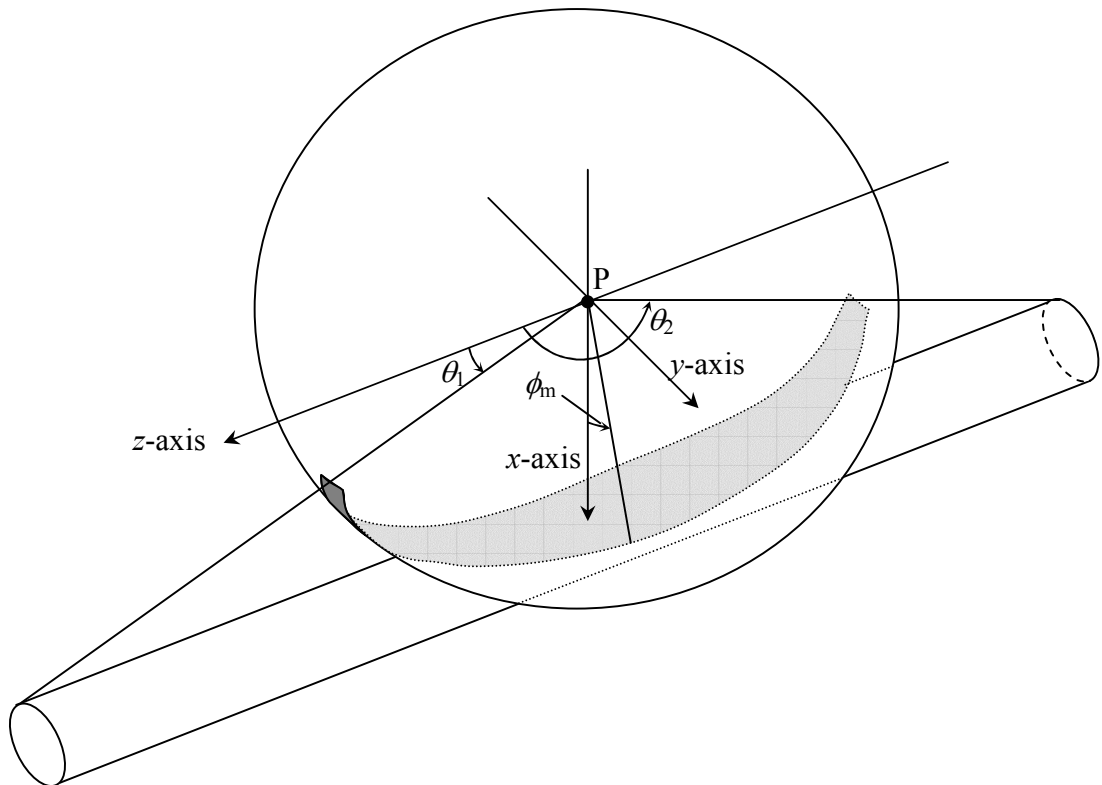
Figure 5-5

An example of the cylindrical projection of a finite-length lamp onto a sphere. The sphere is
centered at an observation point P. Note the use of spherical coordinates θ and ϕ. Here θ_1 and ϕ_m
correspond with the projection boundaries.

Once the equations describing light intensity at any point in space are obtained, a
computer program can be utilized to generate the isolines.

In summary:
The light intensity profile surrounding the lamp will be obtained using spherical
projection. The intensity of rays arriving at the chamber wall will be obtained by direct
integration of light arriving at the wall at P, from the lamp, and then summing over

multiple reflections from the walls and mirrors in the chamber. This summing will take the distance between the mirrors into account, as well as their reflectance.

5.3 The Finite-length Tube

The radiation profile of a finite length cylindrical lamp located in infinite space, i.e. without any reflecting surfaces, will be considered first. Following this treatment, the reflecting properties of a surrounding chamber will be included.

5.2.1 Requirements

There are a number of asymptotic requirements that need to be satisfied by the lamp equations.

- The maximum light intensity should be at the lamp surface.

- Light intensity should vary approximately as $1/r^2$ at distances $r \gg L$

- Close to the lamp, and near the middle, light intensity is assumed to vary approximately as $1/r$.

- Immediately above the lamp surface, light intensity is assumed to vary with r along the entire lamp length, except at the very ends.

- For a given distance r from the lamp, the flux density should be a maximum in the perpendicular plane that passes through the lamp axis centre.

- Due to the finite emissive boundary at either end of a realistic lamp, all isolines are expected to converge to each circular edge at either end of the emitting cylinder of the lamp, rather than meeting at the axis.

5.2.2 The Projection Sphere

It has been stated that Laplacian behavior applies to the radial component of a diffuse emitter. Thus it is only the boundary of the problem that needs to be known. It is necessary therefore to find the integral and its boundaries in terms of spherical coordinates, since the projection lies on a sphere, for simplicity.

Consider an observation point P in the vicinity of the lamp, as shown in Figures 5-5 above. The resulting surface on the projection sphere through which rays from the lamp pass, forms a wedge of constant arc ϕ in relation to the width of the lamp, and spans a range θ according the length of the lamp. In order to find the area of the bounded section, θ must be integrated from θ_1 to θ_2 while ϕ must be integrated from $-\phi_m$ to $+\phi_m$. The complementary angles α and β, as shown in Figure 5-6 below, will be useful in the derivations to follow.

The lamp equation will be an approximation since the projection of an end of the lamp onto the projection sphere will not be straight, as presented in Figure 5-7 below, but will be a convex curve. Figure 5-7 shows the end-effect for a longer lamp with an exaggerated diameter, (about four times that of a standard lamp) in order to enhance the effect.
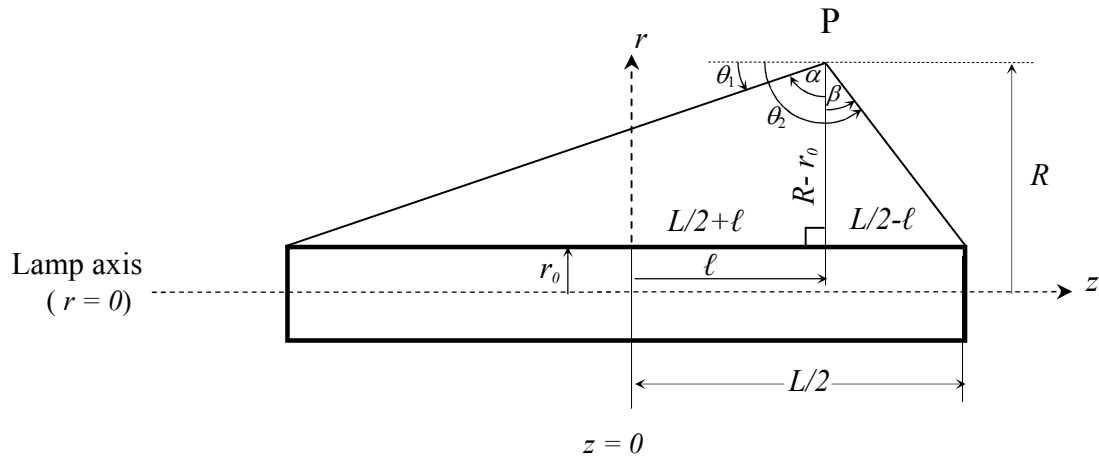
Figure 5-6

The geometry relating the position of the lamp to a point P in space. Length ℓ is the horizontal distance of P from the centre of the lamp. The horizontal distances from P to the left and right ends of the lamp are then $L/2+\ell$ and $L/2-\ell$ respectively. Upper-case R is used for the distance from the lamp axis to observation point P, since the variable will appear later as a parameter of the chamber.

The curvature of the end of the lamp, projected onto the sphere, is more pronounced for longer lamps. For a longer lamp, however, the end of the lamp will be further away from the observation point and hence the projection will be smaller, so that the error is less significant.

This end-effect will therefore be most pronounced where the distance R from the lamp axis is of similar order to L, the length of the lamp. As L increases from zero, the projected boundary due to each end of the lamp appears more curved. The distance between lateral boundaries on the projection sphere decreases, however, so that the error in the integral becomes zero as L tends toward infinity. Also, as L tends toward zero, the mentioned boundary tends toward a straight line, so that the error again tends toward zero.

The error due to the ends of the lamp also depends on the width of the lamp. The boundary due to each end of a very narrow lamp is projected as a relatively short curve on the projection sphere, while the total enclosed area is also small due to the narrower width of the lamp. It will be merely stated here that the error in area tends toward zero as the lamp width decreases. Wide fluorescent tubes are seldom encountered and will not be considered.
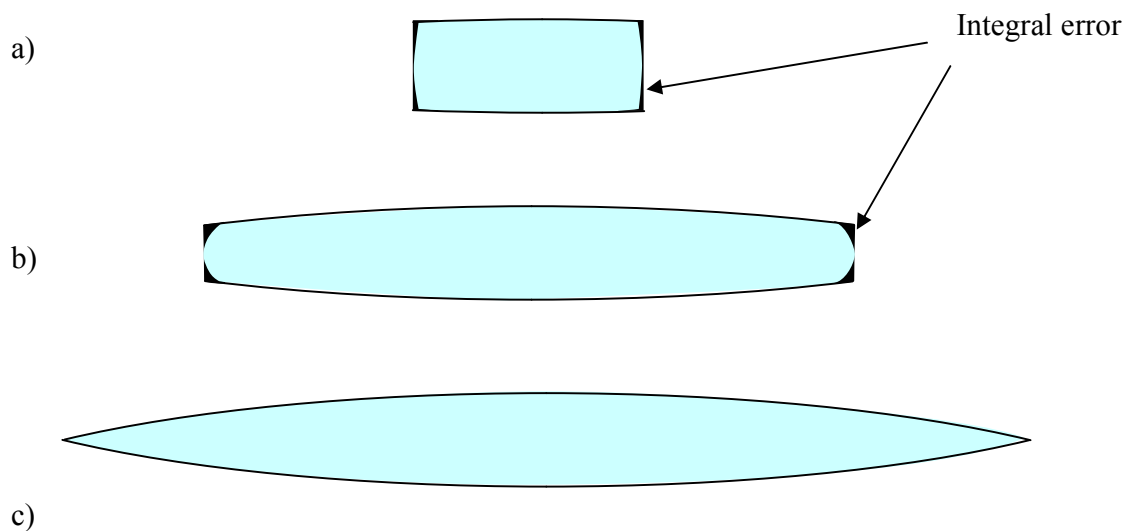
Figure 5-7

Some examples of boundary approximations for several lamp lengths. The area projected onto the sphere has been flattened out. Lamp radius is taken to be about 10% of the distance to the observation point P. The entire area is integrated, whereas the actual area should exclude the darkened sections in the diagram. a) The lamp length is similar to the observation distance. b) The lamp length is 5 times greater than the observation distance. c) The lamp length is infinite. Here there is no error.

5.2.3 The Lamp Equation

The error in projected area as seen in Figure 5-7 is small but noticeable. If necessary, an approximation for the error can be included in the model, but it has been concluded in the previous section that the errors will result in only very slight shifts of a small portion of the isolines. In the following analysis the end-effect will therefore be neglected.

Integration boundaries

Referring to Figure 5-8 below, the integration limit ϕ_m can be written in terms of R and r_0 as

$$\phi_m = \sin^{-1}\frac{r_0}{R}\,.$$
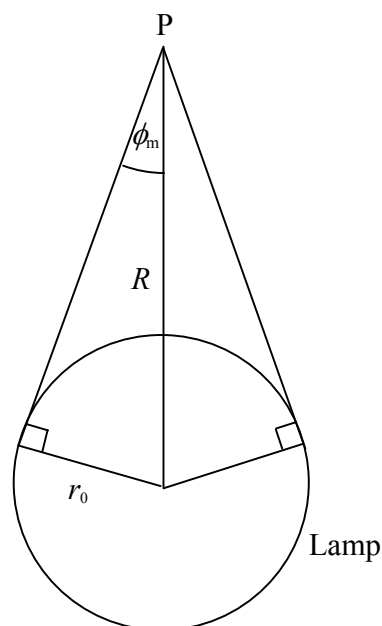
Figure 5-8

The geometry applicable to the lamp projection boundary ϕ_m.

R is the shortest distance from P to the lamp axis.

It is more convenient to express the limits of integration, θ_1 and θ_2, in terms of angles α and β, since they are included in the relevant triangles as shown in Figure 5-6 above.

We have

$$\left.\begin{aligned} \theta_1 &= \frac{\pi}{2} - \alpha \\[2em] \theta_2 &= \frac{\pi}{2} + \beta \end{aligned}\right\} \qquad (5.1)$$

.

The Integral

Let the lamp surface intensity be I_0 (in $W.m^{-2}$). Then there is a flux Φ_0 emitted from an area da. The Lambertian phenomenon distributes the flux Φ_0 over a hemisphere centered over da such that the intensity of a ray decreases as $\cos\theta$ with increasing angle θ of the ray, with respect to the surface norm. A ray in a direction perpendicular to the surface will have the maximum light intensity, which will be denoted as $I_\perp$. A perpendicular ray with this intensity is related to the surface intensity by $I_\perp = \frac{1}{\pi} I_0$ (refer to Appendix C for a proof). The intensity of a ray at an angle φ with the surface norm will then be

$$I(\varphi) = I_\perp \cos\varphi = \frac{1}{\pi} I_0 \cos\varphi .$$

The rays from the projection sphere to point P, projected in the radial direction, must be integrated. The axial component is not detected by a cosine-corrected light-sensor and will therefore not affect calculations.

The contribution from rays from an elemental area da on the projection sphere surface can be obtained in the radial direction by means of vector analysis. Let the vector from the center of the projection sphere to the bounded region be $\vec{\rho}$. Then the unit vector in Cartesian coordinates is

$$\hat{\boldsymbol{\rho}} = \left(\cos\phi\sin\theta, \sin\phi\sin\theta, \cos\theta\right)$$

where θ and ϕ are the variables of the spherical coordinate system. Note that the origin of the coordinate system is at point P, and for the sake of simplicity, point P is located on the x-axis. Therefore the radial direction from the lamps perspective is exactly opposite to the direction of the x-axis from the perspective of point P. Since the projection is not concerned about the sign of the vector, the unit vector $\hat{\mathbf{r}}$ is in this case equivalent to the x-axis unit vector i.e. (1, 0, 0). Thus the projection in the radial direction is

$$\hat{\boldsymbol{\rho}}\cdot\hat{\mathbf{r}} = \left(\cos\phi\sin\theta, \sin\phi\sin\theta, \cos\theta\right)\cdot\left(1,0,0\right)$$

$$= \cos\phi\sin\theta.$$

Therefore the contribution $\delta I_{\hat{\mathbf{r}}}$ to point P is

$$\delta I_{\hat{\mathbf{r}}}\left(R,\theta,\phi\right) = \frac{1}{\pi}I_0\frac{\sin\theta\cos\phi}{R^2}$$

Integration is performed over the projection area:

$$I_{\hat{\mathbf{r}}}\left(R,\ell\right) = \int_{-\phi_m}^{\phi_m}\int_{\theta_1}^{\theta_2}\delta I_{\hat{\mathbf{r}}}\left(\theta,\phi\right)R^2\sin\theta\, d\theta\, d\phi,$$

Therefore,

$$I_{\hat{\mathbf{r}}}\left(R,\ell\right) = \frac{1}{\pi}I_0\int_{-\phi_m}^{\phi_m}\cos\phi\, d\phi\int_{\theta_1}^{\theta_2}\sin^2\theta\, d\theta$$

$$= \frac{1}{\pi} I_0 \cdot 2 \sin \phi_m \cdot \frac{1}{2} \left(\theta - \sin \theta \cos \theta \right) \Big|_{\theta_1}^{\theta_2}$$

$$= \frac{1}{\pi} I_0 \sin \phi_m \cdot \left(\theta_2 - \theta_1 + \sin \theta_1 \cos \theta_1 - \sin \theta_2 \cos \theta_2 \right).$$

Substituting from equations (5.1) yields

$$I_{\hat{\mathbf{r}}} \left(R, \ell \right) = \frac{1}{\pi} I_0 \sin \phi_m \cdot \left[\alpha + \beta + \sin \left(\frac{\pi}{2} - \alpha \right) \cos \left(\frac{\pi}{2} - \alpha \right) - \sin \left(\frac{\pi}{2} + \beta \right) \cos \left(\frac{\pi}{2} + \beta \right) \right].$$

$$= \frac{1}{\pi} I_0 \sin \phi_m \cdot \left(\alpha + \beta + \cos \alpha \sin \alpha + \cos \beta \sin \beta \right) \tag{5.2}$$

by trigonometric reduction.

The variables α and β are more meaningfully expressed in terms of L, ℓ, R, and r_0. From the relevant triangles in Figure 5-6,

$$\tan \alpha = \frac{\frac{L}{2} + \ell}{R - r_0},$$

and

$$\tan \beta = \frac{\frac{L}{2} - \ell}{R - r_0}.$$

Hence

$$\alpha = \tan^{-1} \frac{\frac{L}{2} + \ell}{R - r_0},$$

and

$$\beta = \tan^{-1} \frac{\frac{L}{2} - \ell}{R - r_0}$$

(5.3)

.

The functions $\sin \alpha$, $\cos \alpha$, $\sin \beta$, and $\cos \beta$ must also be expressed in terms of the variable mentioned above.

Let $y = \sin\left(\tan^{-1} x\right)$. See Figure 5-9 below.
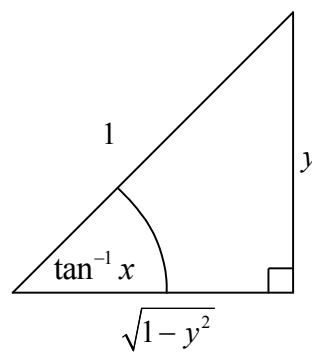
Figure 5-9

A sketch showing trigonometric ratios for $y = \sin(\tan^{-1} x)$.

Then

$$\tan(\tan^{-1} x) = x = \frac{y}{\sqrt{1 - y^2}}$$

i.e.

$$x^2 \left(1 - y^2\right) = y^2$$

$$\Rightarrow y^2 \left(x^2 + 1\right) = x^2$$

$$\Rightarrow y = \frac{x}{\sqrt{x^2+1}} \; .$$

Therefore,

$$\sin \beta = \sin \tan^{-1} \frac{\frac{L}{2}-\ell}{R-r_0} = \frac{\frac{\frac{L}{2}-\ell}{R-r_0}}{\sqrt{\left(\frac{\frac{L}{2}-\ell}{R-r_0}\right)^2 + 1}}$$

i.e.
$$\sin \beta = \frac{\frac{L}{2}-\ell}{\sqrt{\left(\frac{L}{2}-\ell\right)^2 + \left(R-r_0\right)^2}} \; . \tag{5.4}$$

Dimensionless units are preferred in computation. Let $\rho = \dfrac{R}{r_0}$, $s = \dfrac{\ell}{r_0}$ and $s' = \dfrac{L/2}{r_0}$.

Then

$$\sin \beta = \frac{s'-s}{\sqrt{\left(s'-s\right)^2 + \left(\rho-1\right)^2}} \; . \tag{5.5}$$

Similarly,

$$\sin \alpha = \frac{s'+s}{\sqrt{\left(s'+s\right)^2 + \left(\rho-1\right)^2}} \; . \tag{5.6}$$

Now let $y = \cos\left(\tan^{-1} x\right)$. Then $\tan(\tan^{-1} x) = x = \dfrac{\sqrt{1-y^2}}{y}$ in a similar manner, yielding

$$y = \frac{1}{\sqrt{x^2 + 1}} \, .$$

Therefore,

$$\cos \beta = \cos \tan^{-1} \frac{\dfrac{L}{2} - \ell}{R - r_0} = \frac{1}{\sqrt{\left(\dfrac{\dfrac{L}{2} - \ell}{R - r_0} \right)^2 + 1}}$$

$$= \frac{R - r_0}{\sqrt{\left(\dfrac{L}{2} - \ell \right)^2 + \left(R - r_0 \right)^2}}$$

or,
$$\cos \beta = \frac{\rho - 1}{\sqrt{\left(s' - s \right)^2 + \left(\rho - 1 \right)^2}} \tag{5.7}$$

and

$$\cos \alpha = \frac{\rho - 1}{\sqrt{\left(s' + s \right)^2 + \left(\rho - 1 \right)^2}} \, . \tag{5.8}$$

Also,

$$\phi_{\mathrm{m}} = \sin^{-1} \frac{r_0}{R} = \sin^{-1} \frac{1}{\rho} \, . \tag{5.9}$$

Substituting equations (5.3) up to (5.9) into equation (5.2) and simplifying,

$$I_{\hat{r}} = \frac{1}{\pi} I_0 \frac{r_0}{R} \left(\tan^{-1} \frac{\frac{L}{2} - \ell}{R - r_0} + \tan^{-1} \frac{\frac{L}{2} + \ell}{R - r_0} + \frac{\frac{L}{2} - \ell}{\sqrt{\left(\frac{L}{2} - z\right)^2 + (R - r_0)^2}} \frac{R - r_0}{\sqrt{\left(\frac{L}{2} - z\right)^2 + (R - r_0)^2}} \right.$$

$$\left. + \frac{\frac{L}{2} + \ell}{\sqrt{\left(\frac{L}{2} + z\right)^2 + (R - r_0)^2}} \frac{R - r_0}{\sqrt{\left(\frac{L}{2} + z\right)^2 + (R - r_0)^2}} \right)$$

$$= \frac{1}{\pi} I_0 \frac{r_0}{R} \left(\tan^{-1} \frac{\frac{L}{2} - \ell}{R - r_0} + \tan^{-1} \frac{\frac{L}{2} + \ell}{R - r_0} + \frac{\left(\frac{L}{2} - \ell\right)(R - r_0)}{\left(\frac{L}{2} - \ell\right)^2 + (R - r_0)^2} + \frac{\left(\frac{L}{2} + \ell\right)(R - r_0)}{\left(\frac{L}{2} + \ell\right)^2 + (R - r_0)^2} \right).$$

In the defined dimensionless units,

$$I_{\hat{r}}(s, \rho) = \frac{1}{\pi} I_0 \frac{1}{\rho} \left(\tan^{-1} \frac{s' - s}{\rho - 1} + \tan^{-1} \frac{s' + s}{\rho - 1} + \frac{(s' - s)(\rho - 1)}{(s' - s)^2 + (\rho - 1)^2} + \frac{(s' + s)(\rho - 1)}{(s' + s)^2 + (\rho - 1)^2} \right) \quad (5.10)$$

This is the solution, in the radial direction, to the integral representing the light intensity surrounding the fluorescent tube-lamp.

5.2.4 Graphical Results

A program was written in the IDL language specifically for the purpose of plotting the light intensity surrounding the lamp, using equation (5.10). See Figure 5-10 below. Each successive isoline is selected to be one half of the flux density of the preceding line. Since an empirical formula for the isoline has not been obtained, the computer program was required to compute the position of a set intensity level. This was achieved by sweeping over a two-dimensional grid surrounding the lamp.
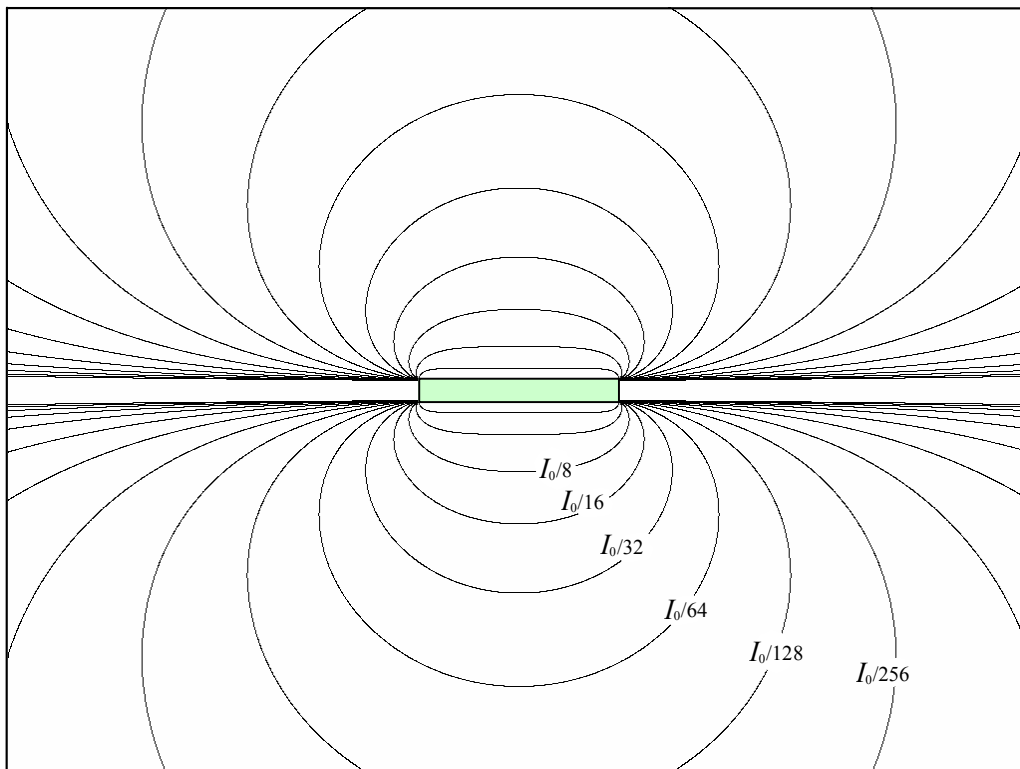
Figure 5-10

A spatial contour-plot of lines of equal light intensity in the radial direction for the fluorescent tube-lamp. Each consecutive isoline represents half of the flux density of the previous line with recession from the lamp. The mathematical model used here has a lamp length that is ten times larger than the lamp diameter. Note that the shaded area represents the lamp, while the areas to the left and to the right of the lamp are the shadowed regions.

An alternative plot was also generated using a colour-table in order to assist in visualization of the solution. The equation (5.10) was applied to calculate the light intensity over a rectangular grid using a program written by the author in the IDL language. The colour-scale was selected for enhanced visualization of the field. Figure 5-11 shows the result. The colour of each pixel represents the magnitude of the light intensity at that point in space.
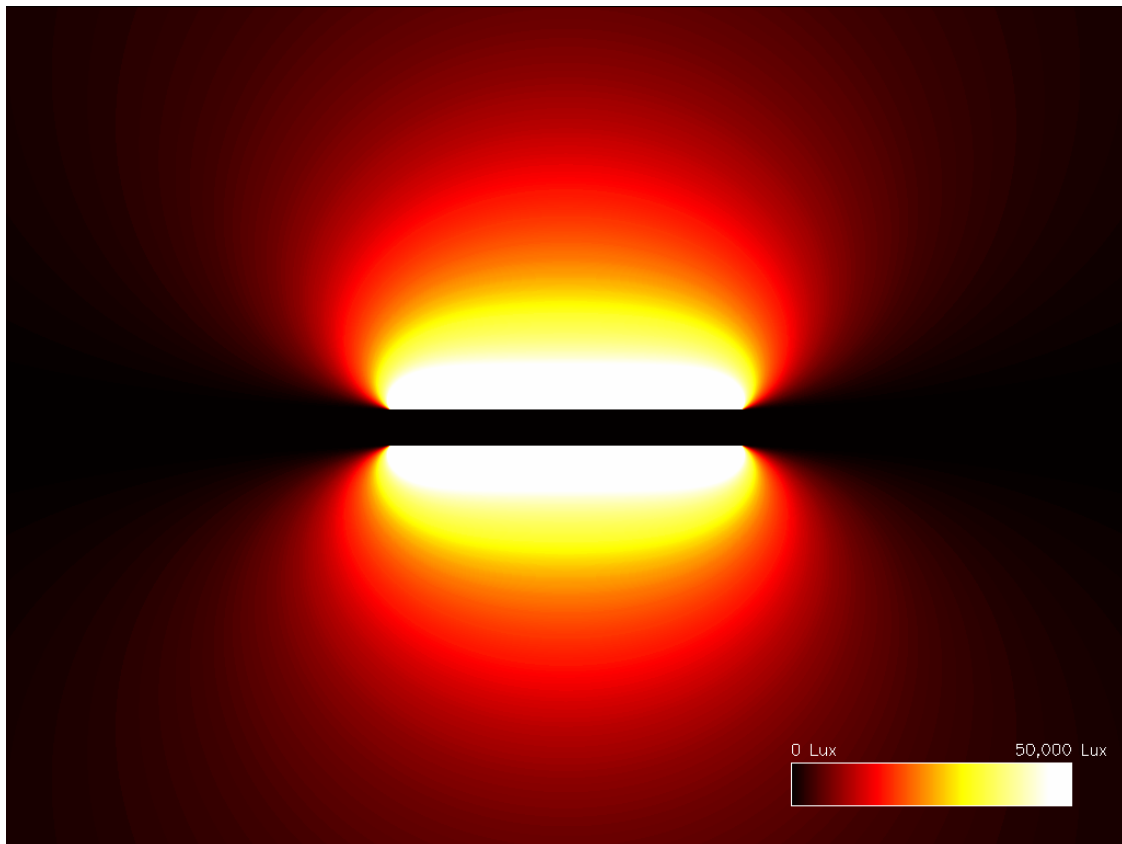
Figure 5-11

A spatial light intensity plot for the fluorescent tube-lamp. The colours are mapped to the values of the light intensity according to the colour-bar shown.

5.2.5 Equation Analysis

The location of observation point P can be varied over a plane that includes the lamp axis, and light intensity can then be determined as a function of position. The quantity ℓ (the z-component of the vector $\vec{r}$ of the observation point P) will be replaced by z from here on since it becomes a variable of the analysis, and is not a fixed value.

The required dimensionless variables are listed here for the sake of clarity.

s: the z-coordinate of P.

s': the z-coordinate of the right end of the lamp. Thus the lamp length is $2s'$.

ρ: the radius of the chamber.

A point halfway between the ends of the lamp will be investigated, since a lamp is usually installed directly over the subject of illumination. With $s = 0$, equation (5.10) becomes

$$I_{\hat{r},\text{lamp}}(\rho)\Big|_{s=0} = \frac{1}{\pi} I_0 \frac{1}{\rho} \left(\tan^{-1} \frac{s'-s}{\rho-1} + \tan^{-1} \frac{s'+s}{\rho-1} + \frac{(s'-s)(\rho-1)}{(s'-s)^2 + (\rho-1)^2} + \frac{(s'+s)(\rho-1)}{(s'+s)^2 + (\rho-1)^2} \right)\Bigg|_{s=0}$$

$$= \frac{1}{\pi} I_0 \frac{1}{\rho} \left(\tan^{-1} \frac{s'}{\rho-1} + \tan^{-1} \frac{s'}{\rho-1} + \frac{s'(\rho-1)}{s'^2 + (\rho-1)^2} + \frac{s'(\rho-1)}{s'^2 + (\rho-1)^2} \right)$$

$$= \frac{1}{\pi} I_0 \frac{1}{\rho} \left(2\tan^{-1} \frac{s'}{\rho-1} + 2\frac{s'(\rho-1)}{s'^2 + (\rho-1)^2} \right)$$

$$= \frac{2}{\pi} I_0 \frac{1}{\rho} \left(\tan^{-1} \frac{s'}{\rho-1} + \frac{s'(\rho-1)}{s'^2 + (\rho-1)^2} \right).$$

It is of interest to analyze the profile close to the lamp surface. Set the observation point P close to the lamp but not too close to the ends, such that the distance to the lamp is much less than the lamp length i.e. $R \ll L$ with $R \sim r_0$ ($\Rightarrow \rho \sim 1$). In order to avoid the end effect, assume that the distance to the lamp surface is much less than the distance to the lamp end i.e. $L/2 - |z| \gg R - r_0$ ($\Rightarrow |s' - s| \gg \rho - 1$ and $|s' + s| \gg \rho - 1$).

$$I_{\hat{r},\text{lamp}}\left(s,\rho\right)\Big|_{\rho\sim 1} = \frac{1}{\pi}I_0\frac{1}{\rho}\left(\tan^{-1}\frac{s'-s}{\rho-1}+\tan^{-1}\frac{s'+s}{\rho-1}+\frac{\left(s'-s\right)\left(\rho-1\right)}{\left(s'-s\right)^2+\left(\rho-1\right)^2}+\frac{\left(s'+s\right)\left(\rho-1\right)}{\left(s'+s\right)^2+\left(\rho-1\right)^2}\right)\Bigg|_{\rho\sim 1}$$

$$\approx \frac{1}{\pi}I_0\frac{1}{\rho}\left(\frac{\pi}{2}+\frac{\pi}{2}+\frac{\left(s'-s\right)\left(\rho-1\right)}{\left(s'-s\right)^2}+\frac{\left(s'+s\right)\left(\rho-1\right)}{\left(s'+s\right)^2}\right)$$

$$= \frac{1}{\pi}I_0\frac{1}{\rho}\left(\pi+\frac{\rho-1}{s'-s}+\frac{\rho-1}{s'+s}\right)$$

$$\approx \frac{1}{\pi}I_0\frac{1}{\rho}\left(\pi\right)$$

$$= I_0\frac{r_0}{R}.$$

Note that the light intensity varies with R as $1/R$ close to the surface of a long cylindrical lamp.

On the other hand, if the observation point P is far from the lamp surface, such that $R \gg L$ ($\Rightarrow \rho \gg s'$), the analysis must be separated into two regions for the radial component, as follows. Refer to Figure 5-12 below.

1) Region 1 *between* the ends of the lamp with $-L/2 < z < L/2$ ($\Rightarrow -s' < s < s'$).
2) Region 2 *beyond* the ends of the lamp with $|z| > L/2$ ($\Rightarrow |s| > s'$)
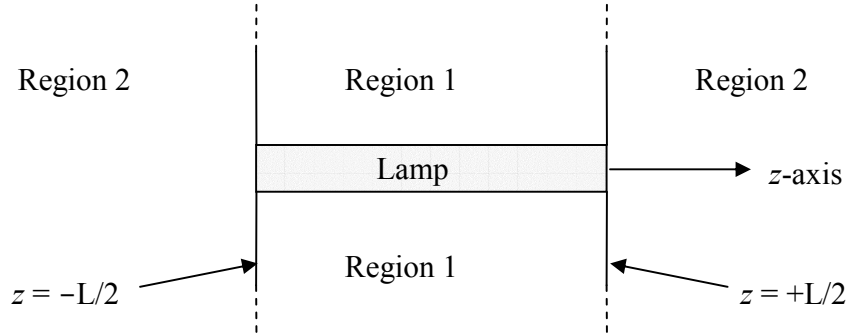
Figure 5-12

Regions in space defined for analysis of light intensity surrounding the tube-lamp

Region 1: $-s' < s < s'$

$$I_{\hat{\mathbf{r}},\text{lamp}}\Big|_{|s|<s'} = \frac{1}{\pi} I_0 \frac{1}{\rho}\left(\tan^{-1}\frac{s'-s}{\rho-1} + \tan^{-1}\frac{s'+s}{\rho-1} + \frac{(s'-s)(\rho-1)}{(s'-s)^2+(\rho-1)^2} + \frac{(s'+s)(\rho-1)}{(s'+s)^2+(\rho-1)^2} \right)\Bigg|_{|s|<s'}$$

$$\approx \frac{1}{\pi} I_0 \frac{1}{\rho}\left(\frac{s'-s}{\rho-1} + \frac{s'+s}{\rho-1} + \frac{(s'-s)(\rho-1)}{(\rho-1)^2} + \frac{(s'+s)(\rho-1)}{(\rho-1)^2} \right)$$

$$= \frac{1}{\pi} I_0 \frac{1}{\rho}\left(2\frac{s'}{\rho-1} + \frac{s'-s}{\rho-1} + \frac{s'+s}{\rho-1} \right)$$

$$= \frac{4}{\pi} I_0 s' \frac{1}{\rho(\rho-1)}$$

$$\approx \frac{4}{\pi} I_0 s' \frac{1}{\rho^2}$$

$$= \frac{4}{\pi} I_0 s' \frac{r_0^2}{R^2}$$

The result is at least valid for a point P between the ends of, but not close to, the lamp.

Region 2: $|s| > s'$

The previous result is actually also valid if P is not too far beyond the ends of the lamp.
The condition $\frac{s' + |s|}{\rho - 1} \ll 1$ must be upheld. If $s' + |s|$ is not small, the tan^{-1} function will
come into play and complicate the analysis. In any case, the extreme lateral regions are of
little concern with typical usage of a cylindrical fluorescent lamp.

Boundary conditions should also be checked: On the surface of the lamp i.e. if $R = r_0$,
intensity is expected to be constant. However, beyond the length of the lamp there is
obviously no lamp surface. There must then be a discontinuity at $z = \pm L/2$.
An examination of the solution reveals that the equation is undefined at the point $R = r_0$
and $z = \pm L/2$.

On the lamp surface, where $R = r_0$ and $|z| \neq \frac{L}{2}$ i.e. with $\rho = 1$ and $-s' < s < s'$, the radial
component is

$$I_{\hat{r}, \rho = 1} = \frac{1}{\pi} I_0 \frac{1}{1} \left(\tan^{-1} \frac{s' - s}{1 - 1} + \tan^{-1} \frac{s' + s}{1 - 1} + \frac{(s' - s)(1 - 1)}{(s' - s)^2 + (1 - 1)^2} + \frac{(s' + s)(1 - 1)}{(s' + s)^2 + (1 - 1)^2} \right)$$

$$= \frac{1}{\pi} I_0 \left(\frac{\pi}{2} + \frac{\pi}{2} + 0 + 0 \right)$$

$$= I_0 .$$

Thus it is shown that the solution yields the correct boundary conditions.

The lamp equation (equation (5.10) will now be reduced to that of a line-source in order to check validity in the limit, as the lamp radius tends to zero.

The line-source intensity has units of flux-per-unit-length rather than flux-per-unit-area; i.e. $I_\ell = I_0.r_0$. The surface area of the lamp is zero, so that the line lamp has an infinite "surface" intensity. But r_0 simultaneously has a value of zero, so that $I_0.r_0$ is undefined. In the limit as is $r_0 \to 0$, $I_0.r_0$ becomes the line intensity I_t. As the lamp radius tends to zero, the radial component becomes

$$I_{\hat{r},\text{line}} = \lim_{r_0 \to 0} I_{\hat{r}}$$

$$= \lim_{r_0 \to 0} \left\{ \frac{1}{\pi} I_0 \frac{r_0}{R} \left(\tan^{-1} \frac{\frac{L}{2}-z}{R-r_0} + \tan^{-1} \frac{\frac{L}{2}+z}{R-r_0} + \frac{\left(\frac{L}{2}-z\right)(R-r_0)}{\left(\frac{L}{2}-z\right)^2 + (R-r_0)^2} + \frac{\left(\frac{L}{2}+z\right)(R-r_0)}{\left(\frac{L}{2}+z\right)^2 + (R-r_0)^2} \right) \right\}$$

i.e.

$$I_{\hat{r},\text{line}} = \frac{1}{\pi} I_\ell \frac{1}{R} \left(\tan^{-1} \frac{\frac{L}{2}-z}{R} + \tan^{-1} \frac{\frac{L}{2}+z}{R} + \frac{\left(\frac{L}{2}-z\right)R}{\left(\frac{L}{2}-z\right)^2 + R^2} + \frac{\left(\frac{L}{2}+z\right)R}{\left(\frac{L}{2}+z\right)^2 + R^2} \right) \quad (5.11)$$

The light intensity of an infinitely long line source is expected to decrease with R as $1/R$ since it is only a one-dimensional system. This should follow from equations (5.11) above: After setting $z = 0$, equation (5.11) becomes

$$I_{\hat{r},\text{line}} = \frac{1}{\pi} I_\ell \frac{1}{R} \left(\tan^{-1} \frac{\frac{L}{2}}{R} + \tan^{-1} \frac{\frac{L}{2}}{R} + \frac{\left(\frac{L}{2}\right)R}{\left(\frac{L}{2}\right)^2 + R^2} + \frac{\left(\frac{L}{2}\right)R}{\left(\frac{L}{2}\right)^2 + R^2} \right)$$

As $L \to \infty$ for a line source,

$$I_{\hat{\mathbf{r}}, \text{line}} \to \frac{1}{\pi} I_\ell \frac{1}{R} \left(\frac{\pi}{2} + \frac{\pi}{2} + \frac{R}{\frac{L}{2}} + \frac{R}{\frac{L}{2}} \right)$$

$$= \frac{1}{\pi} I_\ell \frac{1}{R} (\pi + 0) \qquad\qquad \{\text{since } L \to \infty\}$$

$$= \frac{I_\ell}{R}$$

in agreement with expectations.

If the line lamp length is very small compared with the distance of the observation point P, i.e. $L \ll R$, then the lamp should behave as a point source. Due to the shape of the lamp, however, isotropic point source behavior cannot be expected. Thus the analysis will be carried out at $z = 0$.

$$I_{\hat{\mathbf{r}}, \text{line}} (R)\Big|_{z=0} = \frac{1}{\pi} I_\ell \frac{1}{R} \left(\tan^{-1} \frac{\frac{L}{2}}{R} + \tan^{-1} \frac{\frac{L}{2}}{R} + \frac{\left(\frac{L}{2}\right) R}{\left(\frac{L}{2}\right)^2 + R^2} + \frac{\left(\frac{L}{2}\right) R}{\left(\frac{L}{2}\right)^2 + R^2} \right)$$

$$\approx \frac{1}{\pi} I_\ell \frac{1}{R} \left(\frac{L}{2R} + \frac{L}{2R} + \frac{L}{2R} + \frac{L}{2R} \right)$$

$$= \frac{2}{\pi} I_\ell L \frac{1}{R^2} .$$

The light intensity of a short line lamp varies with R as $1/R^2$, far from the source. The line source therefore increasingly approximates a point source, as the distance from the source increases.

It has been shown that the light intensity surrounding a cylindrical fluorescent lamp can be quantified using reasonable approximations. The result, equation (5.2), will be used in the next chapter to obtain the flux on the chamber wall due to a cylindrical lamp.

6. Analysis of the Cylindrical Integrating Chamber

6.1 Introduction

Projecting the chamber cylinder internal wall onto an internal sphere, as was done in Chapter 5 for a lamp, yields a complicated equation, due to the shape of the projection boundary. The infinitely long virtual chamber, brought about by the mirrors, comprises sections of different orders of f, the mirror reflectance, so that each interval must be integrated separately. Each circular interval edge projects an elliptical boundary onto the projection sphere, which varies in dimensions with progress through the intervals. Analysis of each boundary would therefore be tedious.

Rather, the first method discussed in Section 5.1 was used; i.e. integration was employed over the surface of a chamber interval. The angular part of the integral in this case ranges over a full circle, with the result that double integration is greatly simplified.

The end-mirrors were taken into account by multiplying each successive interval by a further mirror reflection coefficient f. If many intervals were necessary in the calculation i.e. if the interval was small, a computer program was used to calculate the final result, using repetition. The results were then applied to an equation that determines the total lamp flux.

The Monte Carlo method

Another way to find a solution is to use the Monte Carlo method. In this method the chamber is divided into a grid of equal (small) areas (or cells) and a photon from a random point on the lamp is projected in a random direction with a Lambertian (angular) weight. When the photon strikes a surface it is reflected with a probability equal to the reflectance f. For the sake of simplifying the Monte Carlo model, the energy of the

photon can be 'reduced' by multiplying by the reflectance coefficient f, and be re-projected in a random direction again with the Lambertian weighting. After many reflections, an event can be set at which the photon energy has 'expired'. Each grid-cell accumulates the absorbed probability from photons striking it. After many photon emissions from the lamp, a plot of the grid-cell contents will reveal the light profile. The method is not machine-efficient, but accuracy is proportional to computation time.

6.2 Physical Concepts

The light intensity incident at a point on the chamber wall is the sum of contributions of light from all other points of the wall, as well as from the near side of the lamp. The contribution from the mirrors will be regarded as an extension of the chamber, as well as of the cylindrical lamp.

The high paint reflectance ($f_p = 0.97$) causes the majority of photons to "bounce back" into the chamber, thereby resulting in multiple reflections, which significantly boost the measured light intensity at the surface. This is a favorable effect for measurement since then the light level is well above the lower sensitivity threshold of the light-meter.

Theoretically, a chamber with 100% reflective paint and mirrors will produce an ever increasing intensity on any surface within the chamber, with time, as the energy generated by the lamp, collects within the chamber. In reality this situation would not occur because of energy losses, due to heat dissipation. In fact, the heat dissipated by the chamber walls must be exactly equal to the power of the lamp. In Appendix B, the power density of the chamber wall is calculated for a standard lamp, in order to gain a knowledge of the heat requirements of the paint.

The lamp and chamber may be considered as being made up of a real and a virtual part with the aid of mirrors. The virtual part consists of intervals to infinity, identical except for a progressively increasing attenuation coefficient, as reflection order increases. See

Figure 6-1 and Figure 6-2. Each successive image is a result of a further reflection of the image in the previous interval, so that the attenuation coefficient must be multiplied by a further reflection coefficient f.
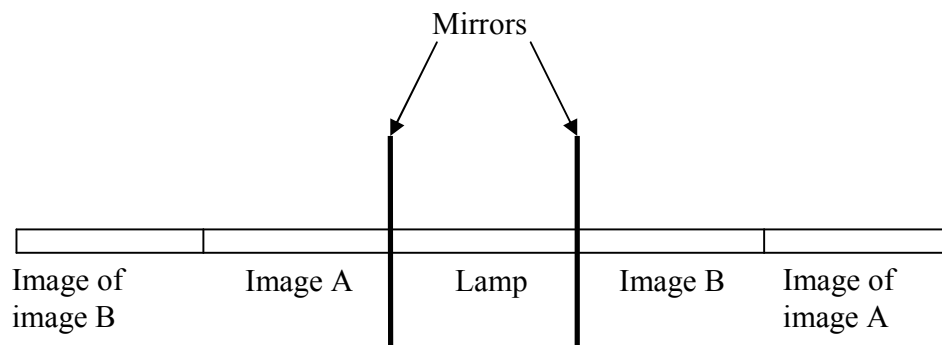
Figure 6-1

An example of the lamp image distribution of virtual sections of the chamber.
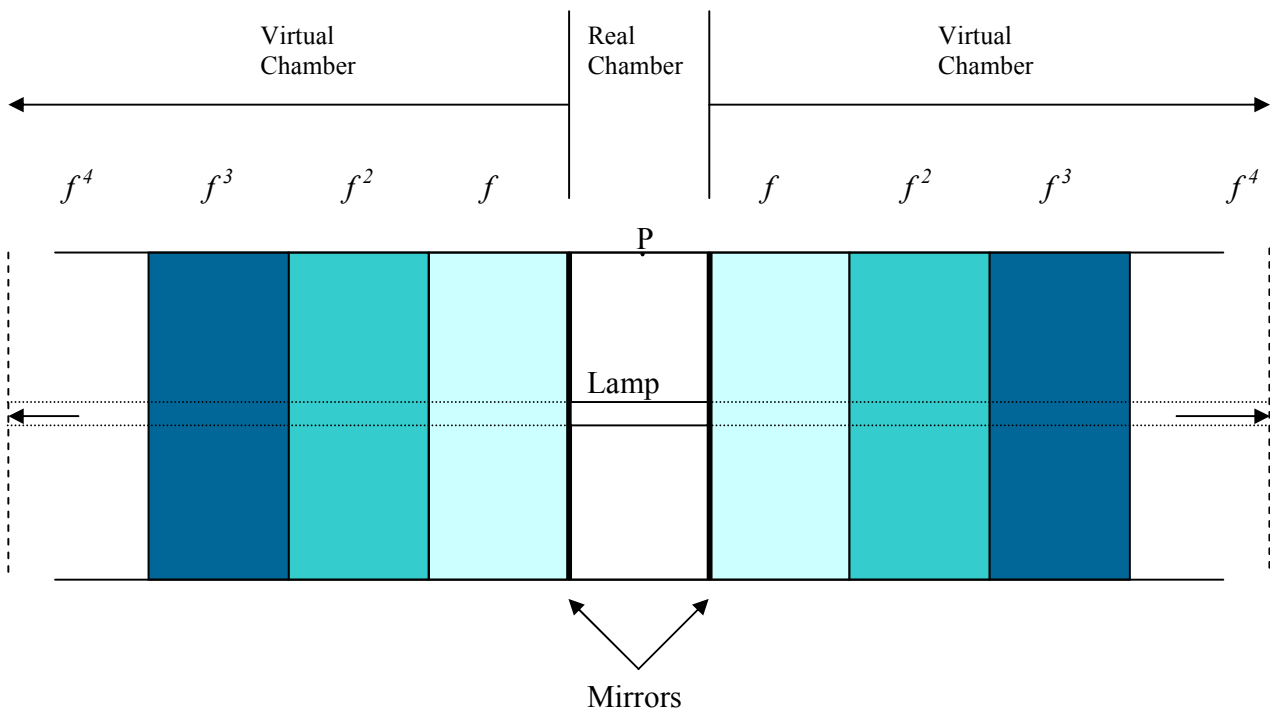
Figure 6-2

The real region of the chamber and the first few virtual intervals.

As an example, for a Perspex mirror, at the 50th interval, light which has been reflected 50 times will be attenuated by a factor of $(f_m)^{50} = (0.83)^{50} = 9 \times 10^{-5}$.

An equation for light intensity at a point P on the real chamber surface, due to reflection from a section of the chamber, was first deduced mathematically, and the result applied to a pseudo-infinite chamber i.e. one with mirrors of reflectance $f < 1$ (various physical assumptions were necessary at this point). Multiple reflections were then taken into account.

6.2.1 Assumptions

1) **The intensity is uniform over the entire chamber surface.** When multiple reflections due to end-mirrors are taken into account, there will be a slight degradation of intensity from the centre to the chamber end. At the centre of the chamber, light comes predominantly from the real chamber, while near an end-mirror the proportion of the light arriving on the sensor from one side is reduced in intensity by a factor of the mirror reflectance compared with the other side.

If the real chamber is very long it will approximate an infinitely long chamber and the influence of the mirrors on the light profile will be minimal. If the chamber is short the virtual intervals will be close together and the average angular position of the real chamber about an axis through the sensor does not vary significantly if the sensor is moved from the chamber centre toward an end-mirror.

It is the mid-range lengths (of the order of the diameter of the chamber, ~ 0.6 m for the chamber constructed for this project) that bring about the largest deviations. However, when multiple reflections are included, it would seem that after each reflection the deviation becomes worse. But the Lambertian nature of the real chamber has not been considered. A high degree of scattering in the real chamber drastically reduces the deviation. Therefore proportional representation of each side of the chamber may be taken as equal irrespective of sensor placement.

2) **The reflective paint is applied uniformly.** For this model paint was applied with a brush, with little guarantee of consistency of thickness or uniformity. However, it is expected that the large degree of scattering will reduce its significance. Measurements were interpreted with the assumption that the paint layer is perfectly uniform.

3) **The reflective paint is Lambertian.** Wet paint can form elevated blobs, can attract dust while drying, and can be applied without having been mixed adequately. Consequently Lambertian characteristics may become localized or deficient. This mathematical model assumes that the paint layer is perfectly Lambertian over the entire surface.

4) **The reflective paint has a flat/uniform spectral absorption curve.** Even high-quality paints exhibit a curved spectral response, thereby creating a band-pass filter [15**Error! Reference source not found.**]. Multiple reflections result in increased selectivity, to the extent that most of the light energy within the chamber is centered about a specific wavelength. The sensor measurement can therefore be quite erroneous.

5) **The spectral curve of the sensor is similar to the emission profile of the lamp.** A fluorescent lamp radiates energy quite non-uniformly across the visible spectrum, and the sensor device is therefore required to represent each wavelength equally, in order for the light meter to produce an accurate power measurement.

6) **Both end-mirrors have the same effective reflectance.** See section 4.2.2 where the apparatus is discussed. The reflectance of a commonly available glass mirror will generally not be identical with that of an equivalent Perspex mirror. It would have been awkward to incorporate two reflection coefficients into the measurement equation. Therefore the average between the two is accepted.

6.2.2 Reflectance of the chamber surfaces

It is established that paint reflectance should be as high as possible. The paint used was white Plascon Road-marking Paint, a durable and stable product with reflectance specified at $f = 0.97$.

Equally important is the diffusivity of the paint, determined by measuring the Lambertian profile. A flat surface was painted and measured using a spectrometer. Details of the experiment are given in Appendix D. The paint was significantly Lambertian up to approximately 60° from the surface norm.

Mirror reflectance was also measured. The experiment is documented in Appendix A. The values obtained were:

Glass mirror: $f = 0.86$,
Perspex mirror: $f = 0.83$.

The average value of the two coefficients ($f = 0.845$) was used in calculations.

6.3 The Chamber Cylinder Integral

In this section, an integral for a section of the chamber cylinder will be obtained.

6.3.1 Cylindrical Geometry

The task of analyzing the geometry of a point P in relation to the chamber cylinder walls, is greatly simplified if P is first set outside the cylinder rather than on it. Thereafter, point P can be translated to the surface by setting the distance from the cylinder axis equal to the cylinder radius. Note that the situation is identical with that of a cylindrical lamp, prior to translation of point P to the cylinder surface. The integrand is therefore also identical, but in the case of the chamber, integration is taken over a full circle of 2π radians, thereby facilitating direct evaluation at the integral boundaries.

Cylindrical coordinates are an obvious choice. For convenience, the z-coordinate of point P will be located at $z = 0$. The parameters defined below are shown in Figure 6-3.

R: shortest distance of any point P from the cylinder axis,

r_0: cylinder radius,

L: cylinder interval length.
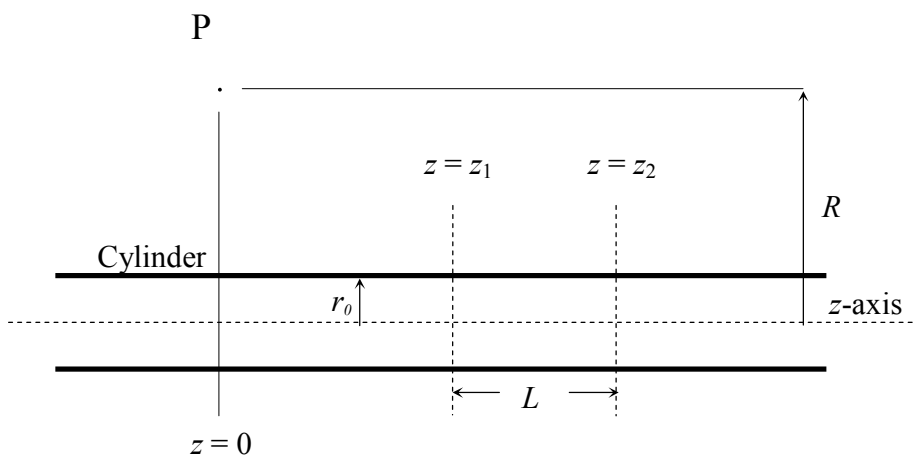
<u>Figure 6-3</u>

The parameters of the cylinder and observation point P. The cylinder has a radius r_0.
Point P is located at coordinates $r = R$, $z = 0$. The relevant cylinder interval, of length
L, begins at $z = z_1$ and ends at $z = z_2$.

The flux arriving at a point P in space from an elemental area *da* at a point Q on an isolated cylindrical emitting surface may be obtained as follows:

Each infinitesimal surface element located at a point Q on the cylindrical surface is assumed to have dimension dz and ds in the longitudinal and azimuthal directions respectively, (as shown in Figure 6-4 below), and can be treated as a point-source, which varies in intensity according to the Lambertian character of a diffuse surface; i.e. as $\cos\varphi$

where φ is the angle of observation with the surface norm ($I_\perp$, the intensity in a direction perpendicular to the surface of such a source, is merely a factor $1/\pi$ of the surface intensity I_0 of the source. A proof is given in Appendix C). Refer to Figure 6-4 below.
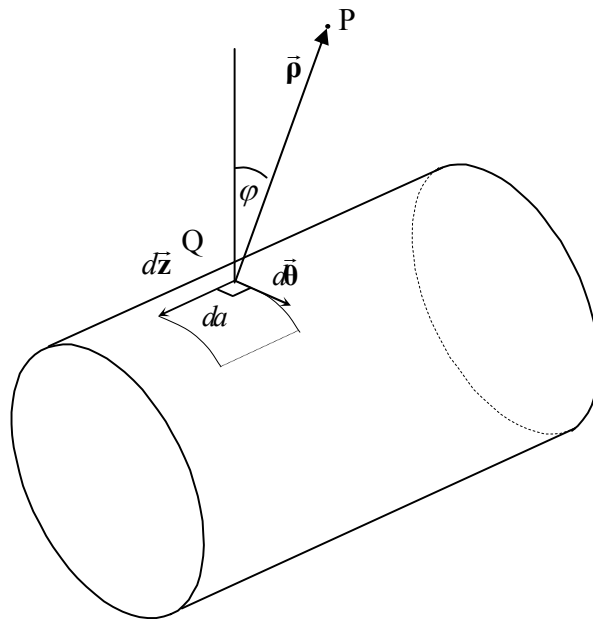
Figure 6-4

An elemental area on the light-emitting cylinder surface, in relation to a point P in space.

The contribution to intensity from the elemental area da at Q, to an elemental area at P is

$$dI_{PQ} = I_{PQ}(\varphi, \rho)\,da = \frac{I_Q(\varphi)}{\rho^2}\,da = I_\perp \frac{\cos\varphi}{\rho^2}\,da \qquad (6.1)$$

The variable ρ here must not be confused with the dimensionless variable used in the previous chapter. Here ρ is the distance between point P and point Q.

The ray arriving at point P must be cosine-corrected by a factor of $\cos\gamma$ due to the increase of surface area with angle of incidence γ (see Figure 6-5 below). Equation (6.1) becomes

$$dI = I_{\perp}\frac{\cos\varphi}{\rho^2}\cos\gamma\, da \qquad\qquad (6.2)$$

The light intensity at point P will be obtained by mathematical integration over the surface area of the cylinder. For the purposes of the calculation, it does not matter whether the intensity of a point on the cylinder is defined in $W.sr^{-1}$, $W.m^{-2}$ or $lm.m^{-2}$. The solution will differ only by a constant factor. Dimensionally, the method used here, of integrating infinitesimal intensities, will result in the units being the same as the units used to describer the lamp surface. The cylinder surface intensity I_0 (and hence $I_{\perp}$) is described in units of $W.m^{-2}$. Thus equation (6.2) becomes

$$I_P = I_{\perp}\int\limits_{Surface}\frac{\cos\varphi\cos\gamma}{\rho^2}\, da \quad W.m^{-2}.$$

Parameter $I_{\perp}$ has been removed from the integrand since the cylinder surface is assumed to have uniform intensity. Note that the summation of Lambertian ray intensities distributed over a hemisphere centered at a point on the surface, yields the surface intensity I_0 at that point.

If the point P in Figure 6-4 is fixed, the variables $\varphi = \varphi(\vec{\rho})$ and $\rho = \|\vec{\rho}\|$ are functions of s and z, the orthogonal coordinates of point Q on the cylinder; i.e. $\varphi = \varphi(s,z)$ and $\rho = \rho(s,z)$. Thus $I_{Q,\hat{r}}(\varphi) = I_{Q,\hat{r}}(s,z)$. The elemental area on a cylinder is simply $da = dsdz = r_0 d\theta dz$ using cylindrical coordinates. Therefore the light intensity at point P is

$$I_{\hat{\mathbf{r}}} = I_{\perp} \int\limits_{Surface} \frac{\cos\varphi \cos\gamma}{\rho^2} r_0 d\theta dz \ . \qquad (6.3)$$

The cosine probability distribution for an area da with intensity I_0 requires a normalization constant $A = \dfrac{1}{\pi}$ such that $I_{\perp} = \dfrac{1}{\pi} I_0$.

Equation (6.3) becomes

$$I_{\hat{\mathbf{r}}} = \frac{1}{\pi} I_0 r_0 \int\limits_{Surface} \frac{\cos\varphi \cos\gamma}{\rho^2} d\theta dz \qquad (6.4)$$

Surface intensity I_0 as well as r_0 are defined as constants and have been moved outside the integral.

The geometry of the problem will now be layed out so that the integral can be expressed in terms of cylindrical coordinates. Refer to Figure 6-5.

It is important to note that for the sake of simplicity, the origin has been moved along the z-axis to a point directly below point Q, rather than point P. This alternative approach suffices until the integrand is obtained in terms of cylindrical coordinate variables.

Let the point P lie in a plane orthogonal to the cylinder axis. Call the plane M. Let M be the point of intersection of the cylinder axis with this plane. Now let $\vec{\rho}$ be the vector from any point Q on the cylinder to observation point P, with magnitude ρ. The shortest distance from Q to plane M is determined in the z-direction and will be labelled as z. Let Q lie in a plane N which is orthogonal to the cylinder axis, intersecting it at N. Clearly the distance between the planes is z. Call the vector from P to the point on the axis cut by plane N, $\vec{v}$. There is a point A in the circle of intersection of plane N with the cylinder

surface such that QA is parallel with the axis MN. Obviously QA $= z$ since it is the distance between the planes M and N. Call the distance PA, d. Then triangle PAQ is right-angled, as is PMN.
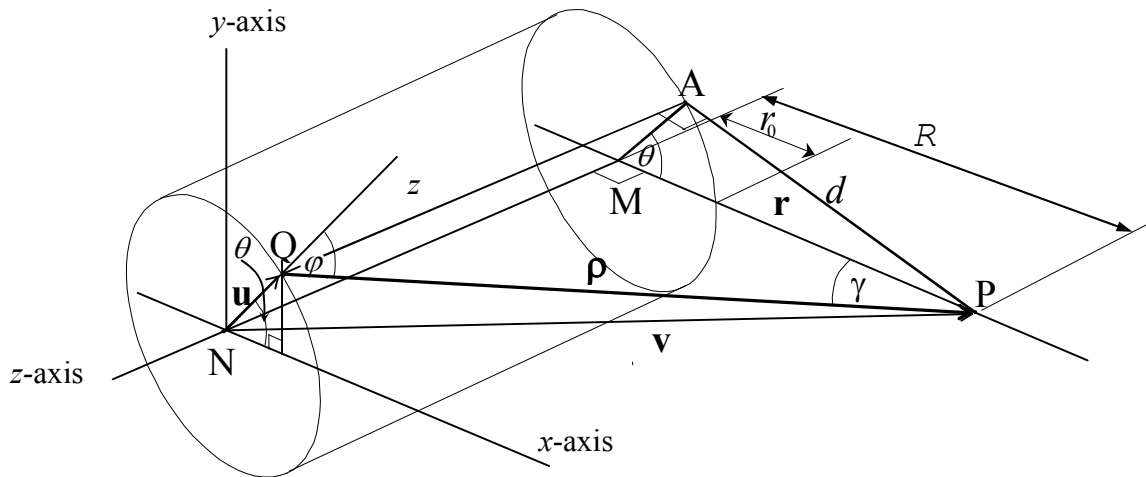
Figure 6-5

The geometry relating an observation point P to a point Q on a cylinder surface.

The required vectors are calculated below in terms of cylindrical coordinate variables z, and θ, and parameters r_0, and R.

$$\vec{u} = \left(r_0 \cos\theta, r_0 \sin\theta, 0\right)$$

$$\left\|\vec{u}\right\| = r_0$$

$$\vec{v} = \left(R, 0, z\right)$$

$$\vec{r} = \left(R, 0, 0\right)$$

$$\vec{\boldsymbol{\rho}} = \vec{\mathbf{v}} - \vec{\mathbf{u}}$$

$$= \left(R - r_0 \cos\theta, -r_0 \sin\theta, z \right)$$

$$\|\vec{\boldsymbol{\rho}}\| = \sqrt{\left(R - r_0 \cos\theta \right)^2 + r_0^{\,2} \sin^2\theta + z^2}$$

$$= \sqrt{R^2 \cos^2\theta - 2Rr_0 \cos\theta + r_0^{\,2} + R^2 \sin^2\theta + z^2}$$

$$= \sqrt{R^2 - 2Rr_0 \cos\theta + r_0^{\,2} + z^2}\ .$$

The projections $\cos\varphi$ and $\cos\gamma$ can now be calculated:

$$\cos\varphi = \frac{\vec{\mathbf{u}} \cdot \vec{\boldsymbol{\rho}}}{\|\vec{\mathbf{u}}\|\|\vec{\boldsymbol{\rho}}\|}$$

$$= \frac{\left(r_0 \cos\theta, r_0 \sin\theta, 0 \right) \cdot \left(R - r_0 \cos\theta, -r_0 \sin\theta, z \right)}{r_0 \rho}$$

$$= \frac{r_0 \cos\theta \left(R - r_0 \cos\theta \right) - r_0^{\,2} \sin^2\theta + 0.z}{r_0 \rho}$$

$$= \frac{Rr_0 \cos\theta \left(R - r_0 \cos\theta \right) - r_0^{\,2} \left(\sin^2\theta + \cos^2\theta \right)}{r_0 \rho}$$

$$= \frac{R\cos\theta - r_0}{\rho}\ .$$

$$\cos\gamma = \frac{\vec{\mathbf{r}} \cdot \vec{\boldsymbol{\rho}}}{\|\vec{\mathbf{r}}\| \cdot \|\vec{\boldsymbol{\rho}}\|}$$

$$= \frac{(R,0,0) \cdot (R - r_0 \cos\theta, -r_0 \sin\theta, z)}{R\rho}$$

$$= \frac{R^2 - Rr_0 \cos\theta}{R\rho}$$

$$= \frac{R - r_0 \cos\theta}{\rho}.$$

The chamber intervals must each be integrated separately, between their respective boundaries $z = z_1$ and $z = z_2$. Note that from here on the origin of the coordinate system is moved along the z-axis below point P, as in Figure 6-3. Equation (6.4) becomes

$$\delta I_{\hat{\mathbf{r}}} = \frac{1}{\pi} I_0 r_0 \int_{z_1}^{z_2} \int_0^{2\pi} \frac{(R - r_0 \cos\theta)(R\cos\theta - r_0)}{\left(z^2 + R^2 + r_0^2 - 2Rr_0 \cos\theta\right)^2} \, d\theta \, dz$$

Dimensionless units are preferred: Let $\rho = \dfrac{R}{r_0}$ and $\sigma = \dfrac{z}{r_0}$. Then at a point P outside a diffuse emitting cylindrical Lambertian surface, the light intensity due to a chamber interval is

$$\delta I = \frac{1}{\pi} I_0 \int_{\sigma_1}^{\sigma_2} \int_0^{2\pi} \frac{(\rho - \cos\theta)(\rho\cos\theta - 1)}{\left(\sigma^2 + \rho^2 + 1 - 2\rho\cos\theta\right)^2} \, d\theta \, d\sigma. \tag{6.5}$$

6.3.2 Mathematical Solutions

The integral equation (6.5) above will be solved using the method of contour integration, but note that z-substitution can also be used.

In the case of the chamber wall $R = r_0$ i.e. $\rho = 1$ and since the *inside* of the chamber is integrated, there is a sign reversal:

$$\delta I = \frac{1}{\pi} I_0 \int_{\sigma_1}^{\sigma_2} \int_0^{2\pi} \frac{(1-\cos\theta)^2}{(\sigma^2 + 2 - 2\cos\theta)^2} d\theta d\sigma$$

It is necessary to first perform the angular part of the integration, since the integrand becomes independent of θ as $\sigma \to 0$ whereas if the integration is performed first with respect to σ, intensity is defined to be zero at $\theta = 0$. The result depends on whether it is the denominator or the numerator that tends toward zero faster, as the elemental area to be integrated approaches P. It amounts to saying that the intensity from a point infinitesimally close to P is zero no matter how much closer the point moves. The Lambertian behavior must dominate the $1/R^2$ behavior for infinitesimal distances.

The angular part of the integral must be evaluated between 0 and 2π, using contour integration. But the denominator must first be written in the form $(1 - p\cos\theta)^2$, $|p| < 1$. Therefore a factor must be removed from the denominator:

$$\frac{1}{\pi} I_0 \int_{\sigma_1}^{\sigma_2} \int_0^{2\pi} \frac{(1-\cos\theta)^2}{(\sigma^2 + 2 - 2\cos\theta)^2} d\theta d\sigma = \frac{1}{\pi} I_0 \int_{\sigma_1}^{\sigma_2} \frac{1}{(\sigma^2 + 2)^2} \int_0^{2\pi} \frac{(1-\cos\theta)^2}{\left(1 - \dfrac{2}{\sigma^2 + 2}\cos\theta\right)^2} d\theta d\sigma.$$

Let
$$p = \frac{2}{\sigma^2 + 2}.$$
(6.6)

Then

$$\delta I = \frac{1}{\pi} I_0 \int_{\sigma_1}^{\sigma_2} \frac{p^2}{4} \int_0^{2\pi} \frac{(1-\cos\theta)^2}{(1-p\cos\theta)^2} d\theta d\sigma .$$

The angular part must now be integrated. Consider integration around a circle of unit radius. Let $e^{i\theta} = z = \cos\theta + i\sin\theta$. Then $dz = ie^{i\theta} d\theta = izd\theta$. Further,

$d\theta = \frac{1}{iz} dz$, $e^{-i\theta} = \cos\theta - i\sin\theta$ and $2\cos\theta = e^{i\theta} + e^{-i\theta} = z + \frac{1}{z} \Rightarrow \cos\theta = \frac{z^2+1}{2z}$.

Thus the integral with respect to θ becomes

$$F_\theta = \int_0^{2\pi} \frac{(1-\cos\theta)^2}{(1-p\cos\theta)^2} d\theta = \frac{1}{i} \int_0^{2\pi} \frac{\left(1 - \frac{z^2+1}{2z}\right)^2}{\left(1 - p\frac{z^2+1}{2z}\right)^2} \frac{1}{z} dz . \qquad (6.7)$$

The contribution from an interval from σ_1 to σ_2 along the lamp is

$$\delta F_\sigma = \int_{\sigma_1}^{\sigma_2} F_\theta(\sigma) d\sigma$$

such that the contribution to flux density is

$$\delta I = \frac{1}{\pi} I_0 . \delta F .$$

After an extensive amount of deduction the following result was obtained for the incident flux at a point on the cylinder wall due to a cylindrical section of the chamber. See Appendix F for details. Equation (F9) is repeated below:

$$\delta I_n = 2 I_0 R^3 \left(\frac{1}{\sqrt{z_n{}^2 + 4R^2}\left(z_n{}^2 + 2R^2 + z_n\sqrt{z_n{}^2 + 4R^2}\right)} - \frac{1}{\sqrt{z_{n+1}{}^2 + 4R^2}\left(z_{n+1}{}^2 + 2R^2 + z_{n+1}\sqrt{z_{n+1}{}^2 + 4R^2}\right)} \right)$$

Here z_{n-1} and z_n are the limits of the nth chamber interval of length $2d$ over which integration is applied. The first interval is that of the real chamber while each successive interval is multiplied by a further mirror reflectance f in order to sum the accumulation of flux at P due to the chamber and mirrors.

$$I_P = \delta I_{real} + 2\delta I_f + 2\delta I_{f^2} + 2\delta I_{f^3} + \ldots$$

$$= \delta I_{real} + 2f\delta I_1 + 2f^2\delta I_2 + 2f^3\delta I_3 + \ldots$$

$$I_P = \delta I_{real} + 2\sum_{n=1}^{\infty} f^n \delta I_n , \qquad (6.8)$$

where

$$\delta I_{real} = I_0\left(1 - \frac{4}{\sqrt{\rho_1{}^2 + 4}\left(\rho_1{}^2 + 2 + \rho_1\sqrt{\rho_1{}^2 + 4}\right)}\right)$$

and

$$\delta I_n = 2 I_0 \left(\frac{1}{\sqrt{\rho_n{}^2 + 4}\left(\rho_n{}^2 + 2 + \rho_n\sqrt{\rho_n{}^2 + 4}\right)} - \frac{1}{\sqrt{\rho_{n+1}{}^2 + 4}\left(\rho_{n+1}{}^2 + 2 + \rho_{n+1}\sqrt{\rho_{n+1}{}^2 + 4}\right)} \right)$$

Substitute $\rho_{n+1} = \rho_n + 2d$;

$$\delta I_n = 2 I_0 \left(\frac{1}{\sqrt{\rho_n{}^2 + 4}\left(\rho_n{}^2 + 2 + \rho_n\sqrt{\rho_n{}^2 + 4}\right)} - \frac{1}{\sqrt{(\rho_n + 2d)^2 + 4}\left((\rho_n + 2d)^2 + 2 + (\rho_n + 2d)\sqrt{(\rho_n + 2d)^2 + 4}\right)} \right)$$

Now since $\rho_{\mathrm{n}} = (2n+1)d$,

$$\delta I_{\mathrm{n}} = 2I_0 \left(\frac{1}{\sqrt{(2n+1)^2 d^2 + 4}\left((2n+1)^2 d^2 + 2 + (2n+1)d\sqrt{(2n+1)^2 d^2 + 4}\right)} \right.$$

$$\left. - \frac{1}{\sqrt{(2n+3)^2 d^2 + 4}\left((2n+3)^2 d^2 + 2 + (2n+3)d\sqrt{(2n+3)^2 d^2 + 4}\right)} \right),$$

$$\delta I_{\mathrm{real}} = I_0 \left(1 - \frac{4}{\sqrt{d^2 + 4}\left(d^2 + 2 + d\sqrt{d^2 + 4}\right)} \right) \qquad (6.9)$$

These equations were used in conjunction with equation (6.8) to plot graphs of the total contribution of the chamber to point P versus chamber interval length for various values of mirror reflectance. The software package Microsoft Excel was used to sum the contributions up to a point where they were insignificant for subsequent n.
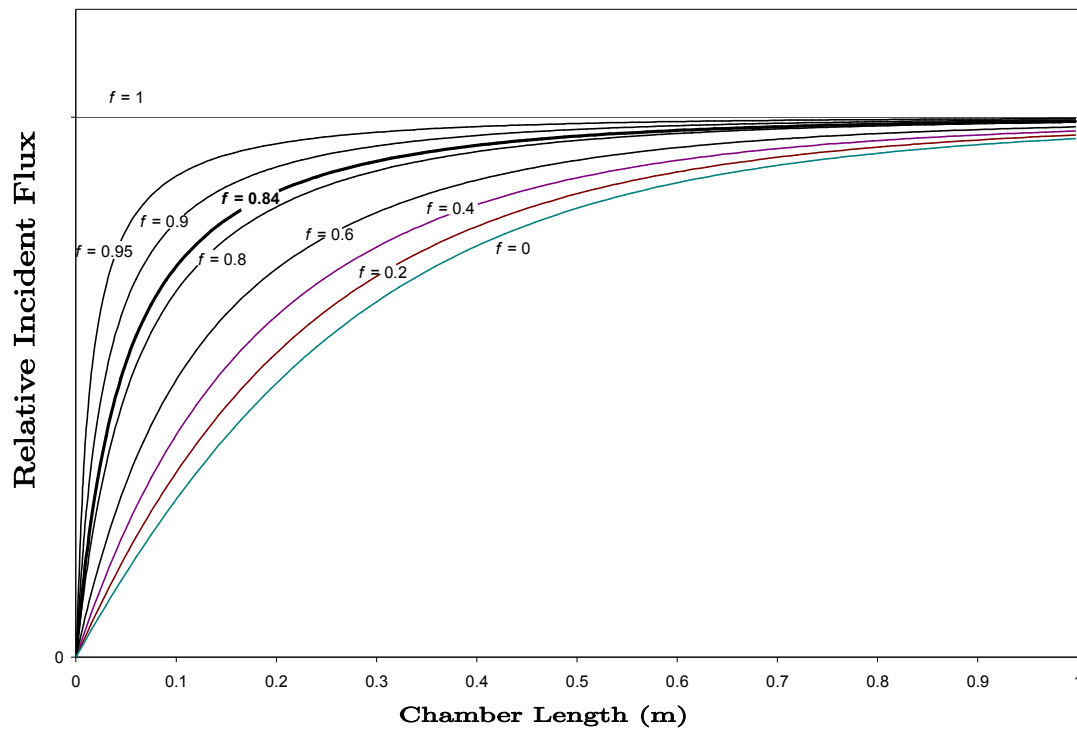
Figure 6-6

A plot of equation (6.8), showing the relative flux arriving at the middle of the chamber. The
arriving flux is plotted for several selections of mirror reflectance f, relative to the level with $f = 1$,
as a function of real-chamber length.

The graph in Figure 6-6 offers some insight into the shape of the function that can be
expected from the measurement equation, but equation (6.8) cannot quantify the intensity
since it does not take multiple reflections from the cylinder walls into account.

6.3.3 Equation Analysis

The equation produced above will now be analyzed primarily to confirm authenticity near
the extremes i.e. for a very long and a very short cylinder.

If the chamber is infinitely long, both sides must be included and since the integrand is an even function,

$$I = 2.2I_0 R^3 \left(\frac{1}{\sqrt{z_1^2 + 4R^2}\left(z_1^2 + 2R^2 + z_1\sqrt{z_1^2 + 4R^2}\right)} - \frac{1}{\sqrt{z_2^2 + 4R^2}\left(z_2^2 + 2R^2 + z_2\sqrt{z_2^2 + 4R^2}\right)} \right)$$

With $z_1 = 0, \ z_2 \to \infty$,

$$I_\infty = 4I_0 R^3 \left(\frac{1}{\sqrt{0 + 4R^2}\left(0 + 2R^2 + 0\sqrt{0 + 4R^2}\right)} - 0 \right)$$

$$= 4I_0 R^3 \frac{1}{2R\left(2R^2\right)}$$

$$= I_0$$

This result is identical with that of an infinitely large plane. The infinitely long diffuse cylinder is thus equivalent to an infinite plane when considering radiance arriving at any point on the inside surface of such a cylinder.

Now, for a very short chamber i.e. from $\sigma = 0$ to $\sigma = \varepsilon$, where $\varepsilon \ll R$

$$I = 4I_0 R^3 \left(\frac{1}{4R^3} - \frac{1}{\sqrt{\varepsilon^2 + 4R^2}\left(\varepsilon^2 + 2R^2 + \varepsilon\sqrt{\varepsilon^2 + 4R^2}\right)} \right)$$

$$\approx 4I_0 R^3 \left(\frac{1}{4R^3} - \frac{1}{2R\left(2R^2 + 2\varepsilon R\right)} \right)$$

with only the first order in ε retained.

$$I = 4I_0 R^3 \left(\frac{1}{4R^3} - \frac{1}{4R^2\left(R + \varepsilon\right)} \right)$$

$$= 4I_0 R^3 \left(\frac{1}{4R^3} - \frac{1}{4R^3\left(1 + \frac{\varepsilon}{R}\right)} \right)$$

$$= I_0 \left(1 - \left(1 - \frac{\varepsilon}{R} + \left(\frac{\varepsilon}{R}\right)^2 - \cdots \right) \right)$$

by cancellation, and expansion of $\left(1 + \frac{\varepsilon}{R}\right)^{-1}$.

$$I = I_0 \left(\frac{\varepsilon}{R} - \left(\frac{\varepsilon}{R}\right)^2 + \cdots \right)$$

$$\approx I_0 \frac{\varepsilon}{R}.$$

(This is an interesting result, which indicates that a ring of light illuminates itself with a flux density that is proportional to the inverse, $1/R$, of its radius and not $1/R^2$, no matter how large the radius).

6.4 Multiple Reflections

Up to this point it has been assumed that the intensity of the chamber wall is uniform throughout. However, due to the imperfect reflectance of the mirrors, flux will distribute non-uniformly. If the mirrors are far apart, the influence of high order multiple reflections will be minimal. However, when the mirrors are close together, multiple reflections will exacerbate non-uniformity. Therefore each phase or 'order' of reflection will set up a different intensity profile along the chamber, each profile contributing differently to the flux at a point. Certain assumptions will have to be made to simplify the deductions.

A light packet of intensity I_0 is traced from the near side of the lamp. After each reflection the density is reduced by a reflection factor f_p of the chamber wall paint. The resulting incident intensity I_i on the wall is due to the sum of multiple reflections of the light packet. For a chamber that is infinitely long, the trajectory of such a packet will not have an angular probability distribution (due to symmetry there cannot be any energy flow along the direction of the chamber axis), and all packets may be considered as reflecting off the surface in a perpendicular direction with no attenuation other than that due to the reflectance f_p of the surface; i.e. the statistics associated with the Lambertian profile do not enter into the calculation.

$$I_i = I_0 + f_p^2 I_0 + f_p^2 \left(f_p^2 I_0 \right) + f_p^2 \left(f_p^2 \left(f_p^2 I_0 \right) \right) + \cdots$$

$$= I_0 + f_p^2 I_0 + f_p^4 I_0 + f_p^6 I_0 + \cdots$$

$$= I_0 \left(1 + f_p^2 + f_p^4 + f_p^6 + \cdots \right)$$

$$= I_0 \sum_{n=0}^{\infty} f_p^{2n} \; .$$

The sum is a G. S. with common ratio f_p^2. It can immediately be written that

$$I_i = I_0 \frac{1}{1 - f_p^2} \qquad (6.10)$$

There is another interesting way to prove this result. Furthermore it paves the way for a more realistic analysis, for example, if the lamp intensity is not uniform over its length. The method involves discrete mathematics.

Consider the light arriving at the chamber wall at event $t = t_2$. It is the contribution from the lamp and from the surrounding wall, i.e.

$$x(t_2) = x_w(t_2) + I_L.$$

The contribution from the wall is

$$x_w(t_2) = f^2 \cdot x(t_1)$$

where t_1 is the previous event.

Thus

$$x(t_2) = f^2 \cdot x(t_1) + I_L.$$

Subtract $x(t_1)$ from both sides;

$$x(t_2) - x(t_1) = (f^2 - 1) \cdot x(t_1) + I_L.$$

Substitute $t_2 = t_1 + \Delta t$ and divide by Δt;

$$\frac{x(t_1 + \Delta t) - x(t_1)}{\Delta t} = (f^2 - 1) \cdot \frac{x(t_1)}{\Delta t} + \frac{I_0}{\Delta t}, \quad t \to \infty$$

Setting $\Delta t = 1$ and letting t approach infinity is completely analogous to finding the limit as $\Delta t \to 0$ so long as a solution exists as $t \to \infty$. If the result is stable as $t \to \infty$ then it is a solution.

$$\frac{x(t+1) - x(t)}{1} = (f^2 - 1) \cdot \frac{x(t)}{1} + \frac{I_0}{1}$$

$$\underset{t \to \infty}{Lim} \frac{x(t+1) - x(t)}{1} = \frac{dx}{dt}\bigg|_{t \to \infty}$$

$$\frac{dx}{dt} = (f^2 - 1) \cdot x(t) + I_0, \quad t \to \infty$$

A stable solution requires $\qquad \dfrac{dx}{dt}\bigg|_{t \to \infty} = 0$.

Therefore,

$$(f^2 - 1) \cdot x(t) + I_0 = 0, \quad t \to \infty$$

$$\Rightarrow x_{t \to \infty} = \frac{I_0}{1 - f^2}.$$

Note that only the near side of the lamp has been taken into account so far. The final intensity at a point on the wall is due to both sides of the lamp. The flux absorbed by the near wall is the sum of contributions of the flux absorbed from the front side of the lamp

as well as from the rear side of the lamp. Using equation (6.10), the front side of the lamp makes a contribution to incident light intensity of

$$I_{i,L} = \frac{I_0}{1-f^2}$$

The contribution from the remote side of the lamp is merely the lamp intensity reflected off the cylinder far wall:

$$I_{i,w} = \frac{I_0}{1-f^2} \cdot f \ .$$

The resultant incident light intensity is

$$I_i = I_{i,L} + I_{i,w}$$

$$= \frac{I_0}{1-f^2} + \frac{I_0}{1-f^2} \cdot f$$

$$= \frac{I_0}{1-f^2}(1+f)$$

$$I_i = \frac{I_0}{1-f} \ . \tag{6.11}$$

Refer to Figure 6-7 below, where the light path is summarized.

$I_{\text{Refl.}}$ Chamber   Multiple
Reflections

Lamp

I_{L} Resultant
Reflection I_{L}

$$I_{\text{Refl.}} = \frac{f}{1-f} I_{\text{a}} \qquad I_{\text{i}} = I_{\text{Refl.}} + \frac{r_0}{R} \cdot I_{\text{L}}$$

$$I_{\text{a}} = (1-f)\frac{r_0}{R} \cdot I_{\text{L}} \qquad\qquad I_{\text{a}} = \frac{r_0}{R} \cdot I_{\text{L}}$$
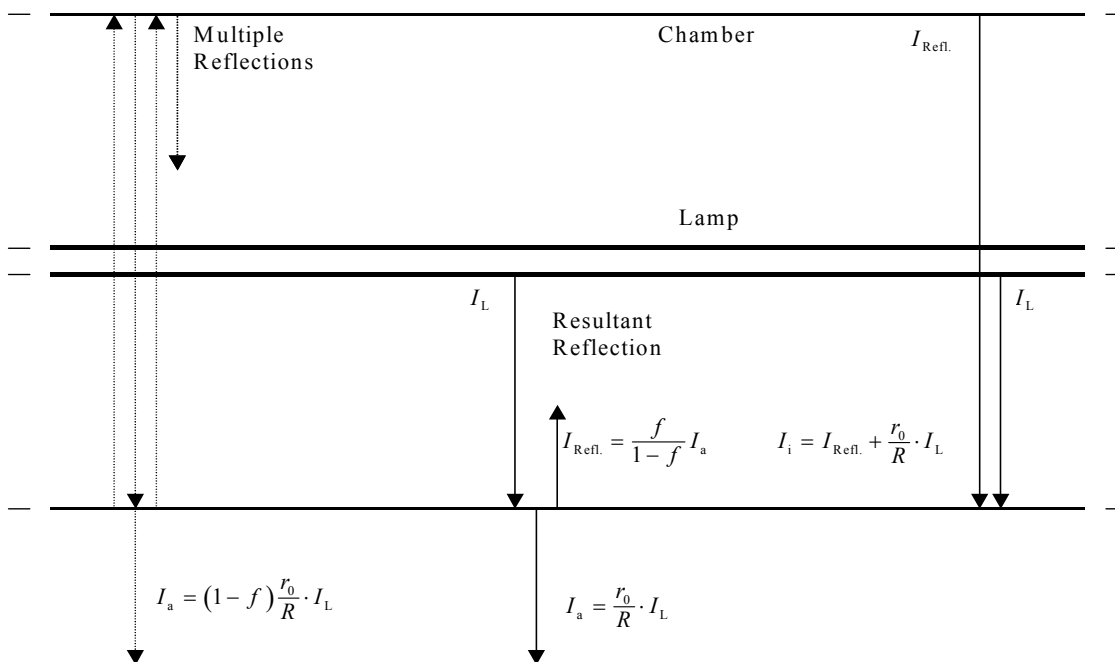
Figure 6-7

A summary of reflections and absorption within the cylindrical chamber.

The mirror surfaces are specular, while the chamber wall is diffuse. In the case of the mirrors, a ray will not scatter upon reflection. A perpendicular ray reflected many times over will remain within the confines of the mirrors. If the chamber wall was a perfectly reflective specular surface, then the end-mirror will appear to present an infinite plane, because of multiple images of the mirror in the chamber wall.

The *diffuse* chamber wall must, however, be viewed from a different perspective. Refer to Figure 6-8. Over the surface of a hemisphere, the mirror "sees" the chamber image in the opposite mirror, plus the chamber wall filling up the rest of the hemisphere. The only distinction between the chamber surface, and what appears to be an infinite plane mirror, is the slightly elevated brightness of the real chamber wall over the virtual chamber wall, because of the less-than-perfect mirror reflectance. Therefore the mirror may be assumed as infinitely large and the rays as not scattered. Note that it applies whether the chamber wall is specular or diffusive.
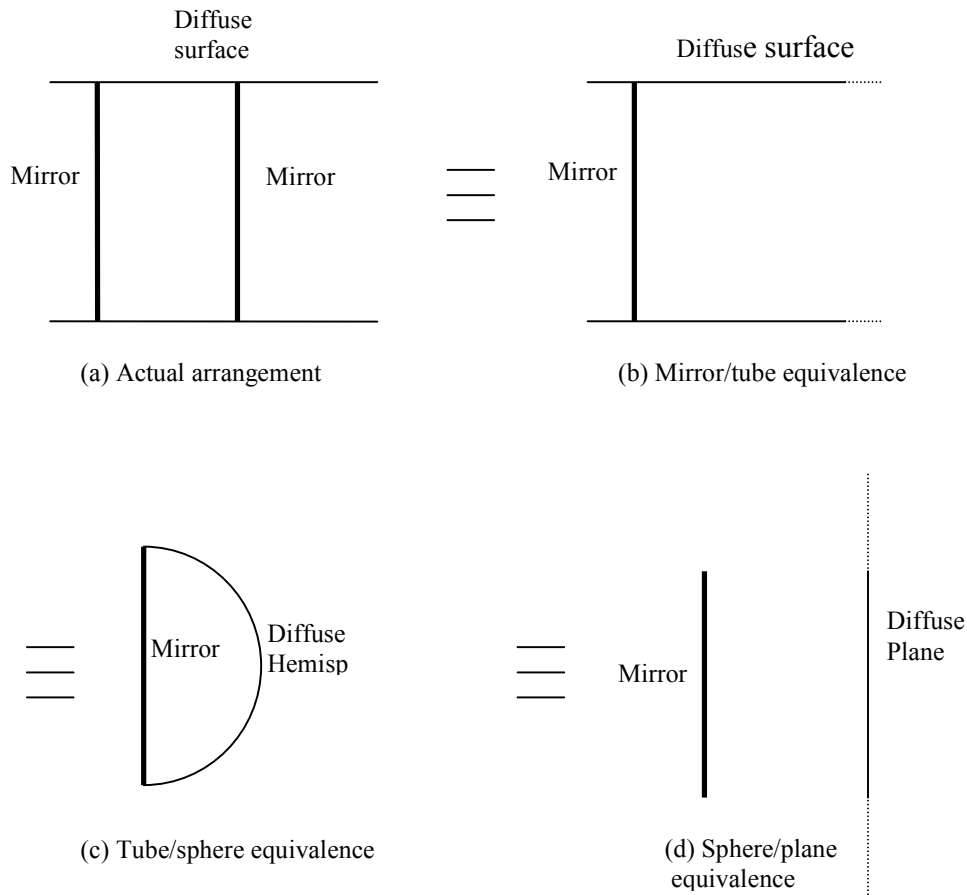
Figure 6- 8

The equivalence of an end-mirror with reflectance $f_m = 1$, to an infinite diffuse plane. (a) The dual end-mirror system. (b) Equivalent infinite chamber. The mirror on the right in (a) presents an infinitely long diffuse chamber to the mirror on the left. Such a mirror can therefore be replaced by an infinitely long chamber. (c) Equivalent spherical plane. Since brightness does not vary with distance or deviation from the norm of a diffuse surface, the infinite chamber can be replaced by a sphere, or an infinite plane, or any other closed shape or infinite surface. (d) Equivalent infinite plane.

For the moment it will be assumed that the mirror reflectance is perfect. Then the virtual chamber will not dissipate any energy from the real chamber, and the wall-to-wall and mirror-to-mirror reflections can be assumed independent of one another.

The mirrors create a pseudo-infinite cylinder for which the resulting surface intensity of reflected light is essentially perpendicular to the cylinder wall everywhere. Although the surface is diffuse and hence the rays are scattered, any ray incumbent on the mirror at any angle, will be reflected back to the chamber (less a small proportion absorbed by the mirror).

Essentially such a statement is not saying anything new. It is simply an alternative way to state that the chamber is infinitely long (due to the mirrors). Hence the diffuse chamber wall surface may be treated as a specular surface insofar as multiple reflections are concerned. Since the mirrors reflect light energy back into the real chamber, Lambertian light scattering will be assumed as negligible in the analysis of multiple reflections.

For an infinitely long lamp, light intensity at a distance R from the lamp is

$$I_{i,L} = \frac{r_0}{R} I_0 .$$ (6.12)

In the case of the real chamber, it is convenient to work with flux rather than intensity. Total flux external to the source, is constant (indirectly due to the Law of Conservation of Energy) as long as the source is in a steady state of constant radiation power.

In all practical situations the chamber will be in equilibrium. That is, in unit time, the total light energy absorbed by the chamber is equal to the light energy radiated from the lamp. This fact proves essential for the deduction of the solution without using statistical methods.

The chamber wall will absorb a proportion of the total flux while the mirrors absorb the rest (a small portion may be absorbed back into the lamp, but will be regarded as negligible). Let the total radiated flux of the lamp be Φ_L. We have

$$\Phi_{c,w} + \Phi_{c,m} = \Phi_L$$

where $\Phi_{c,w}$ and $\Phi_{c,m}$ are the contributions absorbed by the cylinder wall and mirrors respectively.

These fluxes can be considered to be the sum of multiple reflections, perpendicularly between opposite sides of the chamber, in the sense that the mirror system is considered separately from the cylinder. The absorbed flux is thus

$$\Phi_a = (1 - f)\Phi_i$$

where Φ_i is the flux incident on the surface. Let that portion of the lamp flux that is absorbed by the walls be $\Phi_{a,w}$ and the remaining flux absorbed by the mirrors be $\Phi_{a,m}$. The flux absorbed by the nth reflection of the ray is

$$\Phi_{a_n,w} = (1 - f_w)\Phi_{i_n,w} ,$$

$$\Phi_{a_n,m} = (1 - f_m)\Phi_{i_n,m}$$

by the wall and mirror respectively.

As with the intensity, for an infinitely long chamber,

$$\Phi_{i_1} = \Phi_L + f^2\Phi_L + f^4\Phi_L + \cdots$$

$$= \frac{1}{1-f^2} \Phi_L$$

due to the near side of the lamp. The word "near" here more specifically means only a ray that comes directly from the lamp to the point in consideration on the wall, at first incidence, rather than reflecting off the far wall first. It does not imply that the flux is incident on only half of the chamber. The equation applies to the entire chamber.

6.5 The Chamber Measurement Equation

An equation will now be derived which describes the flux distribution along the chamber walls due to a cylindrical fluorescent lamp.

Multiple reflections alter the scenario substantially. Total wall flux and mirror flux will first be analyzed separately. If it is assumed that the flux arriving at the mirrors is equal in density to the flux arriving at the cylinder wall, a ratio of fluxes can be converted to a ratio of intensities, so that the intensity falls away from the equation. The mirror flux is thus obtained in terms of the wall flux. The equations are then combined by summing the total lamp flux distributed throughout the chamber. In this way the total absorbed wall flux is obtained in terms of the total lamp flux. The light intensity on the wall follows by dividing through by the chamber area and equating the absorbed flux in terms of the reflected flux. See the deductions leading up to equation (6.22) below.

The flux on the wall due to the entire lamp is, from equation (6.11),

$$\Phi_i = \frac{1}{1-f} \Phi_L$$

where $a = 1-f$ is an absorption coefficient. The equation above is derived by multiplying equation (6.11) through by the chamber surface area. Unfortunately there are differing

surfaces within the chamber with respectively differing coefficients, namely the wall and the mirrors.

For a finite chamber it will therefore be assumed (see the discussion at the beginning of this section) that the flux on the wall is from the rest of the wall only, and not from the mirrors. Similarly the flux on each end-mirror will be assumed as arriving from the alternate end-mirror only, and not from the cylinder wall. Here the subscript c denotes the contribution (proportion of total lamp light flux) reflected from the given surface, while i denotes the incident flux, and a denotes the absorbed flux, w denotes the wall surface, and m denotes the mirror surface.

$$\left. \begin{array}{l} \Phi_{i,w} = \dfrac{1}{1-f_w}\Phi_{c,w} \\[3em] \Phi_{i,m} = \dfrac{1}{1-f_m}\Phi_{c,m} \end{array} \right\} \qquad (6.13)$$

Equations (6.13) have taken multiple reflections into account. Incident flux is due to multiple reflection of that proportion of lamp light that reflects off the given surface, be it the walls or the mirrors.

Total emitted lamp flux must equal total absorbed flux. Therefore the flux absorbed at the surface is just the relevant contribution.

Thus

$$\left. \begin{array}{l} \Phi_{a,w} = \Phi_{c,w} = \left(1-f_w\right)\Phi_{i,w} \\[2em] \Phi_{a,m} = \Phi_{c,m} = \left(1-f_m\right)\Phi_{i,m} \end{array} \right\} \qquad (6.14)$$

for the wall and mirrors respectively. The total absorbed flux is just the lamp flux:

$$\Phi_{a,w} + \Phi_{a,m} = \Phi_L \qquad (6.15)$$

The incident flux is obtained from shuffling equations (6.14):

$$\Phi_{i,w} = \frac{1}{1-f_w}\Phi_{a,w}$$

$$\Phi_{i,m} = \frac{1}{1-f_m}\Phi_{a,m}$$

Take the flux ratio:

$$\frac{\Phi_{i,w}}{\Phi_{i,m}} = \frac{1-f_m}{1-f_w}\frac{\Phi_{a,w}}{\Phi_{a,m}} \qquad (6.16)$$

Replace the incident fluxes on the left by flux densities, which will later fall away from the equation. Then the relationship between absorbed fluxes by the wall and mirrors will be obtained.

Flux = Intensity $\times$ Surface area: $\Phi = I.S$. Thus

$$\Phi_{i,w} = I_{i,w}S_w$$

$$\Phi_{i,m} = I_{i,m}S_m \ .$$

The cylinder wall area is

$$S_w = 2\pi RL$$

while the total mirror area for both mirrors is

$$S_{\mathrm{m}} = 2\pi R^2 \,.$$

Take the ratio of fluxes:

$$\frac{\Phi_{\mathrm{i,w}}}{\Phi_{\mathrm{i,m}}} = \frac{I_{\mathrm{i,w}} S_{\mathrm{w}}}{I_{\mathrm{i,m}} S_{\mathrm{m}}}$$

$$= \frac{I_{\mathrm{i,w}}}{I_{\mathrm{i,m}}} \frac{2\pi R L}{2\pi R^2}$$

i.e.
$$\frac{\Phi_{\mathrm{i,w}}}{\Phi_{\mathrm{i,m}}} = \frac{I_{\mathrm{i,w}}}{I_{\mathrm{i,m}}} \frac{L}{R} \,. \qquad (6.17)$$

It will be assumed that the light incident at the cylinder wall has the same flux density as the light incident at the mirror, due to the high degree of light scattering in the chamber;

i.e.
$$\frac{I_{\mathrm{i,w}}}{I_{\mathrm{i,m}}} = 1 \,.$$

Also, let
$$\Gamma = \frac{L}{R} \,.$$

Then equation (6.17) becomes

$$\frac{\Phi_{\mathrm{i,w}}}{\Phi_{\mathrm{i,m}}} = \Gamma \qquad (6.18)$$

Now equate equations (6.16) and (6.18):

$$\frac{\Phi_{i,w}}{\Phi_{i,m}} = \Gamma = \frac{1-f_m}{1-f_w}\frac{\Phi_{a,w}}{\Phi_{a,m}}.$$

Rearrange for the flux absorbed by the mirrors

$$\Phi_{a,m} = \frac{1}{\Gamma}\frac{1-f_m}{1-f_w}\Phi_{a,w} \tag{6.19}$$

Substitute equation (6.16) into equation (6.15). Then the flux absorbed by the wall is obtained exclusively in terms of reflection coefficients (and other constants).

$$\Phi_{a,w} + \frac{1}{\Gamma}\frac{1-f_m}{1-f_w}\Phi_{a,w} = \Phi_L$$

Multiply by the denominator, $\Gamma\left(1-f_w\right)$:

$$\Gamma\left(1-f_w\right)\Phi_{a,w} + \left(1-f_m\right)\Phi_{a,w} = \Gamma\left(1-f_w\right)\Phi_L$$

Factorize the left side:

$$\left[\Gamma\left(1-f_w\right) + \left(1-f_m\right)\right]\Phi_{a,w} = \Gamma\left(1-f_w\right)\Phi_L.$$

Finally,

$$\Phi_{a,w} = \Gamma\frac{1-f_w}{\Gamma\left(1-f_w\right) + \left(1-f_m\right)}\Phi_L. \tag{6.20}$$

However, it is the reflected flux that is required. Reflected flux and absorbed flux are related. The reflected flux is $\dfrac{f}{1-f}$ times the absorbed flux (see Appendix G for a proof).

i.e.
$$\Phi_{r,w} = \frac{f_w}{1-f_w}\Phi_{a,w} \qquad (6.21)$$

Substitute equation (6.20) into equation (6.21):

$$\Phi_{r,w} = \frac{f_w}{1-f_w}\Gamma\frac{1-f_w}{\Gamma(1-f_w)+(1-f_m)}\Phi_L$$

$$= \Gamma\frac{f_w}{\Gamma(1-f_w)+(1-f_m)}\Phi_L$$

Divide the flux on each side by the respective area to obtain the flux density

$$\frac{\Phi_{r,w}}{2\pi RL} = \Gamma\frac{f_w}{\Gamma(1-f_w)+(1-f_m)}\frac{\Phi_L}{2\pi r_0 L}\frac{r_0}{R}$$

$$I_{r,w} = \Gamma\frac{f_w}{\Gamma(1-f_w)+(1-f_m)}I_0\frac{r_0}{R}$$

$$I_{r,w} = \frac{\Gamma}{\rho}\frac{f_w}{\Gamma(1-f_w)+(1-f_m)}I_0. \qquad (6.22)$$

The measured incident flux density on the wall of an infinitely long chamber must be identical with the summation of reflected flux density from the entire cylinder wall, if the lamp is excluded from measurement, e.g. with a baffle. The validity of such a statement might be questioned on the grounds that the reflected flux must be less than the incident

flux by an amount of the absorbed flux. However, the absorbed flux is considered as due to the lamp only, so that when only the chamber wall light intensity is measured, the wall may be regarded as perfectly reflective i.e. $f = 1$.

Of course, the sensor will also measure the actual light coming from the lamp directly:

$$I_m = I_{r,w} + I_{i,L} \tag{6.23}$$

Substitution of equation (6.12) and equation (6.22) into equation (6.23) yields

$$I_m = \frac{\Gamma}{\rho} \frac{f_w}{\Gamma\left(1 - f_w\right) + \left(1 - f_m\right)} I_0 + \frac{1}{\rho} \cdot I_0 \tag{6.24}$$

It has been assumed up to now that the intensity on the 'surface' of the virtual part of the chamber is identical with intensity on the surface of the real part. Although the presence of the mirrors has indirectly influenced the calculation of the intensity of light reflected from the cylinder surface, the *measured* light is influenced directly by the mirrors since the detector will measure light from both the real part and the virtual part of the chamber.

A non-ideal chamber will not exhibit the same uniform intensity for each and every interval due to the order n of reflection, so that the measurement equation must therefore be adjusted; i.e. the intensities from the virtual part of the chamber must be modified by an order n of the mirror reflectance f.

Before such steps are taken, a plot is produced to show comparison of results so far, with measurement. See Figure 6-9 below. A log of the measured results is shown in Table 6.1. The light intensity at the middle of the chamber cylinder wall was measured for various chamber widths. The chamber width was adjusted by locating the circular internal mirror at various specified intervals along the cylinder.

The mirror reflectance used in the calculations is $f_m = 0.845$, the average between the glass- and Perspex-mirror. See Appendix A where the details of the experiment to determine reflectance have been documented.
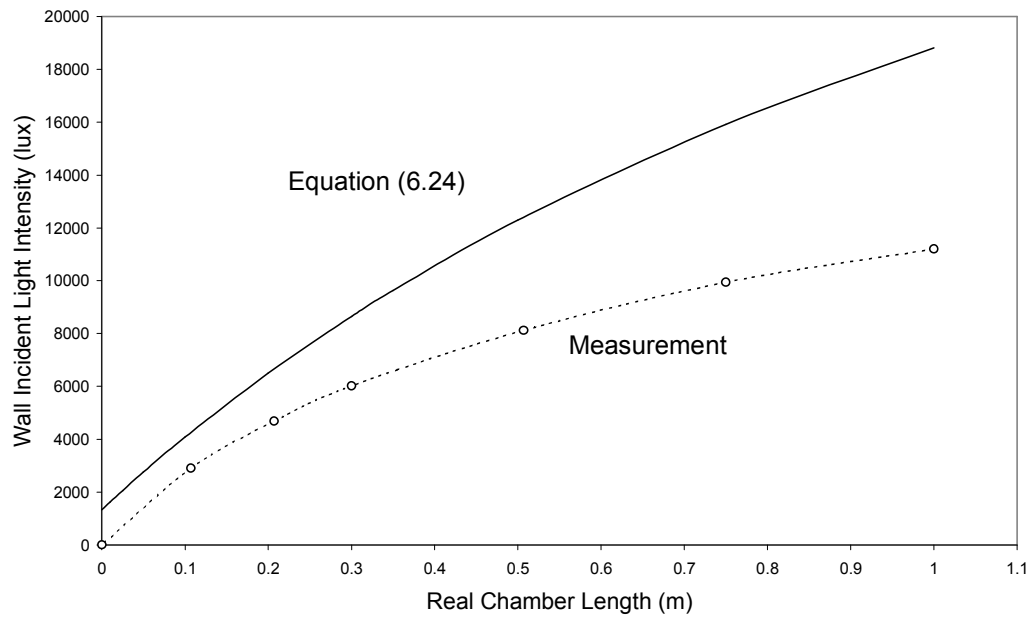
Figure 6-9

A plot of measurement equation (6.24), which excludes mirror absorption.

Table 6.1

Measured luminous flux density at the centre of the chamber wall.

Chamber Length (m)	0.1	0.2	0.3	0.5	0.75	1.0
Flux Density (lx)	2900	4680	6020	8120	9950	11200

Lamp intensity I_0 used for the plot, was computed using the manufacturers specification of 2850 lumens for a standard 1.2 metre long 1-inch tube. The surface of the lamp is $S_w = 2\pi r_0 L$. Thus if it is assumed that radiation is uniform over the entire surface, with

$r_0 = 0.0127\,\text{m}$

$L = 1.2\,\text{m}$

$\Phi = 2850\,\text{lm},$

then $I_0 = \dfrac{\Phi}{S} = \dfrac{2850\,\text{lm}}{2\pi \cdot 0.0127\,\text{m} \cdot 1.2\text{m}} = 29763\,\text{lux} \approx 30{,}000\text{ lux}.$

The calculation possesses no more than two-digit accuracy since L is approximated to be 1.2 m due to cathode fall at the ends of the tube. The effective length will be slightly less.

The graph is not very encouraging at this point. The measurement-equation (6.24) does not take into account the fact that the mirror reflection coefficient influences the chamber wall intensity directly. Thus the intensity at a point on the wall is not due to flux arriving from a uniform infinitely long chamber, as was assumed. Rather, the intensity of the virtual chamber wall decreases with distance from the chamber centre.

In reality, what is measured is a proportion F of the intensity of an infinitely long real chamber or lamp, due to the reduced intensity of the virtual part of the chamber. The proportion F will be approximated by integrating over the real- and virtual-chamber

surface to infinity, and then taking the ratio with the integral of an infinitely long real chamber.

The mirrors will have the effect of reducing the intensity in the virtual, and hence the real chamber. A point at the centre of the chamber will be surrounded by the real chamber immediately on both sides while a point at the edge (near a mirror) will experience the real chamber on one side only. This point then is expected to have a slightly lower intensity. It has already been assumed in the calculations that flux is constant throughout the real chamber. Therefore any small variations in intensity along the wall of the real chamber will be ignored.

Equation (6.24) must be adjusted by the factor F to take into account the reduction of overall measured intensity caused by mirrors with $f_{m} < 1$. The chamber radius differs significantly from the lamp radius, so that a unique factor F is required for each, namely F_{w} and F_{L}, for the chamber wall and lamp respectively.

These proportionality factors have been calculated for several interval sizes by integrating over each interval and summing the contributions of all intervals. Microsoft Excel was the software package used to perform the summation of intervals. Equations (6.25) below were programmed into a spreadsheet.

$$I_{\hat{r},\text{wall}} = I_0 \left(1 - \frac{4}{\sqrt{d^2 + 4}\left(d^2 + 2 + d\sqrt{d^2 + 4}\right)} \right)$$

$$+ f_m 2I_0 \left(\frac{1}{\sqrt{9d^2 + 4}\left(9d^2 + 2 + 3d\sqrt{9d^2 + 4}\right)} - \frac{1}{\sqrt{25d^2 + 4}\left(25d^2 + 2 + 5d\sqrt{25d^2 + 4}\right)} \right)$$

$$+ f_m{}^2 \left[\cdots \right.$$

$$I_{\hat{r},\text{lamp}} = \frac{2}{\pi} I_0 \frac{1}{\rho} \left(\tan^{-1} \frac{2d}{\rho-1} + \frac{2d(\rho-1)}{4d^2+(\rho-1)^2} \right) - \frac{4}{\pi} I_0 \frac{1}{\rho} \left(\tan^{-1} \frac{d}{\rho-1} + \frac{d(\rho-1)}{d^2+(\rho-1)^2} \right)$$

$$+ f_m \left[\frac{2}{\pi} I_0 \frac{1}{\rho} \left(\tan^{-1} \frac{4d}{\rho-1} - \tan^{-1} \frac{2d}{\rho-1} + \frac{2d(\rho-1)}{4d^2+(\rho-1)^2} + \frac{16d^2(\rho-1)}{16d^2+(\rho-1)^2} \right) - \frac{2}{\pi} I_0 \frac{1}{\rho} \left(\tan^{-1} \frac{2d}{\rho-1} + \frac{2d(\rho-1)}{4d^2+(\rho-1)^2} \right) \right]$$

$$+ f_m^{\,2} \left[\cdots \right. \tag{6.25}$$

Since the integrand is an even function, only one half of the chamber was evaluated and the result doubled. The factor $1/\pi$ is the normalization constant.

The dependence on interval size was then graphed using equations (6.25) with a value for mirror reflectance $f_m = 0.845$, which is the average between the reflectance of the Perspex mirror and the glass mirror. The relative flux density at the centre of the chamber can be read from the respective graph by selecting the appropriate interval size. See Figure 6-10 and Figure 6-11 below (a separate graph was produced for the lamp, since the situation of the lamp is not identical with that of the chamber, the reason being the difference in ratio of radius to length).

The chamber equation (6.24) becomes

$$I_m = F_w \cdot I_{r,w} + \frac{1}{\rho} \cdot F_L \cdot I_0$$

i.e.
$$I_m = \frac{1}{\rho} \left(F_w \Gamma \frac{f_w}{\Gamma(1-f_w)+(1-f_m)} + F_L \right) I_0. \tag{6.26}$$
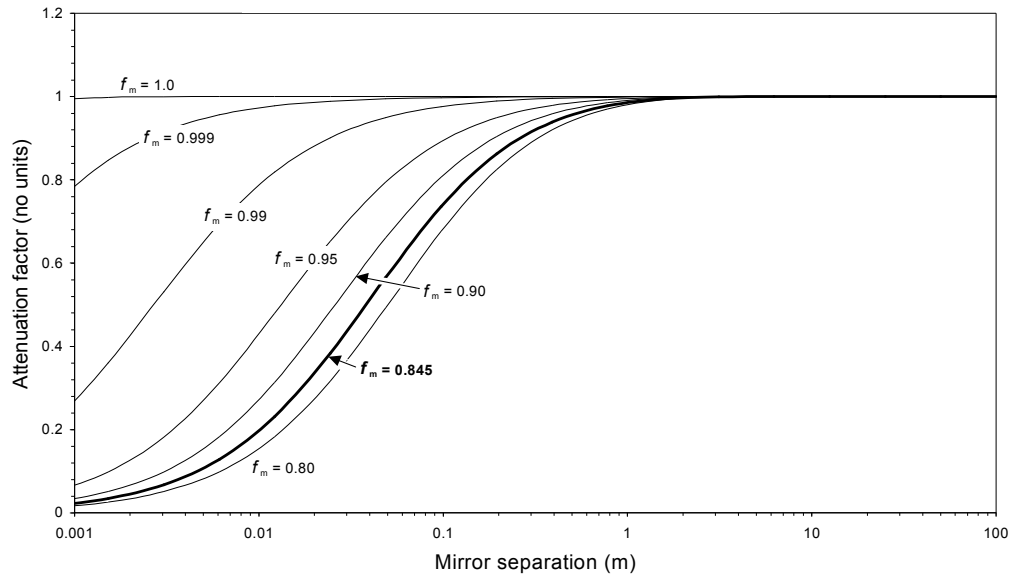
Figure 6-10

A plot of the chamber attenuation factor F_w. Note the logarithmic horizontal scale.
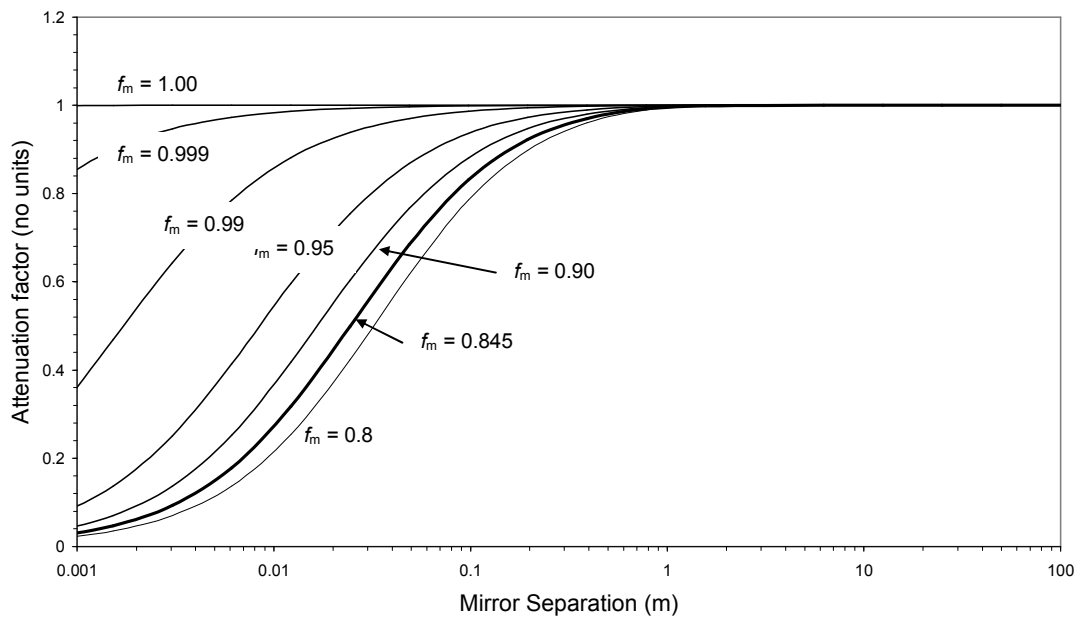
Figure 6-11

A plot of the lamp attenuation factor F_L.

It is worth again comparing theory with measurement. See Figure 6-12 below.
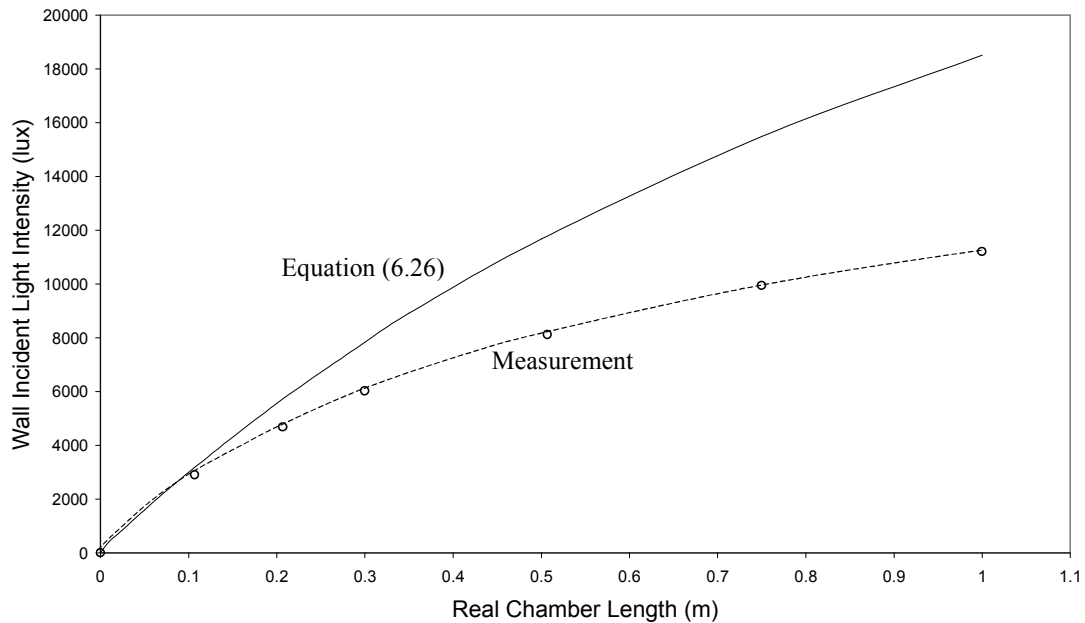
Figure 6-12

A plot of measurement equation (6.26), which includes mirror absorption. Note the improved correlation for small chamber lengths of $L < 0.1$ m.

It seems certain that the two curves above approach widely differing asymptotic values as the chamber length L increases, indicating some fundamental shortcoming in the analysis thus far.

Clearly more light than expected is being absorbed somewhere within the chamber. Some possible reasons were investigated: If the mirrors were responsible, then their effect should reduce as L is increased. Mirror absorption cannot therefore account for the asymptotic discrepancy.

The lamp may be responsible for some re-absorption of light. The curves in Figure 6-12 above diverge as chamber length increases, suggesting that the theoretical value for

infinite L is significantly larger than the expected measurement. The lamp would have absorbed some of its own light. Lamp re-absorption could not be excluded but it was concluded that such a phenomenon would have far less effect than what was observed.

By elimination, it must be concluded that the diffuse paint is absorbing more light than is expected, for longer chamber lengths, indicating that the paint reflectance is not as close to unity as the value quoted by Plascon.

It is expected that the effective paint reflectance will vary slightly with the chamber length, in the following way:

Consider a mirror of high absorption coefficient with a beam of light incident on it at some angle θ. As the angle of the incident beam increases, the component normal to the mirror surface decreases. This component is the only portion of the incident beam that is attenuated by the mirror. As θ approaches 90°, more of the beam is reflected and less is absorbed until at 90°, the entire beam passes along the mirror surface parallel to it, and is then not reflected or absorbed in any way. The reflection is specular. Such behavior can easily be observed when a sheet of glass is held at an angle to the eye. Beyond a certain angle, an image of the surroundings may be observed as reflected off the surface.

Now consider a black diffuse surface with $f = 0$, in the same way. Almost no light is reflected at a large angle. The surface still appears black. Even when the ray is almost parallel to the surface, virtually all of the ray energy is absorbed. There is no cosine dependence. This demonstrates the fact that a diffuse surface does not absorb a portion of the perpendicular component only, but of the entire incident ray. Furthermore, the entire ray is scattered upon reflection.

In the calculations, the integration has treated the chamber surface as specular, using the $\cos \theta$ function to satisfy the requirements of the measurement sensor. This is still acceptable insofar as the beam area on the surface increases with θ as $1/\cos \theta$, and therefore the summing at a point is correct. But absorption does not take place on a

component only, as is the case with specular reflection, where the component parallel with the surface is excluded from absorption. It is the whole ray that is subjected to absorption. Therefore the factor cos θ must be excluded.

Of course, the absorption coefficient of the paint is only 0.03, so that the effect might not be expected to be large. But the measurement equation is very sensitive to the paint reflectance (and hence the absorption coefficient), as shown in Figure 6-13 below.
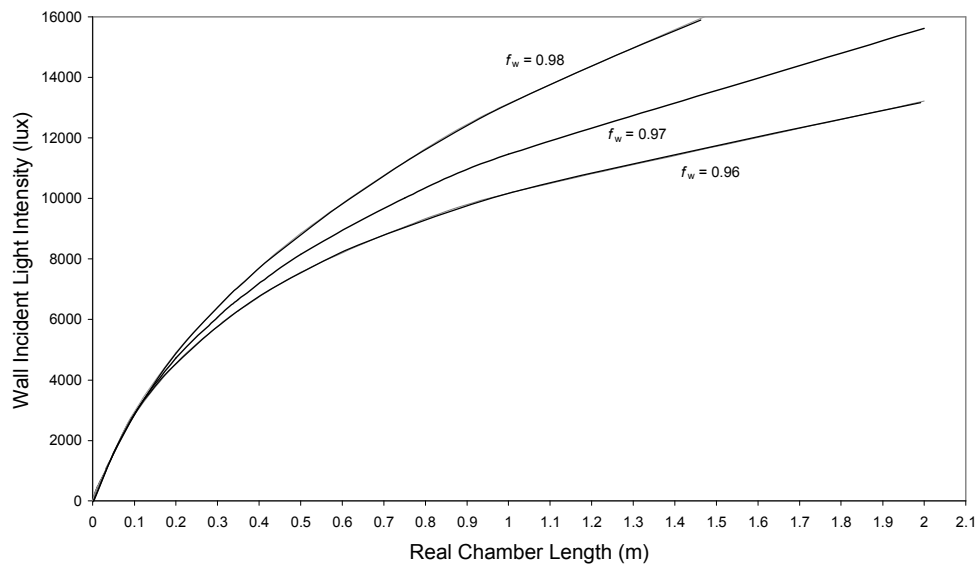
<u>Figure 6-13</u>

A plot of equation (6.26) for several values of chamber wall paint reflectance. Note
how sensitive the function is to small changes in wall-paint reflectance.

A convenient way to adjust the measurement equation, without introducing complicated statistics, is to vary the paint reflectance coefficient with the chamber length. Indeed, it is the absorbed flux which is greater due to increased relevant incident intensity after exclusion of the factor cos θ. For an infinitely long real chamber, it can be shown that the incident intensity in this case should be exactly twice the value relevant to a specular surface. See Appendix H. With the maximum value of f_p set at 0.97 (and absorption

coefficient $a_p = 0.03$), f_p can be adjusted down to $f_p = 0.91$ ($0.91 = 0.97 - 2 \times 0.03$). Figure 6-14 below shows a plot of the measurement equation with revised f_p, while Figure 6-15 shows the manually adjusted effective paint reflectance f_p used to obtain the improved agreement of theory with measurement.
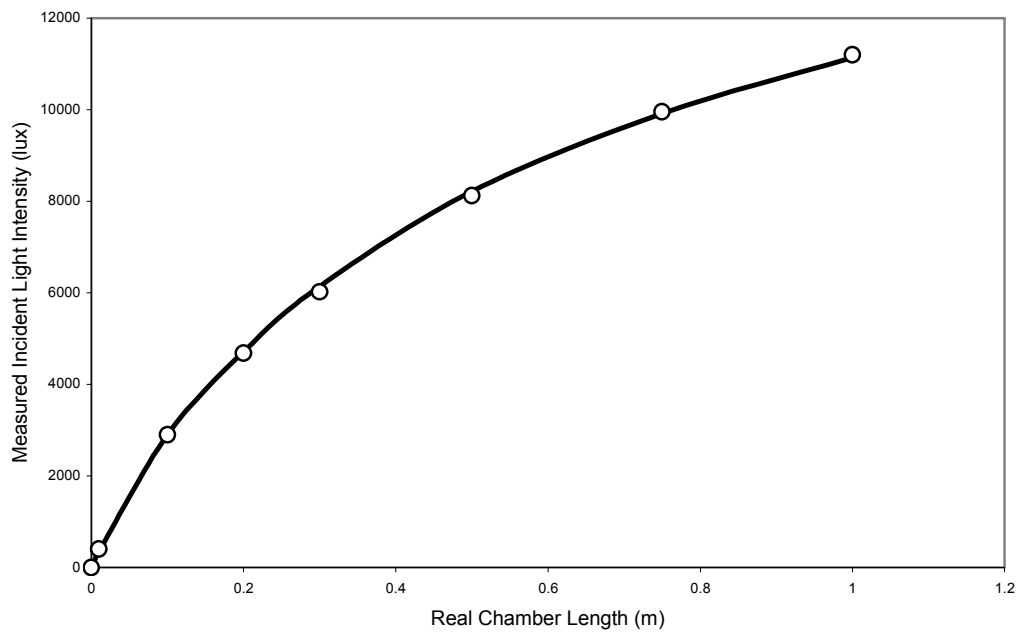
<u>Figure 6-14</u>

A plot of the improved measurement equation, with paint reflectance adjusted.
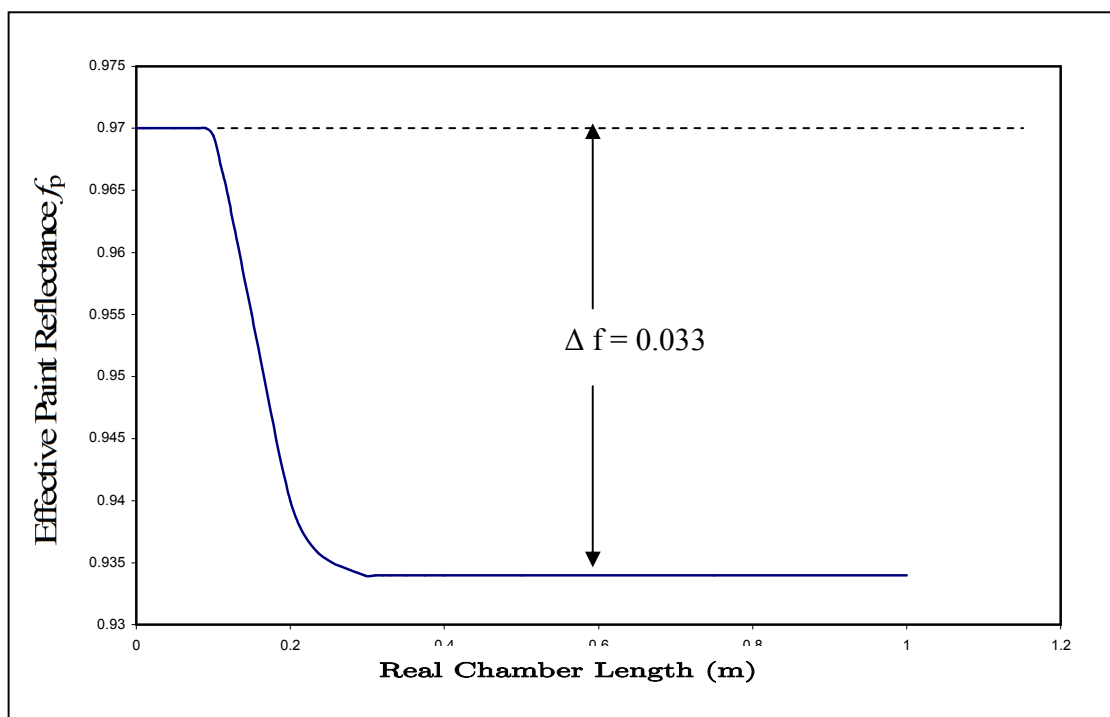
Figure 6-15

A plot of the effective paint reflectance as a function of chamber length.

There may be several reasons why the difference between the maximum of 0.97 and the minimum of 0.935 is not quite twice the value of the absorption coefficient. Fore-mostly, the paint absorption may actually be lower than expected at larger incident angles, due to irregularities in the painted surface, or microscopic properties of the paint. The paint is not perfectly diffuse, as shown in Figure D-2 of Appendix D.

The Figure 6-15 above was produced by a manual adjustment of the paint reflectance f_p. It turns out that there is a straightforward way to quantify the adjustment if one small approximation is made.

The measurement equation is presented in terms of the reflected flux, since it is what is measured by the light-meter. A factor k will be introduced to reduce the reflected flux, and then k will be quantified.

The reduced reflected flux must be linked with the increased effective incident flux on which absorption takes place, due to exclusion of the cosine function. This will be done via the absorbed flux.

The larger incident flux involved in Lambertian absorption will be regarded as the new flux, while the original cosine-corrected incident flux will be regarded as the old incident flux. Clearly

$$\Phi_{i,new} = \frac{\Phi_{i,new}}{\Phi_{i,old}} \Phi_{i,old} \, .$$

The ratio $\dfrac{\Phi_{i,new}}{\Phi_{i,old}}$ appears as a correction factor for calculating the new larger effective incident flux in terms of the original incident flux, thereby avoiding complicated backtracking in the calculations in an attempt to exclude the cosine function. In other words, the present cosine model is preserved but effective incident flux is increased, i.e.

$$\Phi_{i,new} = k_a' \Phi_{i,old} \tag{6.27}$$

There is no way to change the incident flux in the measurement equation directly, since there is no incident flux term present.

The constant k' will be connected with the measurement equation, through the absorbed flux since reflected flux can be written in terms of the absorbed flux. The new absorbed flux will be

$$\Phi_{a,new} = a\Phi_{i,new}$$

$$= a\left(k_a'\Phi_{i,old}\right) = \left(ak_a'\right)\Phi_{i,old}$$

Thus k' can be viewed as a correction factor for the absorption coefficient, if the original incident flux is used.

Consider the flux reflected from a surface, from equation (6.21):

$$\Phi_r = \frac{f}{1-f} \Phi_a$$

The reflectance can be written in terms of the absorption coefficient a:

$$\Phi_r = \frac{1-a}{a} \Phi_a$$

The correction factor will now be introduced through the absorption coefficient. The new reflected flux is

$$\Phi_{r,new} = \frac{1-k'a}{k'a} \Phi_a .$$

It will be shown further on that k' ranges between 1 and 2. Since $a = 0.03$, $k = 0.06 \ll 1$. Therefore the change in the numerator is much less than the change due to k in the denominator. The maximum change due to k' in the numerator, is 3%, while the maximum change due to k' in the denominator, is 100%. The change in the numerator will be considered as negligible, in order to make the calculation manageable. However, it must be considered that the final measurement equation will exhibit a possible 3% maximum error for a long chamber. But it will be further shown that this error can be "tuned out" by a very small adjustment of the paint reflectance.

Thus

$$\Phi_{r,new} \approx \frac{1-a}{ak'}\Phi_a = \frac{1-a}{a}k\Phi_a$$

where
$$k = \frac{1}{k'}$$
(6.28)

Here k can be seen as a proportionality coefficient, operating on absorbed flux, to reduce reflected flux.

$$\Phi_{r,\,new} \approx k\frac{1-a}{a}\Phi_a = k\Phi_{r,\,old}$$

The light intensity of the chamber wall becomes

$$I_{r,\,new} \approx kI_{r,\,old}$$

and thus the measured intensity is

$$I_m \approx kF_w \cdot I_{r,w} + \frac{F_L}{\rho} \cdot I_L.$$

The reflected flux must be adjusted by the correction factor k. From equation (6.27) it is shown to be the ratio between old and new effective incident flux. The old flux is the sum of contributions of chamber wall flux from all real- and virtual-chamber intervals, with cosine correction included, while the new flux is the sum of contributions with no cosine correction. Factor k can be calculated as a function of the chamber length.

$$k(L) = \frac{\sum\limits_{\text{Interval}} \int f(S)\cos\gamma \, dS}{\sum\limits_{\text{Interval}} \int f(S) \, dS} = \frac{F_w(L)}{F_a(L)}$$

Here $\gamma = 90° - \theta$ is used as the angle of incidence rather than θ, in order to prevent confusion with the notation for spherical coordinates. The variable S has been used here for area, in order to avoid confusion with the absorption coefficient a.

The function $f(S) = f((S(\theta))$ is calculated from the flux contribution of a ray from any point on the chamber wall, using spherical coordinates. However, the dependence on azimuthal angle ϕ cancels out in the ratio, so that it is not necessary to include it in $f(S)$.

It should be noted that since k is a ratio of the sums of integrals, the actual intensity of the wall cancels out, so that k depends only on the dimensions of the chamber, and reflection coefficients.

The function $\int f(S)\cos\theta \, dS$ in the numerator is simply equation and after summation over intervals, the numerator is just F_w. The function $f(S)$ can easily be shown to be

$$f(S) = f(S(z,\theta)) = \frac{R\cos\theta - r_0}{\left(z^2 + R^2 + r_0^2 - 2Rr_0\cos\theta\right)^{\frac{3}{2}}}$$

The function $f(S)$, turns out to have square-roots of polynomials in the denominator, and was therefore integrated numerically, using the Trapezoid Rule [16]. Figure 6-16 shows a portion of the denominator F_a of k.
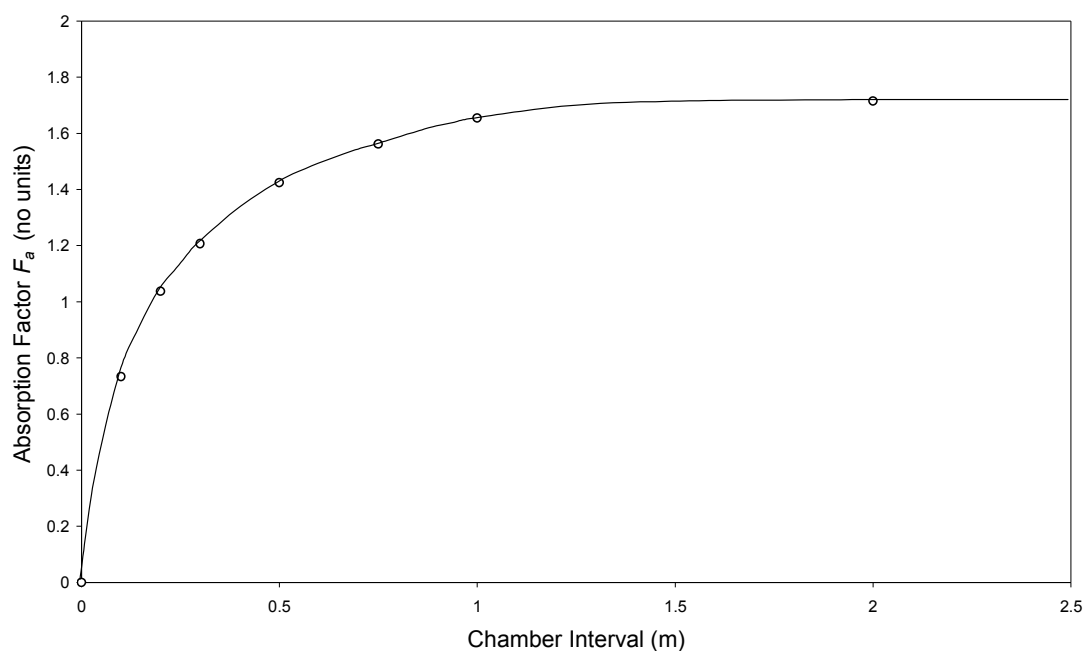
Figure 6-16

A plot of the chamber absorption factor F_a. The theoretical asymptotic value is $F_a = 2$. The value of $F_a = 1.7$ at $L = 2$, is not asymptotic by any means.

In the limit as $L \to \infty$, the theoretical value of the factor k becomes $k = 0.5$ exactly. It is shown in appendix G that k' has a maximum value of $k' = 2$. Since k is just the inverse, from equation (6.28), k has a minimum value of $k = 0.5$. The approximate value of $k = 0.58$ beyond $L = 2.5$, is by no means asymptotic. The curve levels off to some degree, but, beyond the plotted portion for L up to 2.5 m in Figure 6-17, will gradually progress toward the asymptotic value of $k = 0.5$, as $L \to \infty$. As the chamber becomes shorter, the factor k approaches unity, the correct theoretical value; i.e. $L \to 0$ as $k \to 1$. A plot of the function follows.
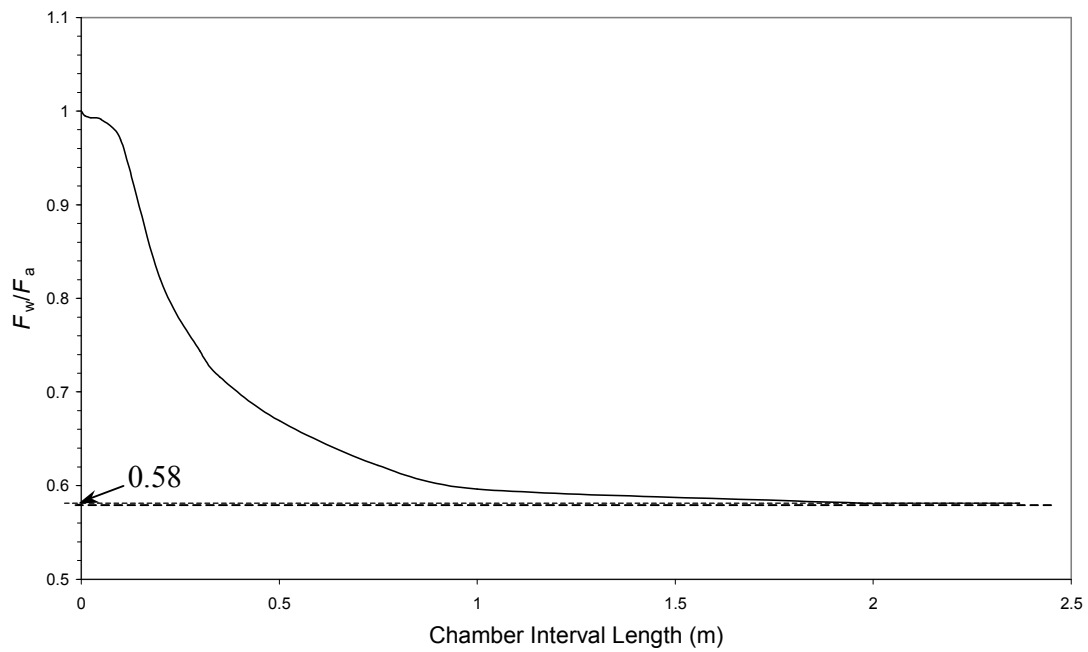
Figure 6-17

A plot of the absorption correction factor k, up to $L = 2.5$m. Note that the dotted line indicating the value of $k = 0.58$, at $L = 2.5$ m, is not an asymptote. The asymptote lies at $k = 0.5$.

The improved equation has the following form

$$I_{\mathrm{m}}(L) = k(L)F_{\mathrm{w}}(L) \cdot I_{\mathrm{r,w}} + \frac{F_{\mathrm{L}}(L)}{\rho} \cdot I_0$$

$$= \frac{1}{\rho}\left(k(L)F_{\mathrm{w}}(L)\Gamma(L)\frac{f_{\mathrm{w}}}{\Gamma(L)(1-f_{\mathrm{w}})+(1-f_{\mathrm{m}})} + F_{\mathrm{L}}(L) \right)I_0 \qquad (6.29)$$

and is plotted below in Figure 6-18.
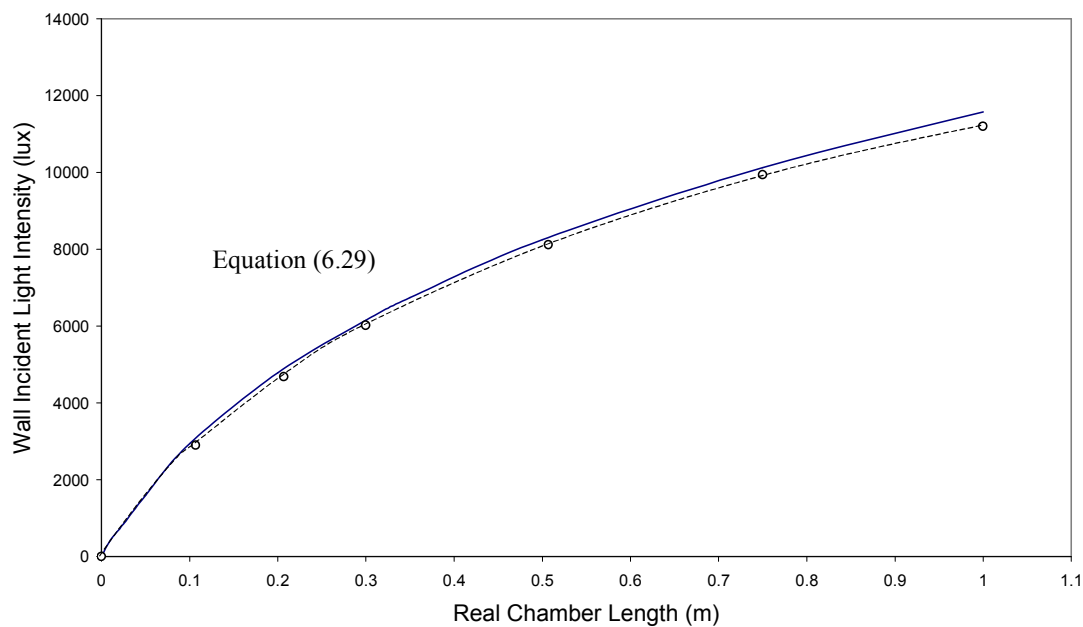
Figure 6-18

A plot of the measurement equation (6.29), which includes absorption-correction. The solid line
corresponds to the measurement equation and the dashed line represents the measured results.

An improved fit between the theoretical result and the experimental data may be obtained
as shown in Figure 6-19 by adjusting the reflectance coefficients of the wall and mirrors.
See Table 6.2. The adjustment for the mirrors occurs within experimental error of the
reflectance of the Perspex- and glass-mirror. The paint reflectance adjustment also occurs
within specification accuracy.

Table 6.2

The reflectance adjustment for the cylinder wall and end-mirrors

Parameter	Measured/specified	Adjusted
f_w	0.97	0.969
f_m	0.845	0.842
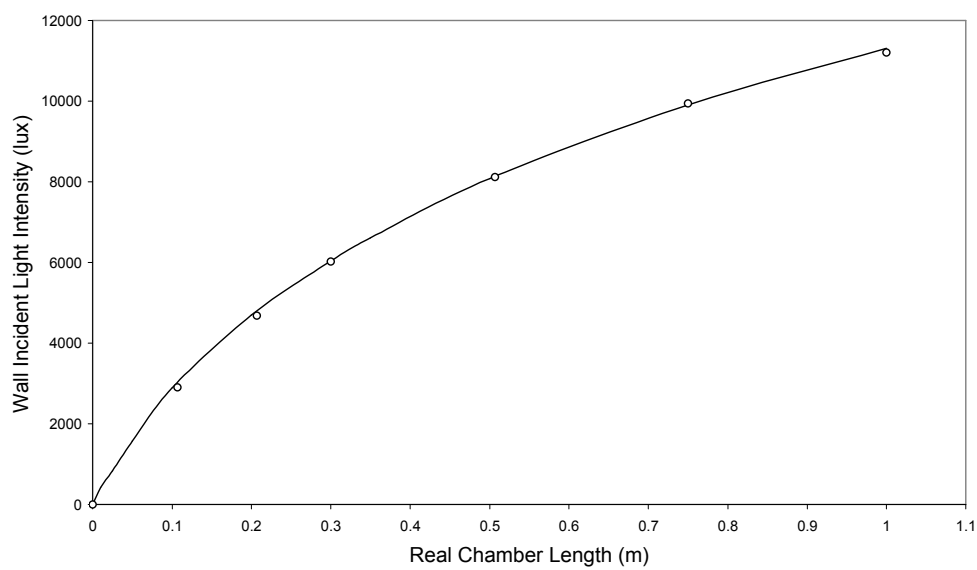
Figure 6-19

A plot of the improved measurement equation (6.29), with adjusted reflectance. The wall-paint reflectance and the mirror reflectance were each adjusted by approximately 0.1%.

Equation (6.29) is more useful when written in terms of lamp flux Φ_L. From the intensity

$$I_m = \frac{1}{\rho} \frac{kF_w \Gamma f_w + F_L \left[\Gamma \left(1 - f_w\right) + \left(1 - f_m\right) \right]}{\Gamma \left(1 - f_w\right) + \left(1 - f_m\right)} I_L$$

$$\Rightarrow I_L = \rho \frac{\Gamma \left(1 - f_w\right) + \left(1 - f_m\right)}{kF_w \Gamma f_w + F_L \left[\Gamma \left(1 - f_w\right) + \left(1 - f_m\right) \right]} I_m \,,$$

the lamp flux is

$$\Phi_L = I_L \cdot 2\pi r_0 L = 2\pi RL \frac{\frac{L}{R}\left(1 - f_w\right) + \left(1 - f_m\right)}{kF_w \frac{L}{R} f_w + F_L \left[\frac{L}{R}\left(1 - f_w\right) + \left(1 - f_m\right) \right]} I_m$$

$$= 2\pi RL \frac{L\left(1 - f_w\right) + R\left(1 - f_m\right)}{kF_w L f_w + F_L \left[L\left(1 - f_w\right) + R\left(1 - f_m\right) \right]} I_m.$$

$$\Phi_L = 2\pi RL \frac{L.\left(1 - f_w\right) + R.\left(1 - f_m\right)}{L\left[k\left(L\right).F_w\left(L\right) f_w + F_L\left(L\right).\left(1 - f_w\right) \right] + F_L\left(L\right).R.\left(1 - f_m\right)} I_m. \tag{6.30}$$

Equation (6.30) is the so-called *measurement equation* (see the self-study manual by NIST, Part 1 *Preface*, page iii. [17]).

6.6 Calculations

As an example of using the chamber, a sample calculation follows. The chamber that was built for this analysis had a radius of 28.5 cm, and was coated with a white Plascon Road-

paint with a photometric reflectance of $f_p = 0.97$. A lamp with a rated intensity of 2850 lm was mounted inside the chamber.

The chamber length was set up at 1.00 m. An intensity of 11200 lx was measured at the centre of the chamber, with the sensor mounted on the wall, facing the lamp. From the relevant charts of Figure 6-10 and Figure 6-11, corresponding to a chamber length of 1.00 m,

$F_L = 0.994$

$F_w = 0.982$

Using the above values in equation (6.30) produces a lamp light power of $2386\,lm$ emitted from a lamp of length 1.0 meter. A 1.2 metre long lamp will emit $2863\,lm$.

The calculated value is slightly higher than the rated value of 2850 lumens, suggesting an effective length of $L = 1.195$m, about 0.5 cm less, due to cathode fall.

The next calculation shows how the lamp efficacy may be obtained from a light intensity measurement.

Suppose that a lamp of length 1.2 m, and a power rating of 36 W has a total flux output of 2850 lumens. Then the lamp efficacy is

$$f = \frac{2850\,\text{lm}}{36\,\text{W}} = 79.2 \ \text{lm.W}^{-1}$$

The lamp efficacy can be used to calculate electrical efficiency. For a spectrum identical with the human eye sensitivity curve

$$1 \ \text{W} = 683 \ \text{lm}$$

or
$$1 \text{ lm} = \frac{1}{683} \text{ W} .$$

The incandescent lamp has a spectrum shape not very different from the sensitivity curve shape of the human eye so that statistically, the incandescent lumen is approximately the same.

$$1 \text{ lm}_{inc.} = \frac{1}{683} \text{ W}$$

The lux-meter adjusts the light level by a factor of 0.95 between incandescent and fluorescent settings. Thus

$$1 \text{ lm}_{fl.} = \frac{1}{0.95 \cdot 683} \text{ W} \approx 0.0015 \text{ W}$$

$$79.2 \text{ lm} = 79.2 \cdot 0.0015 \text{ W} \approx 0.12 \text{ W}.$$

That is, only 12 % of the total electrical power is converted to light visible by the human eye. The electrical power consumption is rated at 36 W. The efficiency of the lamp is therefore about 12 %. This is to be compared with the efficiency of a 40 W incandescent light bulb which has a typical efficiency of 2 %. The fluorescent lamp is therefore about 6 times more efficient than an incandescent light-bulb with a similar electrical power rating.

6.7 Final Error Considerations

The chamber length of $L = 0.1$m is a practical size for local measurement. Local accuracy improves as the interval width is reduced but the lux-meter sensor must be accommodated between the mirrors. Errors will therefore be referred to a chamber with a length of 0.1 m.

At $L = 0.1$m the measured value was 2900 $\pm$10 lux. The error of $\pm$10 lux is due to drift (with time, of the lamp or sensor). The calculated value is 2897 lux for the chosen value of $f_w = 0.969$ and is not very dependent on f_w for small L. The average error is 3 lux, less than 0.2%, and is well within the drift error quoted above. Any further error analysis would require the source of drift to be quantified, prevented or nulled, in combination with many more measurements.

7. Conclusions and Suggestions

7.1 Conclusions

It has been shown that the cylindrical chamber can be successfully quantified, using only a handful of physical and mathematical tools. By applying several acceptable assumptions and logical mathematical deductions, an absolute value for the light power was obtained without resorting to statistical methods. The dynamics of the light profile within the chamber have been revealed, and the combination of a diffuse wall along with specular end-mirrors provides a chamber that can be characterized for tubular lamps.

Figure 6-19 reveals that the measurement equation (6.30) agrees favorably with experimental results. The variation of measured lamp flux with chamber length has been modeled successfully, by using realistic physical arguments, pertaining to the geometry of a cylindrical diffuse chamber, incorporating specular mirrors at the ends.

This dissertation has successfully described the reflection dynamics within the cylindrical chamber, to the end that the chamber can be utilized to obtain the efficiency of a cylindrical fluorescent lamp. The Monte Carlo method (see Section 6.1) will almost certainly reveal a more accurate measurement factor after some computation. However, if the Monte Carlo method had been employed from the start it would not have revealed many of the chamber dynamics.

Paint with high reflectance has successfully enhanced the level of measurable light within the chamber. The paint diffusivity has significantly scattered light throughout the chamber, to the extent that an acceptable degree of integration has taken place. It must be noted however, that the results of the experiment are quite sensitive to the paint reflectance coefficient, as shown in Figure 6-13.

In respect of the above statements, it can be concluded that the cylindrical chamber may be applied in the following areas:

- Research and Development testing of new cylindrical lamp designs.
- Pre-production testing of fluorescent lamps, to determine efficiency, and to determine cathode effects near the ends of the lamp.
- Production testing with a view to quality control.
- Market testing and comparison of lamp makes and models.
- Aftermarket testing to develop ageing profiles for lamps, as well as to determine the remaining lifetime of an installed lamp.

7.2 Suggestions

Front-coated mirrors would increase accuracy of the mathematical model and hence the results. Employing mirrors with high reflectance can reduce the error for intermediate values of chamber length. Front-coated mirrors are capable of achieving values of $f = 0.95$.

The Monte Carlo method is not restricted to tubular lamps. Combined with the mathematical tractability of the cylindrical chamber, the Monte Carlo method could be utilized to obtain a chamber measurement factor for various lamp forms.

With regard to paint reflectance sensitivity, it is important that a paint of high quality be used. The paint should have uniform reflectance, high textural consistency, must be capable of being applied evenly, preferably spray-able, must be washable and have little sensitivity to moisture.

Further investigation into the use of the cylindrical chamber should include tests on a variety of lamps, as well as a determination of the extent of dependence on spectral selectivity of the paint.

Appendix A

The experiment undertaken to determine mirror reflectance.

The basic requirement of this experiment is to compare light intensity from a fixed source with and without the mirror in the optical path. Mirror reflectance can then be calculated over the visible spectrum using these two quantities. Finally an average reflectance can be calculated over the effective spectral region.

 Refer to Figure A-1 for the following discussion of the apparatus.

The light source consists of an opalescent sheet in front an incandescent lamp, which is shielded within a blackened collimating tube. The combination of the opalescent sheet and the two apertures greatly reduces sensitivity of the system to path length. Only a small central portion of the opalescent sheet is "visible" to the spectrometer, and since brightness does not change with distance for a diffuse radiator, small offsets in path-length will not affect measurements.

 Two apertures of 5 mm diameter were utilized, with aperture-1 being placed as close as possible to the source.

The collimating tube serves several purposes. The opalescent sheet is remote from the lamp, thereby preventing bright zones and enhancing uniformity of intensity. Since it is made from plastic, it is also prevented from distortion due to heat in the immediate vicinity of the incandescent lamp. The tube prevents stray light from the outside from striking the opalescent sheet. Furthermore, the tube blocks stray light.

The internal surface of the tube is painted a matte black to reduce internal reflections, which can lead to rings of brightness at the opalescent sheet.

Light intensity was measured with the aid of a sweeping spectrometer so that an average could be calculated over the visual spectrum. The focusing lens concentrates the light from the aperture onto the spectrometer grating via the spectrometer aperture, which was set at 200 μm. The spectrometer-lens separation is a crucial dimension in the experiment. It is vital that the lens remains precisely in one position throughout the test.
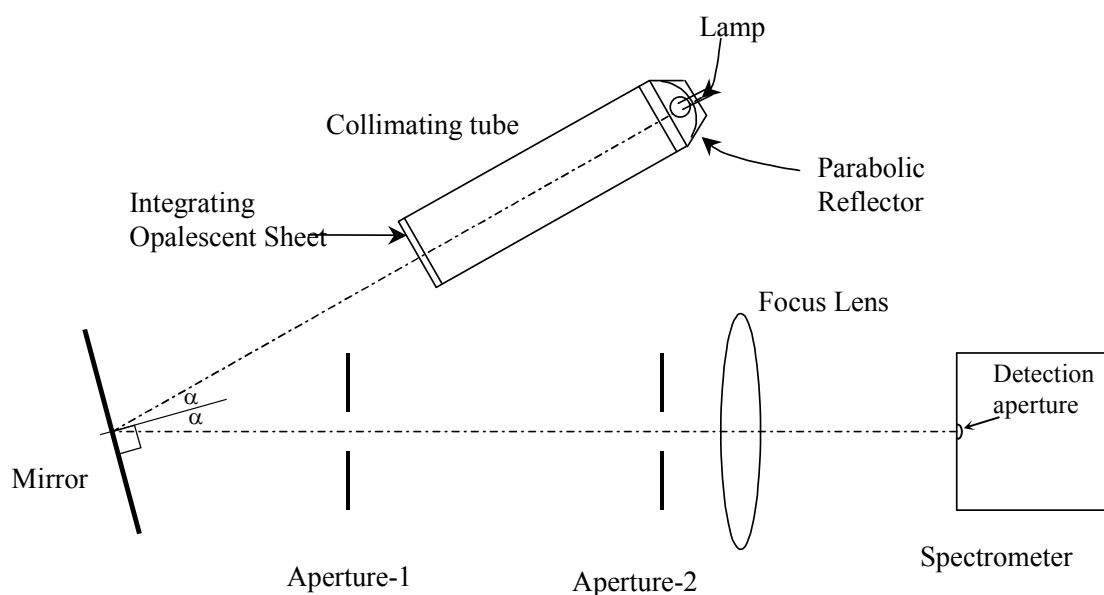
Figure A-1

The experimental setup used for measuring mirror reflectance. Source/mirror separation is 20 cm; mirror/aperture-1 separation is 10cm; aperture-1/aperture-2 separation is 20 cm; aperture-2/focus lens separation is 5 cm; focus lens/spectrometer separation is 10 cm; total path-length is 65cm.
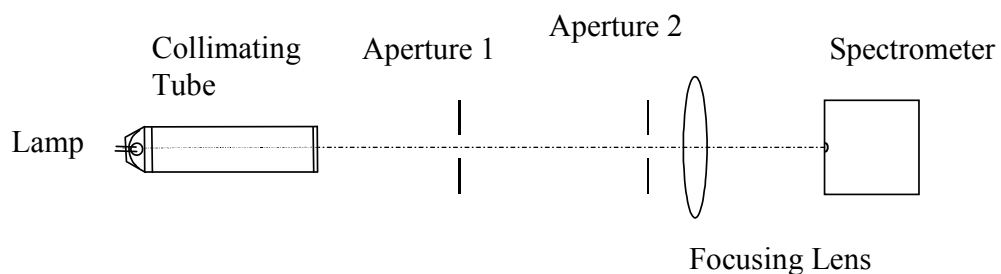
Figure A-2

The experimental setup used for measuring the intensity of a diffuse source. Source/aperture-1 separation is 30 cm; total path-length is 65 cm. All other relevant parameters are identical to those for the setup in Figure A-1.

The spectrum was swept across the light-band (λ = 4000 Å - 6600 Å) firstly with the mirror in place, and then without the mirror, in which case the collimating tube was lined up along the optical axis, at the same optical distance. Direct and reflected intensities are compared in Figure A-3 below.
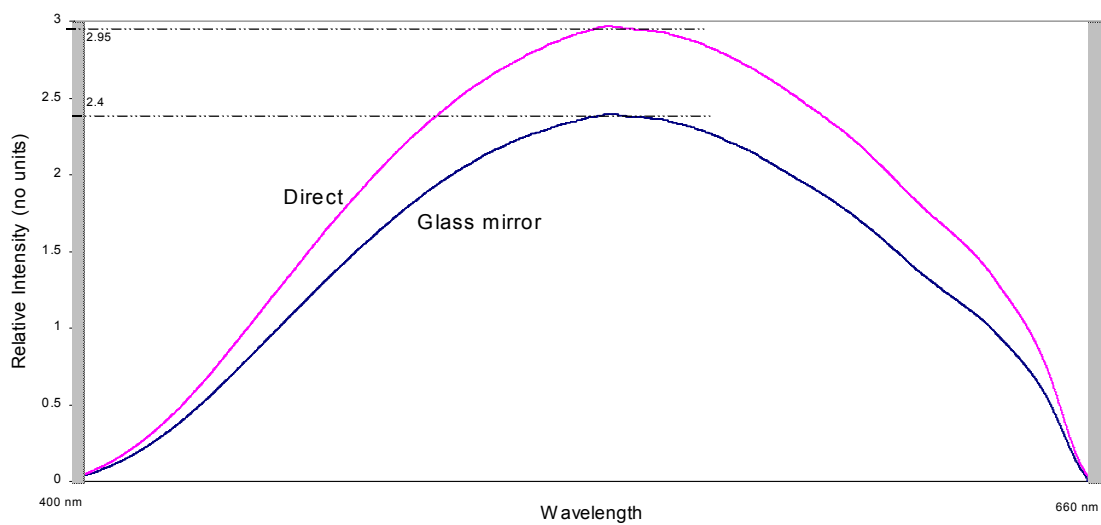
Figure A-3

A comparison of light levels with and without a glass mirror along the optical path. The intensity was measured by means of a sweeping spectrometer.

Both Perspex- and glass-mirrors were measured. Reflected light values were divided by direct light values to obtain reflectance as a function of wavelength. See Figure A-4 below.
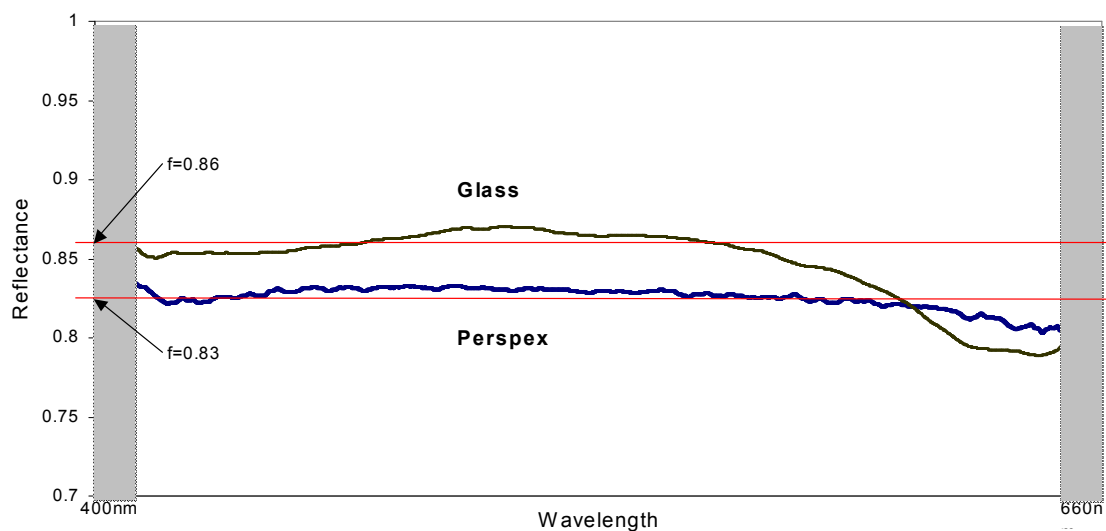
<u>Figure A-4</u>

A comparison of the measured reflectance for the glass and Perspex mirrors. The shaded regions represent data at wavelengths for which the spectrometer sensitivity is reduced, or for which the lamp emission is unreliably low.

The response of glass mirror is somewhat less uniform than for a Perspex mirror at the higher wavelengths (at the red end of the visual spectrum). Therefore, average values were calculated over the most linear part of the spectrum i.e. from 420 nm to 600 nm. A typical fluorescent lamp emits virtually almost all of its light power in this range. See Figure A5 below.
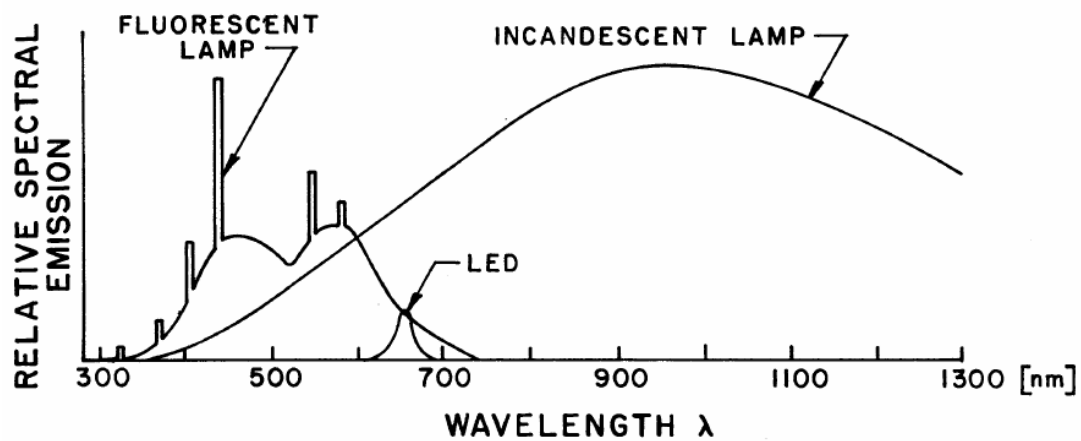
Figure A-5

The relative spectral emission profile of a typical fluorescent lamp. The curve is compared with the emission of an incandescent lamp.

The reflectances were calculated to be:

Perspex: $f_m = 0.83$

glass: $f_m = 0.86$.

One mirror in the chamber was made of glass while it was necessary to machine the second internal mirror. Perspex was chosen for the ease with which it can be machined. The average of the two reflectances is used in calculations:

Chamber mirrors: $f_m = 0.845$

Appendix B

Power dissipation of the paint.

The energy absorbed by the paint will be checked in terms of power dissipation density over the inner surface of the chamber, in order to quantify the power dissipation density of the paint. Any effects due to the mirrors will be ignored.

The chamber surface is much larger than the lamp surface and therefore lamp power dissipation need not be of concern. The cylinder radius is approximately 20 times larger than the lamp radius. The resulting cylinder area is larger than that of the lamp by the same factor since the wall area is proportional to the cylinder circular perimeter and hence radius.

It was shown in Section 6.6 that at typical lamp of length 1.2 m might radiate 4.3 W of light power. The area of the chamber is $A = 2\pi R L$ excluding mirrors. Using values of $R = 0.3$ m, $L = 1.2$ m one obtains an area of $A = 2.26$ m^2. Intensity is therefore

$$\frac{P}{A} = \frac{4.3 \text{ W}}{2.26 \text{ m}^2} = 1.9 \text{ W. m}^{-2}.$$

Appendix C

The Lambertian Probability Normalization Constant.

The constant $1/\pi$ will be obtained for a radiating point on a Lambertian surface.

Let the normal component of a Lambertian point source on a surface be $I_\perp = AI_0$ where A is the normalization constant and I_0 is the lamp surface intensity in $W.m^{-2}$. Integrating the probability over all possible directions in a hemisphere must yield a total probability of unity. The angle of the ray with the surface norm will be denoted as θ here rather than φ, to distinguish it from the rather similar-looking ϕ. For a Lambertian surface the probability density function is just

$$p_r(\theta) = \frac{\cos\theta}{r^2}$$

for some given r. (Refer to F. Mandl [18] for the statistical meaning of the probability density function). Thus

$$A\int_0^{2\pi}\int_0^{\frac{\pi}{2}} p_r(\theta).r^2\sin\theta d\theta d\phi = 1$$

i.e.

$$A\int_0^{2\pi}\int_0^{\frac{\pi}{2}} \frac{\cos\theta}{r^2}.r^2\sin\theta d\theta d\phi = 1$$

$$\Rightarrow A \int_{0}^{2\pi} \int_{0}^{\frac{\pi}{2}} \cos\theta \sin\theta d\theta d\phi = 1$$

$$\Rightarrow -\pi A \int_{0}^{\frac{\pi}{2}} \sin 2\theta d\theta = 1$$

$$\Rightarrow -\frac{\pi}{2} A \cos 2\theta \bigg|_{0}^{\frac{\pi}{2}} = 1$$

$$\Rightarrow \pi A = 1$$

$$\Rightarrow A = \frac{1}{\pi}.$$

Hence $I_{\perp} = \frac{1}{\pi} I_0$; i.e. the light intensity of a ray emitted from a Lambertian surface, in a direction perpendicular to the surface, is less than the surface intensity by a factor of $1/\pi$.

Appendix D

Paint diffusive profile measurement.

The method used here is one of comparison of light levels with and without a reflecting plane in the optical path.
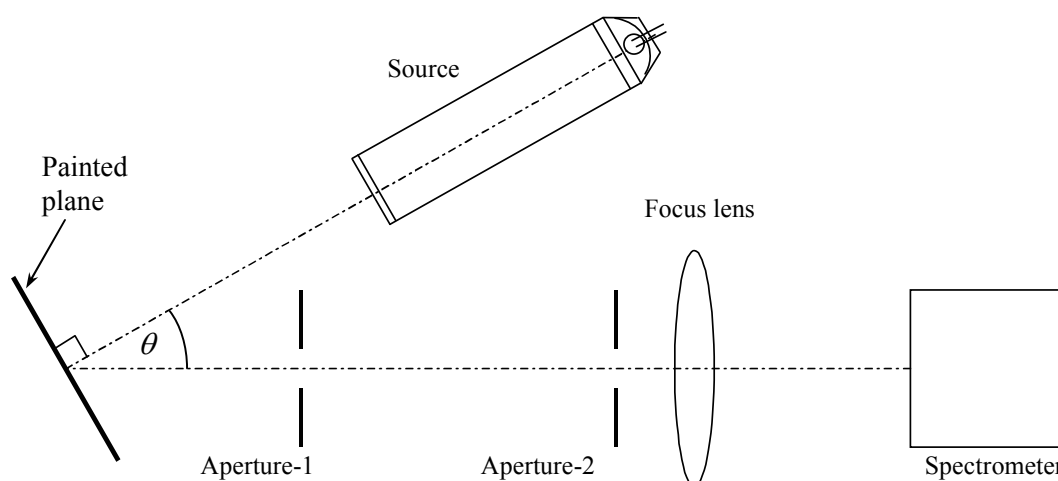
Figure D-1

The experimental setup used to measure angular dependence of paint reflectance.

An incandescent lamp was used because of the broad spectral emission compared with other lamps. The spectrum was swept across the light-band from 400 Å to 650 Å for several reflector angles. The collimating tube was lined up so that the incident beam was orthogonal to the reflecting surface.

The results are plotted in Figure D-2 below. Beyond an angle of about 60˚ with the norm the profile deviates from Lambertian. Nevertheless, the profile may comfortably be

regarded as Lambertian since the method of analysis leans strongly on the notion of orthogonal rays dominating the chamber characteristics.

The reason for deviation can largely be attributed to inconsistency of the applied matte paint. It is also well known that the microscopic spheres responsible for diffuse reflection cause a small enhancement of reflection flux density within a 5° cone centered about the incident ray, as documented by Delta Developments [7].

Orthogonal source, rotated reflector
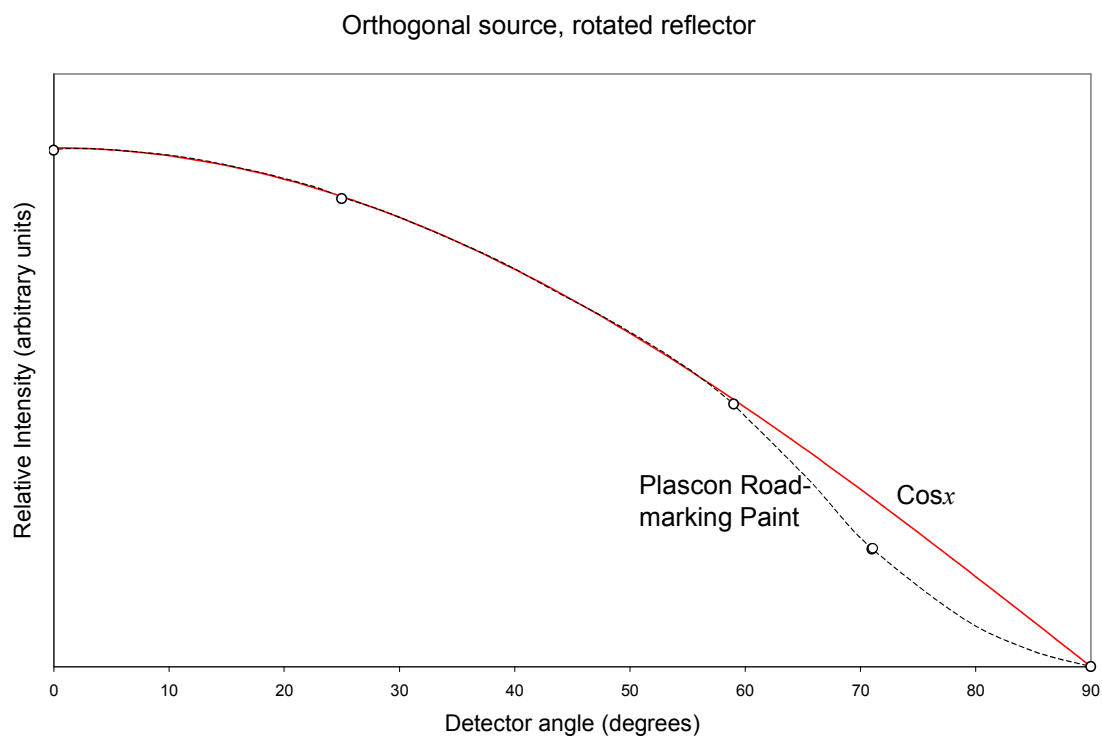
Figure D-2

A plot showing the diffusivity of white Plascon Road-marking paint. The data was obtained experimentally using the configuration of Figure D-1.

Appendix E

<u>*Definitions.*</u>

Many of the definitions were interpreted from the texts written by A. Stimson [19] and W. G. Driscoll [20].

Steradian: unit of solid angle. There are 4π steradians of solid angle in a sphere. Steradians cannot simply be marked off on a sphere surface, as radians can on a circle perimeter, since the surface area corresponding to one steradian can take on any shape.

Projection: precisely the mathematical definition. In vector form $\vec{u} \cdot \vec{v} = uv\cos\theta$ is the projection of $\vec{u}$ on $\vec{v}$. Projected area is equivalently the area of the shadow of a given area A, produced by a distant light-source. Shadow size will vary with the angle of area A, as $\cos\theta$.

Flux: energy transported across an area per-unit-time. From a theoretical perspective, flux is measured as *energy per-unit-time*, in units of *joules per second* (J/s). The SI unit is the *watt* (W). In the field of photometry, the *lumen* (lm) is adopted. The lumen, in comparison with the watt, is scaled up by a factor of at most 683 to account for the sensitivity of the human eye. Eye sensitivity changes with the frequency-distribution of light and is peaked or "centered" near 555 nm. If the measured light spectrum does not have the same form, a different factor must be calculated.

Flux density: flux-per-unit-area, or energy flow-rate per unit area. Measured as *power per-unit-area* in units of *watts per square meter* (W.m^{-2}), or in *lumens per square meter* (lm.m^{-2}) in photometry.

Intensity: the light energy passing through a surface area in space per unit time. In the context of this thesis, it is required that intensity be regarded is a *surface* density, not to be confused with the *radial* density of a *point source* in *watts per steradian* (W.sr^{-1}), referred to the source point only. The surface referred to formerly may be the finite emissive surface of a source. For a single point source, a surface flux density is meaningless, as is a radial flux density for a non-spherical source such as a cylinder wall surface. Intensity is measured in W.m^{-2} or W.sr^{-1}.

Luminous Intensity: the flux density of light, referred to the lumen. Measured as *lumens per-square-meter* (lm/m^2). The SI unit is the *lux.*

Illuminance: a measure of illumination level at a point and direction in space. By the Cosine Law of Illuminance, illuminance = intensity $\times \cos\theta$, where θ is the angle of the surface considered, with the flux direction. Thus illuminance is the projection of luminous intensity on a defined surface. Obviously maximum illuminance = luminous intensity. A simple comparison is the case of a small ball placed in the vicinity of a point source. The *luminous intensity* of light approaching any point on the illuminated side of the ball is essentially constant, while *illuminance* is a maximum at the centre, going off to zero on approach toward the circular illumination edge. Illuminance is measured as *power per-unit-area* in units of lumens.m^{-2}. The SI unit is the lux (lx) [21].

Lambertian: cosine emissive/reflective characteristic of a diffuse surface. Due to the diffuse nature of the surface, light is radiated in all directions, the statistical weights resulting in a factor $\cos\theta$ in the intensity formulation [22].

Luminance: projected effective luminous intensity of an emissive/reflective surface. If an area da on an emissive/reflective surface is observed at an angle θ with the norm, the area is effectively reduced by a factor $\cos\theta$, with the interpretation that there is an increase in point-source density in an equal projected area da. Therefore, it is possible for luminance to be greater than luminous intensity. However, in the case of a diffuse material surface, the projected intensity also is reduced by a factor $\cos\theta$ due to

Lambertian nature. The factors cancel, resulting in a projected surface with exactly the same intensity as for the perpendicular to the diffuse surface.

The term *luminance* is associated with observed light *from* an emissive/reflective surface while *illuminance* refers to the light *responsible* for the luminance of a reflective surface. Thus illuminance is an entity whether there exists a reflecting surface or not, while luminance of a uniform surface is a characteristic of the surface only, and is not a function of distance from the surface. In contrast, illuminance of such a surface varies with distance from the source and azimuthal angle of the source.

Brightness: Absolute brightness is the luminance of a diffuse material surface, while apparent brightness varies with the inverse square of distance. Note that brightness is a *scalar* quantity. It does not vary with angle of observation, due to the Lambertian nature of a diffuse surface. In contrast, the term 'brightness' cannot be ascribed to the surface of a mirror, since the projected intensity will certainly be directional.

Isoline: used in this document to denote a contour line representing axially symmetric surfaces of equal (luminous) intensity. The measured quantity is called *luminous intensity* as defined previously.

Reflection order: the number of reflections a ray of light undergoes before being measured.

Reflectance: the degree to which an incident ray is reflected by an *object*.

Reflectivity: the degree to which an incident ray is reflected by a *substance*. For example, the reflectivity of the glass in a thin glass mirror is much closer to unity than the reflectance, which occurs at the *surfaces* of the glass.

Appendix F

Evaluation of the chamber integral.

The integral for the light contribution of an interval of the cylindrical chamber to an observation point on the inner wall surface will be evaluated between the limits of integration in the complex domain. Much of the methodology is adopted from the books written by E. Butkov [23], and A. C. BajPai [24].

The integral δF over an interval between axial positions σ_1 and σ_2 is

$$\delta F_\sigma = \int_{\sigma_1}^{\sigma_2} F_\theta(\sigma)d\sigma$$

where F_θ is the angular integral obtained in Section 6.3.2. Equation (6.7) is repeated here:

$$F_\theta = \int_0^{2\pi} \frac{(1-\cos\theta)^2}{(1-p\cos\theta)^2}d\theta = \frac{1}{i}\int_0^{2\pi} \frac{\left(1-\frac{z^2+1}{2z}\right)^2}{\left(1-p\frac{z^2+1}{2z}\right)^2}\frac{1}{z}dz$$

with z as a variable in the complex plane. The angular integral F_θ will now be evaluated.

$$F_\theta = \frac{1}{i}\int_0^{2\pi} \frac{\left[2z-\left(z^2+1\right)\right]^2}{\left[2z-p\left(z^2+1\right)\right]^2 z}dz \quad \{\text{multiply by } \frac{z^2}{z^2}\}$$

$$= \frac{1}{i} \int_0^{2\pi} \frac{\left(z^2 - 2z + 1\right)^2}{\left(pz^2 - 2z + p\right)^2 z} dz$$

$$= \frac{1}{i} \int_0^{2\pi} \frac{\left(z - 1\right)^4}{\left(pz^2 - 2z + p\right)^2 z} dz .$$

Complete the square on the denominator:

$$pz^2 - 2z + p = p\left(z^2 - \frac{2}{p}z\right) + p$$

$$= p\left(z - \frac{1}{p}\right)^2 - \frac{1}{p} + p$$

$$= p\left[\left(z - \frac{1}{p}\right)^2 - \left(\frac{1}{p^2} - 1\right)\right]$$

$$= p\left(z - \frac{1}{p} + \sqrt{\frac{1}{p^2} - 1}\right)\left(z - \frac{1}{p} - \sqrt{\frac{1}{p^2} - 1}\right)$$

$$= p\left(z - \frac{1}{p} + \frac{1}{p}\sqrt{1 - p^2}\right)\left(z - \frac{1}{p} - \frac{1}{p}\sqrt{1 - p^2}\right)$$

$$= \frac{1}{p}\left(pz - 1 + \sqrt{1 - p^2}\right)\left(pz - 1 - \sqrt{1 - p^2}\right).$$

Hence

$$F_\theta(z) = \frac{p^2}{i} \oint_C \frac{(z-1)^4}{\left(pz-1+\sqrt{1-p^2}\right)^2 \left(pz-1-\sqrt{1-p^2}\right)^2 z} \, dz \ .$$

The closed integral is taken along a circle in the complex domain. [23, [24, 25, [26, [27, [28].

The poles are at $z = 0$, $z = \frac{1}{p} - \frac{1}{p}\sqrt{1-p^2}$ and $z = \frac{1}{p} + \frac{1}{p}\sqrt{1-p^2}$ on the real axis. The constant of integration p ranges from 0 up to 1.

Consider the third pole:

$$\frac{1}{p} + \frac{1}{p}\sqrt{1-p^2} \ > \ \frac{1}{p} + \frac{1}{p}.0$$

$$= \ \frac{1}{p} \geq 1$$

i.e.
$$\frac{1}{p} + \frac{1}{p}\sqrt{1-p^2} > 1.$$

The third pole therefore lies outside the contour.
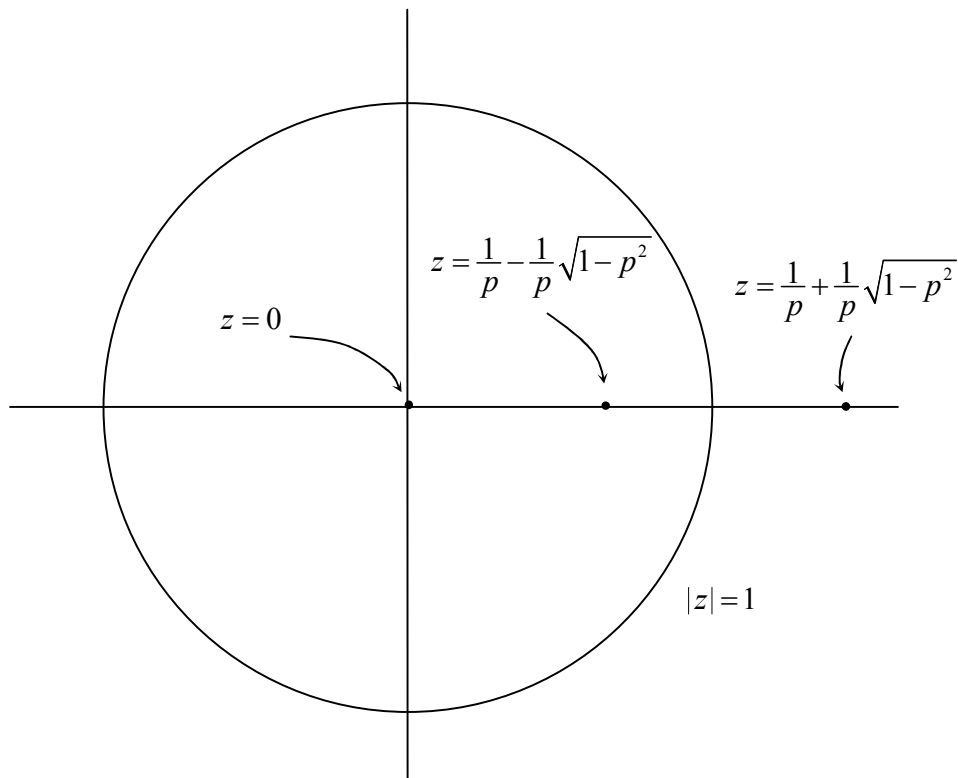
Figure F-1

The poles and the integration contour in the complex plane.

Consider the second pole:

$$\frac{1}{p} - \frac{1}{p}\sqrt{1-p^2} = \left(\frac{1}{p} - \frac{1}{p}\sqrt{1-p^2}\right) \cdot 1 \leq \left(\frac{1}{p} - \frac{1}{p}\sqrt{1-p^2}\right)\left(\frac{1}{p} + \frac{1}{p}\sqrt{1-p^2}\right)$$

$$= \frac{1}{p^2} - \frac{1}{p^2}\left(1-p^2\right)$$

$$= 1.$$

i.e.
$$\frac{1}{p} - \frac{1}{p}\sqrt{1-p^2} \leq 1$$

and thus lies inside the contour. The residue must be hence be evaluated at the simple pole $z_1 = 0$, and the pole $z_2 = \frac{1}{p} - \frac{1}{p}\sqrt{1-p^2}$, of second order. Let

$$f(z) = \frac{(z-1)^4}{\left(pz - 1 + \sqrt{1-p^2}\right)^2 \left(pz - 1 - \sqrt{1-p^2}\right)^2 z} \cdot$$

The residue at $z = 0$ is easily calculated:

$$\operatorname{Res} f(0) = \left. \frac{(z-1)^4}{\left(z - \frac{1}{p} + \frac{1}{p}\sqrt{1-p^2}\right)^2 \left(pz - 1 - \sqrt{1-p^2}\right)^2} \right|_{z=0}$$

$$= \frac{(-1)^4}{\left(-\frac{1}{p} + \frac{1}{p}\sqrt{1-p^2}\right)^2 \left(-1 - \sqrt{1-p^2}\right)^2}$$

$$= \frac{p^2}{\left(1 - \sqrt{1-p^2}\right)^2 \left(1 + \sqrt{1-p^2}\right)^2}$$

$$= \frac{p^2}{\left[1 - \left(1-p^2\right)\right]^2}$$

$$= \frac{p^2}{p^4}$$

$$= \frac{1}{p^2} \ .$$

The integral evaluated at the simple pole is then

$$F_{1\theta} = \frac{p^2}{i} 2\pi i \cdot \operatorname{Res} f_{\theta}(z_1)$$

$$= 2\pi \ .$$

Finding $\operatorname{Res} f\left(\frac{1}{p} - \frac{1}{p}\sqrt{1-p^2}\right)$ is not straightforward, as the pole is not of first order.

The denominators must be converted into a Taylor series, but for simplicity the pole shall

be transferred to the origin. Let $w = pz - 1 + \sqrt{1-p^2}$. Then $pz = w + 1 - \sqrt{1-p^2}$ and

$dz = \frac{1}{p} dw$ so that

$$F_{2\theta}(p) = \frac{p^2}{4} \frac{1}{p^2 i} \oint_C \frac{\left(w+1-p-\sqrt{1-p^2}\right)^4}{w^2 \left(w-2\sqrt{1-p^2}\right)^2 \left(w+1-\sqrt{1-p^2}\right)} dw$$

$$= \frac{1}{4i} \oint_C g(w) dw$$

where

$$g(w) = \frac{\left(w+1-p-\sqrt{1-p^2}\right)^4}{w^2 \left(w-2\sqrt{1-p^2}\right)^2 \left(w+1-\sqrt{1-p^2}\right)} \ .$$

$$F_{2\theta} = \frac{1}{4i} \cdot 2\pi i \operatorname{Res} g(0)$$

$$= \frac{\pi}{2} \operatorname{Res} g(0) \ .$$

The residue of $g(w)$ at $w = 0$ will now be evaluated.

$$\operatorname{Res} g(0) = \frac{d}{dw}\left(w^2 \cdot g(w)\right)\bigg|_{w=0}$$

$$= \frac{d}{dw}\left\{\frac{\left(w+1-p-\sqrt{1-p^2}\right)^4}{\left(w-2\sqrt{1-p^2}\right)^2\left(w+1-\sqrt{1-p^2}\right)}\right\}\bigg|_{w=0} \ . \qquad \text{(F1)}$$

It is convenient to represent the constant expressions as symbols. Let

$$a = 1 - p - \sqrt{1-p^2} \ , \qquad\qquad\qquad\qquad \text{(F2)}$$

$$b = 2\sqrt{1-p^2} \ , \qquad\qquad\qquad\qquad \text{(F3)}$$

$$c = \sqrt{1-p^2} - 1 \ . \qquad\qquad\qquad\qquad \text{(F4)}$$

The following interpretations will be required in the deductions.

$$a = 1 - p - \frac{b}{2} \qquad\qquad\qquad\qquad \text{(F5)}$$

$$b^2 = 4\left(1 - p^2\right) \qquad\qquad\qquad\qquad \text{(F6)}$$

$$c = \frac{b}{2} - 1.$$ (F7)

Then from equation (F1),

$$\text{Res } g(0) = \frac{d}{dw}\left(\frac{(w+a)^4}{(w-b)^2(w-c)}\right)\Bigg|_{w=0} , \quad b \neq 0, \quad c \neq 0$$

$$= \frac{-1}{b^2 c}\frac{d}{dw}\left(\frac{(w+a)^4}{\left(1-\frac{w}{b}\right)^2\left(1-\frac{w}{c}\right)}\right)\Bigg|_{w=0}$$

Expand the fractions as Taylor series, using the fact that $\frac{1}{1-t} = 1 + t + t^2 + \cdots$ for $|t| < 1$.

$$\text{Res } g(0) = \frac{-1}{b^2 c}\frac{d}{dw}\left[\left(w^4 + 4aw^3 + 6a^2w^2 + 4a^3w + a^4\right)\left(1 + \frac{w}{b} + \ldots\right)^2\left(1 + \frac{w}{c} + \ldots\right)\right]\Bigg|_{w=0}$$

$$= \frac{-1}{b^4 c^2}\frac{d}{dw}\left[\left(4a^3w + a^4\right)\left(b + w + \ldots\right)^2\left(c + w + \ldots\right)\right]\Bigg|_{w=0}$$

$$= \frac{-1}{b^4 c^2}\frac{d}{dw}\left[\left(4a^3w + a^4\right)\left(b^2 + 2bw\right)\left(c + w\right)\right]\Bigg|_{w=0}$$

$$= \frac{-1}{b^4 c^2}\frac{d}{dw}\left[\left(4a^3w + a^4\right)\left(b^2 c + b(2c + b)w\right)\right]\Bigg|_{w=0}$$

$$= \frac{-1}{b^4 c^2}\left[4a^3b^2c + a^4b(2c + b)\right]$$

$$= \frac{-a^3}{b^3 c^2} \left[4bc + a(2c+b) \right].$$

Insert equation (F7):

$$\operatorname{Res} f(0) = \frac{-a^3}{b^3 c^2} \left[4b\left(\frac{b}{2}-1\right) + a\left(2\left(\frac{b}{2}-1\right)+b\right) \right]$$

$$= \frac{-a^3}{b^3 c^2} \left[2b^2 - 4b + 2a(b-1) \right]$$

Insert equation (F5):

$$\operatorname{Res} f(0) = \frac{-a^3}{b^3 c^2} \left[2b^2 - 4b + 2\left(1-p-\frac{b}{2}\right)(b-1) \right]$$

$$= \frac{-a^3}{b^3 c^2} \left[b^2 - b - 2pb - 2 + 2p \right].$$

Insert equation (F6):

$$\operatorname{Res} f(0) = \frac{-a^3}{b^3 c^2} \left[4\left(1-p^2\right) - (1+2p)b - 2 + 2p \right]$$

$$= \frac{-a^3}{b^3 c^2} \left[2 + 2p - 4p^2 - (1+2p)b \right]$$

$$= \frac{-a^3}{b^3 c^2} \left[2(1+2p)(1-p) - (1+2p)b \right]$$

$$= \frac{-2a^3}{b^3 c^2} (1+2p) \left[(1-p) - \frac{b}{2} \right]$$

$$= \frac{-2a^3}{b^3 c^2} (1+2p) a$$

$$= -2(1+2p) \frac{a^2 a^2}{b^3 c^2}.$$

Insert equation (F2):

$$\mathrm{Res}\, f(0) = -2(1+2p) \frac{\left[(1-p) - \sqrt{1-p^2} \right]^2 \left[(1-p) - \sqrt{1-p^2} \right]^2}{b^3 c^2}$$

$$= -2(1+2p) \frac{\left[(1-p)^2 - 2(1-p)\sqrt{1-p^2} + 1 - p^2 \right]^2}{b^3 c^2}$$

$$= -2(1+2p) \frac{\left[2 - 2p - 2(1-p)\sqrt{1-p^2} \right]^2}{b^3 c^2}$$

$$= -8(1+2p)(1-p)^2 \frac{\left[1 - \sqrt{1-p^2} \right]^2}{b^3 c^2}$$

$$= -8(1+2p)(1-p)^2 \frac{c^2}{b^3 c^2}$$

$$= -8(1+2p)(1-p)^2 \frac{1}{b^3}.$$

Insert equation (F3):

$$\operatorname{Res} f(0) = -8(1+2p)(1-p)^2 \frac{1}{8(1-p^2)^{\frac{3}{2}}}$$

$$= -\frac{(1+2p)(1-p)^2}{(1-p^2)^{\frac{3}{2}}}$$

$$= -\frac{(1+2p)(1-p)^2}{\sqrt{1-p^2}\,(1-p^2)}$$

$$= -\frac{(1+2p)(1-p)}{\sqrt{1-p^2}\,(1+p)}$$

$$= -\frac{(1+2p)(1-p)}{\sqrt{1-p}\sqrt{1+p}\,(1+p)}$$

$$= -\frac{(1+2p)\sqrt{1-p}}{(1+p)^{\frac{3}{2}}}.$$

Therefore

$$F_{2\theta}(p) = \frac{\pi}{2}\operatorname{Res} f(z_2)$$

$$= -\frac{\pi}{2}\frac{(1+2p)\sqrt{1-p}}{(1+p)^{\frac{3}{2}}}.$$

The integrand due to both poles is

$$f_\sigma\left(p(\sigma)\right) = F_\theta = F_{1\theta} + F_{2\theta} = \frac{\pi}{2} - \frac{\pi}{2}\frac{1+2p}{\left(1+p\right)^{\frac{3}{2}}}\sqrt{1-p}$$

The contribution from an interval from σ_1 to σ_2 along the lamp is

$$\delta F_\sigma = \int_{\sigma_1}^{\sigma_2} f_\sigma d\sigma .$$

Rearranging equation (6.6),

$$\sigma^2 + 2 = \frac{2}{p}$$

and therefore

$$2\sigma d\sigma = -\frac{2}{p^2}dp$$

after differentiation. Also,

$$\sigma = \sqrt{\frac{2}{p} - 2}$$

after making σ the subject of equation (6.6). Hence

$$d\sigma = -\frac{1}{p^2\sqrt{\frac{2}{p}-2}}dp$$

$$= -\frac{1}{\sqrt{2}\,p^{\frac{3}{2}}\sqrt{1-p}}dp$$

after appropriate division and substitution of σ, so that

$$\delta F_\sigma = \int_{p_1}^{p_2} \left(\frac{\pi}{2} - \frac{\pi}{2} \frac{1+2p}{(1+p)^{\frac{3}{2}}} \sqrt{1-p} \right) \frac{-1}{\sqrt{2}\, p^{\frac{3}{2}} \sqrt{1-p}} \, dp$$

$$= \frac{\pi}{2\sqrt{2}} \int_{p_1}^{p_2} \frac{1+2p}{(1+p)^{\frac{3}{2}} p^{\frac{3}{2}}} \, dp - \frac{\pi}{2\sqrt{2}} \int_{p_1}^{p_2} \frac{1}{p^{\frac{3}{2}} \sqrt{1-p}} \, dp \, .$$

In the first integral, let

$$p = \tan^2 \omega \,. \tag{F8}$$

Then

$$dp = 2 \tan \omega . \sec^2 \omega . d\omega \, .$$

In the second integral, let $\qquad p = \sin^2 \mu \, .$

Then

$$dp = 2 \sin \mu . \cos \mu . d\mu \, .$$

Now

$$\delta F = \frac{\pi}{\sqrt{2}} \int_{\omega_1}^{\omega_2} \frac{1+2\tan^2\omega}{\left(1+\tan^2\omega\right)^{\frac{3}{2}}\tan^3\omega} \tan\omega \sec^2\omega\, d\omega - \frac{\pi}{\sqrt{2}} \int_{\mu_1}^{\mu_2} \frac{1}{\sin^3\mu\sqrt{1-\sin^2\mu}} \sin\mu\cos\mu\, d\mu$$

$$= \frac{\pi}{\sqrt{2}} \int_{\omega_1}^{\omega_2} \frac{\sec^2\omega+\tan^2\omega}{\sec^3\omega\tan^3\omega} \tan\omega \sec^2\omega\, d\omega - \frac{\pi}{\sqrt{2}} \int_{\mu_1}^{\mu_2} \frac{1}{\sin^2\mu}\, d\mu$$

using the identities $\sec^2 x = 1+\tan^2 x$ and $\sin^2 x + \cos^2 x = 1$. Perform the integration:

$$\delta F = \frac{\pi}{\sqrt{2}} \int_{\omega_1}^{\omega_2} \left(\csc\omega\cot\omega + \cos\omega\right) d\omega - \frac{\pi}{\sqrt{2}} \int_{\mu_1}^{\mu_2} \csc^2\mu\, d\mu$$

$$= \frac{\pi}{\sqrt{2}} \left(-\csc\omega + \sin\omega\right)\Big|_{\omega_1}^{\omega_2} + \frac{\pi}{\sqrt{2}} \cot\mu\Big|_{\mu_1}^{\mu_2}.$$

From equation (F8),

$$\omega = \tan^{-1}\sqrt{p}.$$

Let $y = \csc\omega = \csc\tan^{-1}\sqrt{p}$. Then from trigonometric ratios,

$$\tan\left(\tan^{-1}\sqrt{p}\right) = \sqrt{p} = \frac{1}{\sqrt{y^2-1}}.$$

Square both sides:

$$p = \frac{1}{y^2 - 1}$$

and solve for y.

$$y = \sqrt{\frac{1+p}{p}} \; .$$

i.e.

$$\csc \omega = \sqrt{\frac{1+p}{p}}$$

and

$$\sin \omega = \sqrt{\frac{p}{1+p}} \; .$$

Similarly

$$\cot \mu = \sqrt{\frac{1-p}{p}} \; .$$

Thus

$$\delta F = \frac{\pi}{\sqrt{2}} \left(-\sqrt{\frac{1+p}{p}} + \sqrt{\frac{p}{1+p}} + \sqrt{\frac{1-p}{p}} \right) \Bigg|_{p_1}^{p_2}$$

As p approaches zero the expression as it stands becomes undefined, and must be placed in alternate form [26]:

$$-\sqrt{\frac{1+p}{p}} + \sqrt{\frac{p}{1+p}} + \sqrt{\frac{1-p}{p}} = \frac{-(1+p) + p + \sqrt{1-p^2}}{\sqrt{p}\sqrt{1+p}}$$

$$= \frac{\sqrt{1-p^2}-1}{\sqrt{p}\sqrt{1+p}}$$

$$= \frac{\sqrt{1-p^2}-1}{\sqrt{p}\sqrt{1+p}} \cdot \frac{\sqrt{1-p^2}+1}{\sqrt{1-p^2}+1}$$

$$= \frac{1-p^2-1}{\sqrt{p}\sqrt{1+p}\left(\sqrt{1-p^2}+1\right)}$$

$$= \frac{-p^{\frac{3}{2}}}{\sqrt{1+p}\left(\sqrt{1-p^2}+1\right)}$$

It is now evident that as $p \to 0$,

$$\frac{-p^{\frac{3}{2}}}{\sqrt{1+p}\left(\sqrt{1-p^2}+1\right)} \to 0 \ .$$

The new result is

$$\delta F = \frac{\pi}{\sqrt{2}}\left(\frac{-p^{\frac{3}{2}}}{\sqrt{1+p}\left(1+\sqrt{1-p^2}\right)}\right)\Bigg|_{p_1}^{p_2} \ .$$

Now restore σ by substitution of the expression for $p(\sigma)$ (equation (6.6)). The unevaluated integral is

$$\frac{p^{\frac{3}{2}}}{\sqrt{1+p}\left(1+\sqrt{1-p^2}\right)} = \frac{\left(\frac{2}{\sigma^2+2}\right)^{\frac{3}{2}}}{\sqrt{1+\frac{2}{\sigma^2+2}}\left(1+\sqrt{1-\left(\frac{2}{\sigma^2+2}\right)^2}\right)}$$

Multiply both numerator and denominator on the right hand side by $\left(\sigma^2+2\right)^{\frac{3}{2}}$:

$$\frac{p^{\frac{3}{2}}}{\sqrt{1+p}\left(1+\sqrt{1-p^2}\right)} = \frac{(2)^{\frac{3}{2}}}{\sqrt{\sigma^2+2+2}\left(\sigma^2+2+\sqrt{\left(\sigma^2+2\right)^2-4}\right)}$$

$$= \frac{2\sqrt{2}}{\sqrt{\sigma^2+4}\left(\sigma^2+2+\sqrt{\sigma^4+4\sigma^2}\right)}$$

$$= \frac{2\sqrt{2}}{\sqrt{\sigma^2+4}\left(\sigma^2+2+\sigma\sqrt{\sigma^2+4}\right)}.$$

Upon evaluation,

$$\delta I = \frac{1}{\pi}I_0.\delta F$$

$$= 2I_0\left(\frac{1}{\sqrt{\sigma_1^2+4}\left(\sigma_1^2+2+\sigma_1\sqrt{\sigma_1^2+4}\right)} - \frac{1}{\sqrt{\sigma_2^2+4}\left(\sigma_2^2+2+\sigma_2\sqrt{\sigma_2^2+4}\right)}\right).$$

In terms of the original constants,

$$\delta I = 2I_0 R^3 \left(\frac{1}{\sqrt{z_1^2 + 4R^2}\left(z_1^2 + 2R^2 + z_1\sqrt{z_1^2 + 4R^2}\right)} - \frac{1}{\sqrt{z_2^2 + 4R^2}\left(z_2^2 + 2R^2 + z_2\sqrt{z_2^2 + 4R^2}\right)} \right) \quad \text{(F9)}$$

This is the final result, for the flux contribution at an observation point on the chamber wall, of a cylindrical chamber interval between planes perpendicular to the axis at z_1 and z_2.

Appendix G

The intensity of the surface within a spherical integrating chamber.

The intensity of light reflected off the surface of a spherical integrating sphere, will be obtained by considering the path of a single ray.

It will first be noted that the reflected flux can be written in terms of the absorbed flux.

$$\Phi_a = a\Phi_i = (1-f)\Phi_i$$

$$\Phi_r = f\Phi_i$$

$$\frac{\Phi_r}{\Phi_a} = \frac{f\Phi_r}{(1-f)\Phi_r} = \frac{f}{1-f}$$

Therefore,

$$\Phi_r = \frac{f}{1-f}\Phi_a \, .$$

Now suppose a source radiates a flux of Φ_s watts isotropically. There are 4π steradians in a sphere. Then the intensity of the source is $I_s = \dfrac{\Phi_s}{4\pi} \, W.sr^{-1}$ and is equivalently the intensity on a unit sphere. The intensity of light incident on the surface of a sphere of radius r is

$$I_i(r) = \frac{\Phi_i}{4\pi r^2} \, W.m^{-2}.$$

Similarly the reflected intensity is

$$I_r(r) = \frac{\Phi_r}{4\pi r^2} \; W.m^{-2}.$$

Total reflected flux is

$$\Phi_r = \frac{f}{1-f} \Phi_a \; .$$

Therefore,

$$I_r(r) = \frac{\Phi_a}{4\pi r^2} \frac{f}{1-f} \; .$$

Total absorbed flux is just the source flux,

$$\text{i.e. } \Phi_a = \Phi_s$$

so that

$$I_r = \frac{\Phi_s}{4\pi r^2} \frac{f}{1-f} \qquad \text{(G-1)}$$

Equation (G-1) is the intensity on the surface of a spherical integrating sphere.

Appendix H

The ratio of actual flux to cosine-corrected flux, arriving at a point, from an infinite diffuse plane.

For an infinite plane, integration takes place over an entire hemisphere. In the case of cosine-corrected flux, the relevant part (all other constants cancel out in the ratio) of the integral is

$$F_{i,c} = \int_0^{\frac{\pi}{2}} \sin\theta \cos\theta \, d\theta$$

$$= \frac{1}{2}$$

while if cosine-correction is excluded, the integral just yields the area of the hemisphere.

$$F_{i,c} = \int_0^{\frac{\pi}{2}} \sin\theta \, d\theta = 1.$$

The ratio becomes

$$\frac{F_i}{F_{i,c}} = \frac{1}{\frac{1}{2}} = 2.$$

i.e. the flux at a point in space, due to an infinite Lambertian emissive plane, is exactly twice the value measured at that point by a cosine-corrected device.

References

[1] J. D. Simpson, D. J. Drake & T. Speziale, *Light-integrating cylinder for inertial confinement fusion balance measurements in mirror illumination systems,* Rev. Sci. Instrum. 57 (12), 2951-2957, (1986).

[2] A. M. Maher & P. D. Swift, *Providing a homogeneous visual field with an integrating sphere*, IOP Publishing Ltd, Physiol. Meas. Vol. 23, N9–N15, (2002).

[3] Labsphere, *A Guide to Integrating Sphere Theory and Applications*, 231 Shaker st. North Sutton, New Hampshire, U.S.A.; website: **www.labsphere.com**, (2005).

[4] Labsphere, *A Guide to Reflectance Coatings and Materials*, (2005).

[5] J. W. T. Walsh, M.A, MSc, & W. Barnett, *The Effect of Slightly Selective Absorption in the Paint used for Photometric Integrators*, (1926).

[6] H. Shitomi, Y. Mishima & I. Saito, *Development of a new integrating sphere with uniform reflectance for absolute diffuse reflectance measurements*, BIPM and IOP Publishing Ltd, Metrologia Vol. 40, S185–S188, (2003).

[7] Delta Developments, *Integrating Spheres*, PO Box 115, Liss, Hants GU33 6DF, UK, (2005).

[8] C. J. Y. Lerebourg, D. A. Pilgrim, G. D. Ludbrook & R. Neal, *Development of a point source integrating cavity absorption meter,* IOP Publishing, J. Opt. A: Pure Appl. Opt. Vol. 4, S56–S65 (2002).

[9] J. A. Bastin, *Use of an integrating sphere to distinguish between absorption and scattering in solids,* Vol. 10, 412-416, British Journal of Applied Physics, (1959).

[10] Hanssen & Prokhorov, *Numerical modeling of an integrating sphere radiation source,* National Institute of Standards and Technology, (2003).

[11] S. W. Brown & B. C. Johnson, *Development of a portable integrating sphere source for the Earth Observing System's calibration validation programme*, International Journal of Remote Sensing Vol. 24 (2), 215–224, (2003).

[12] P. Saunders, A. B. Trotter, H. Edgar & D. Cochrane, In situ *measurement of catalyst tube emissivity by means of a portable solid integrating sphere reflectometer,* Meas. Sci. Technol. Vol. 12, 622–626, (2001).

[13] M. Kiguchi & M. Kato, *Near-field optical microscopy using an integrating sphere*, Appl. Phys. B Vol. 73, 727–730, (2001).

[14] D. J. Griffiths, *Introduction to Electrodynamics,* 2nd edn, Prentice-Hall, (1989).

[15] Meyer/ Arendt, *Introduction to Classical and Modern Optics*, 4th edn, Prentice-Hall, (1995).

[16] Gerald/ Wheatley, *Applied Numerical Analysis*, 6th edn, Wesley, (1999).

[17] NIST, *Self-study Manual on Optical Radiation Measurements*, eDoc Publish Inc.; 100 Bureau drive, Gaithersburg, Maryland, (2005).

[18] F. *Mandl Statistical Physics* 2nd edn, Wiley, (1988).

[19] A. Stimson, *Photometry and Radiometry for Engineers*, Wiley, (1974).

[20] W. G. Driscoll, *Handbook of Optics*, McGraw-Hill, (1978).

[21] R. W. Boyd, *Radiometry and the detection of Optical Radiation*, Wiley, (1983).

[22] R. W. Wood, *Physical Optics*, Macmillan, (1988).

[23] E. Butkov, *Mathematical Physics*, Wesley, (1968).

[24] A. C. BajPai, *Mathematics for Scientists & Engineers* Vol.2, Wiley, (1973).

[25] Finney/ Thomas, *Calculus and Analytical Geometry*, 6th edn, Wesley, (1983).

[26] K. A. Stroud, *Engineering Mathematics*, 2nd edn, Macmillan, (1982).

[27] Finney/ Thomas, *Calculus*, 2nd edn, Wesley, (1994).

[28] K. Nicholson, *Linear Algebra*, 3rd edn, PWS Boston, (1995).